THE GENERATION OF UNSTABLE WAVES AND THE GENERATION OF TRANSVERSE UPWELLING: TWO PROBLEMS IN GEOPHYSICAL FLUID DYNAMICS

by

CLINTON ARTHUR LEE

B.A., University of California, La Jolla, 1968

M.Sc., University of British Columbia, 1970

A THESIS SUBMITTED IN PARTIAL FULFILLMENT OF THE REQUIREMENTS FOR THE DEGREE OF DOCTOR OF PHILOSOPHY

in the Institute of Oceanography and

the Intitute of Applied Mathematics and Statistics

We accept this thesis as conforming to the required standards

THE UNIVERSITY OF BRITISH COLUMBIA

February, 1975

In presenting this thesis in partial fulfilment of the requirements for an advanced degree at the University of British Columbia, I agree that the Library shall make it freely available for reference and study. I further agree that permission for extensive copying of this thesis for scholarly purposes may be granted by the Head of my Department or by his representatives. It is understood that copying or publication of this thesis for financial gain shall not be allowed without my written permission.

Department of Mathematics

The University of British Columbia
Vancouver 8, Canada

Date April 30, 1975

ABSTRACT

In this thesis two different problems in geophysical fluid dynamics are studied. In Part A we consider the general problem of the generation of unstable shelf waves, a problem that relates to the generation of the meanders in the Gulf Stream. In Part B we consider the generation of transverse motions of the thermocline in long two layer bodies of water by general wind stresses.

The instability of fluid systems has been studied for a long time, but the problem of how the instabilities are generated and grow has been neglected. Recently, however, in the study of the interaction of plasmas with electron streams, techniques have been developed to study the growth of instabilities. These techniques can in principle be applied to any unstable linear system that is excited by stationary forcing. In Part A we describe these techniques and extend them to cover the case of moving forcing effects. We then use the results to study the generation of unstable shelf waves.

Long barotropic waves trapped on an abrupt change in bottom topography are shelf waves; the presence of lateral shear in the persistent ocean currents gives rise to unstable shelf waves. The possible presence of such waves in the Gulf Stream system could explain the generation of

the meanders in the Gulf Stream. Thus we study the response of a model Gulf Stream that supports unstable shelf waves to the wind. Only curl free wind stress is considered, mainly for convenience. It is found that only on the offshore side of the stream, where the response is always larger than on the inshore side, are the unstable waves always dominant. A wind system moving slowly in the direction of the stream is the most efficient at generating the unstable waves, but its efficiency is affected quite drastically by the duration of the disturbance. A wind system moving counter to the stream is less efficient by about a factor of eight, but is practically uneffected by a change in duration.

In Part B we consider a stable system. We use simple Fourier expansion to study the motions of the thermocline in an infinitely long two layer body of water generated by both long axis and cross channel winds. It is found that in a wide lake, such as Lake Michigan, cross channel winds are more efficient in generating transverse motions which in all cases are multi-modal. Here wide means wide in comparison to the Rossby radius of curvature. These results agree only qualitatively with observations made on Lake Michigan. In fact reasonable wind stresses only give responses about one-tenth of those observed. In a narrow lake it is found that the response to a long axis wind is larger than that to a cross channel wind, both giving a uni-modal response.

Observations of wind and thermocline depth taken at Babine Lake in northern B. C. agree quite well with the theory.

TABLE OF CONTENTS

LIST OF FIGURES FOR PART A

(b) $\psi_F(2,y,100)$ and $\psi_F(2,y,200)$ for $V^*=.03$ and $s^*=-.06$.

Figure IV.15 $\psi_T(2,y,100)$ and $\psi_T(2,y,200)$ for $V^*=-.1$ and $s^*=-.06$.

LIST OF FIGURES FOR PART B

ACKNOWLEDGEMENTS

I am indebted to Dr. L. A. Mysak for his advice and encouragement in the writing of this thesis and the work that led up to it. I would also like to thank Dr. D. M. Farmer for giving me the opportunity to spend two weeks at Babine Lake during which time I made some of the observations reported here. During part of the time I was working on this thesis I was supported by a National Research Council Postgraduate Scholarsphip, and during the whole period I was given the opportunity by the Mathematics Department at U. B. C. to obtain extra support by lecturing.

Finally I would like to thank my wife Marion. Without her help and encouragement I would not have been able to complete this task.

PART A

The Generation of Unstable Waves with Applications to the Meanders in the Gulf Stream

CHAPTER I - Introduction

A common problem in many branches of physical science is to determine under what conditions or parameter ranges, if any, a physical system is unstable when perturbed by a certain class of time dependent disturbances. One technique used to solve this problem is that developed in linear hydrodynamic stability theory (Lin, 1955; Chandrasekhar, 1961; Ried, 1967). For a one-dimensional system the scalar or vector valued function $\phi(x,t)$ describing the perturbations to the system due to the disturbance is written as a travelling wave with

$$\phi(x,t) = A \exp[i(\omega t - kx)] . \tag{I.1}$$

Introducing (I.1) into the equations for $\phi(x,t)$ that describe the system it is assumed that the amplitudes of the perturbations are small enough so that any products of perturbations are negligible. Thus a set of linear equations for the amplitudes A is obtained that has a solution only if a certain relation between k and ω,

$$\Delta(k,\omega) = 0, \tag{I.2}$$

is satisfied. This relation is called the dispersion relation and the graph of $\omega = \omega(k)$ obtained by solving (I.2) for ω with k real is called the disperion curve. If for some real k a solution $\omega(k)$ of (I.2) is complex with $\mathrm{Im}\{\omega(k)\}<0$, the system is said to be unstable since the wave with wavenumber k grows exponentially in time.

In most problems this is as far as the study of stability is taken. The intervals on the real k axis for which there are unstable roots of the dispersion relation are determined. Alternatively, ω is assumed real and roots of the dispersion relation with k complex are sought. In the former case the system has a temporal instability, and in the latter a spatial instability. Another approach to the instability problem that is useful in systems with damping is through "neutral stability" curves (or surfaces) along which $\mathrm{Im}\{\omega(k)\}=0$, in a suitable parameter space. For example, in the stability of parallel flows (Betchov and Criminale, 1967) neutral stability curves are drawn in the (k,R) plane. Here R is the Reynolds number. Such curves represent transitions from stability to instability. These approaches have yielded much useful information about many interesting and important systems (Chandrasekhar, 1961). In most cases it is difficult to go beyond this "simple" stability analysis. In fact, it is often impossible even to obtain a closed form expression for the dispersion relation (Reid, 1967).

However, if $\Delta(k,\omega)$ can be expressed in closed form and is a simple enough function, it would be useful to solve the initial value problem for $\phi(x,t)$ in order to see how the unstable waves actually grow. This would serve at least as a check on the assumption implicit in all the approaches to the stability problem mentioned above, i.e. if the system has a temporal instability it will eventually dominate the response of the system. As will be seen, it is possible for the unstable waves to propagate out of a finite geophysical system before it grows to significant size. This problem has been neglected, especially in geophysical problems, mainly due to the difficulties mentioned above. However, Criminale and Kovasznay (1962) have solved the problem of the growth of an initial disturbance in a laminar boundary layer. Also, in the study of the interaction of electron streams with plasmas the growth of unsatble waves is important, and in that field techniques have been developed to find the asymptotic behaviour for large time of an unstable system (Briggs, 1964).

In the study of unstable plasma systems it is useful to classify the instability of a system into two types, absolute and convective. Both types are unstable by the criterion given above, i.e. $\mathrm{Im}\{\omega(k)\}<0$ for some real k. In a system with an absolute instability an observer at any point sees exponential growth in time. In a system with only convective instabilities only observers moving with non-zero velocities in a certain range see exponential growth. Thus in a convectively unstable system a stationary observer at a distance from some initial disturbance sees growth with time initially, but eventually he must see the perturbations decay with time as the instability is "convected" past him. It is important to be able to distinguish between convective and absolute instabilities in designing plasma systems because in a convectively unstable system it is possible for a potentialy dangerous instability to convect out of the finite system before it has a chance to grow to destructive proportions (Hall and Heckrotte, 1968).

Another way to state the distinction between absolute and convective instabilities is in terms of the group velocity. Recall that the group velocity, $V_g(k)$, is given by

$$V_g(k) = \omega'(k). \tag{I.3}$$

An observer moving at the velocity $V_g(k)$ sees a wave of the form $\exp\{i[\omega(k)t-kx]\}$. This is derived using the method of stationary phase (e.g. Lighthill, 1965). An absolutely unstable system is one for which there is an unstable wave that has zero group velocity; a convectively unstable system is one for which there are no unstable waves with zero group velocity. Theoretical plasma physicists have developed methods for determining whether an unstable system has an absolute instability or only convective instabilities (Briggs, 1964 and Derfler, 1970) and the velocity ranges in which growth will be observered for both absolutely and convectively unstable systems (Hall and Heckrotte, 1968).

The results referred to above can be used to obtain explicit asymptotic expressions for the response of an unstable system to a stationary disturbance. In Part A of this thesis these results are used to study the growth of unstable waves in a geophysical system. Since it is of interest to find the response for travelling disturbances, the results are also extended to cover this case. To my knowledge this is the first time that such methods have been used to study the response of an unstable geophysical system.

The system that we study here is a laterally sheared flow over a variable bottom topography. The flow is assumed to be vertically homogeneous and uniformly rotating. With or without a basic flow, low frequency waves with periods of the order of days propagate as perturbations on the fluid velocities in a direction perpendicular to the depth gradient. Such waves are called shelf waves and are said to be "trapped" by the depth gradient (Robinson, 1964; Mysak, 1967; Buchwald and Adams, 1968). Niiler and Mysak (1971), hereafter referred to as NM, have found that the presence of the lateral shear gives rise to unstable waves propagating in the direction of the flow, these are unstable shelf waves. Here the generation of such waves by a wind stress acting at the surface is studied. In the case of stable shelf waves this problem has been studied by Adams and Buchwald (1969). This problem is of interest in that it relates to the problem of the meanders in the Gulf Stream.

For many years it has been known that the Gulf Stream changes position over periods of days. Such changes have been termed meanders. The Gulf Stream is a phenomenon that is similar to phenomena seen on the western side of most of the ocean basins of the world. It is a region of an intense poleward surface current that is the return flow of the overall surface circulation of the North Atlantic. The flow is concentrated strongly along the coast due to the variation of the Coriolis paramter with latitude (Stommel, 1948 and Munk, 1950; for a physical explanation see Stewart, 1964). Associated with the Gulf Stream are large surface temperature gradients with temperature increasing away from the coast. It is found that these large gradients coincide with the maximum surface current velocities (Stommel, 1966). Thus the location of Gulf Stream can be accomplished by determining the position of the large surface temperature gradients. Observations of the position of the Gulf Stream over many years have revealed that its position is not at all steady; in fact this meandering seems to be an intrinsic property of the Gulf Stream and other western intensified currents.

Haurwitz and Panofsky (1950) were the first to suggest that the meanders might be the result of low frequency unstable waves propagating along the Gulf Stream. Their model includes fairly realistic piecewise continuous approximations to the laterally sheared flow of the Gulf Stream but does not include the effects of bottom topography. Since vertical variations of density and velocity are also neglected it is called a barotropic model. With this simple model they predicted that the system will support unstable waves if the region of lateral shear is far enough from the boundary. The unstable waves predicted by their model have properties similar to the wave properties of the meanders in the Gulf Stream.

Since the work of Haurwitz and Panofsky many models that are applicable to the Gulf Stream and support unstable waves have been studied. Most of these models have included the most important feature of the Gulf Stream ignored by Haurwitz and Panofsky--the vertical variation of density and velocity. Such models are called baroclinic. Two methods for modeling such variations have been used. The simplest is to assume the flow to be divided into horizontal layers in which there are no vertical variations; properties change discontinuously across the interface between layers. Two-layer models in which the lower layer is stationary and the upper layer is laterally sheared have been studied by Stern (1961), Lipps (1963), Jacobs (1971) and Sela and Jacobs (1971). Orlanski (1969) has studied two layer models that include the dynamics of the lower layer in order to examine the effect of bottom topography on the stability of the flow. Vertical structure may also be modeled by continuous vertical changes. This has been done by Pedlosky (1964 a and b) who considered both two-layer and continuous variation models. All of the models mentioned above are complicated enough that, even though they by no means include all of the physics of the Gulf Stream, it is possible to only do the "simple" stability analysis described above. Much work has been expended in determining the parameter ranges in which the models are unstable and the simplest properties of the unstable waves, e.g. growth rate, wavelength, frequency and phase speed.

The baratropic model of NM on the other hand is simple enough that the asymptotic techniques developed for unstable plasma systems are easily applied. Thus the response of the model to various disturbances can be calculated. The model is similar to that of Haurwitz and Panofsky except that it includes bottom topography. In Part A of this thesis we calculate the response of this model to curl free wind systems both stationary and moving. This may be regarded as a first step in the problem of calculating the response of more complicated models to more general wind systems. Also, as will be seen, the response to a curl free wind stress certainly gives a lower bound to the total response of the system. Further, this problem also serves the purpose mentioned above of checking the basic assumption of stability theory that in an unstable system the instablity eventually dominates the response. It is already apparent that in a convectively unstable system, as the NM model is, this assumption must be treated with care, but explicit calculations indicate further ramifications. For example, it is found that in the NM model while the response on the offshore side of the stream is always dominated by the unstable waves, that on the inshore side is not. Finally, again to my knowledge this is the first time that the explicit asymptotic response of an unstable geophysical system has been calculated, in spite of the large number of such systems that have been studied.

It might be useful here to give a brief history of this project. When first proposed it was intended as a qualifying problem for the Institute of Applied Mathematics at U. B. C. to be completed in a couple of months. The initial boundary value problem for the response of the NM model was to be solved using Fourier-Laplace transforms with the resulting inversion integrals,

$$\psi(y,t) = \frac{1}{4\pi^2 i}\int_{\gamma-i\infty}^{\gamma+i\infty} e^{st}\,ds \int_{-\infty}^{\infty} \frac{F(k,s)\,e^{-iky}}{\Delta(k,s)}\,dk \qquad (I.4)$$

to be evaluated using standard asymptotic techniques, such as the method of steepest descent. Using this approach the Laplace inversion integral is evaluated first by summing residues, and then the Fourier inversion integral is evaluated asymptotically for large time and small y by the method of steepest descent. In order to extend the results to finite y let $y=y_0+Vt$ and do the asymtotics for each V of interest.

In the method of steepest descent integrals of the form

$$I(t) = \int_A^B g(k)\exp[t f(k)]\,dk \qquad (I.5)$$

are to be evaluated asymtotically for large t by deforming the path of integration in the complex k plane into a path of steepest descent, i.e. a path along which $Re\{f(k)\}$ decreases most rapidly. Obviously the most important contribution to the integral comes from the point on the new path of integration at which $Re\{f(k)\}$ is a maximum. There are only two possibilities. Either the maximum occurs at an endpoint A or B, or the maximum occurs at an interior point, k_o, at which $f'(k_o)=0$. The point k_o is a saddle point of $f(k)$. Only in the second case does the saddle point contribute to the aysmptotic development of $I(t)$. The form of the asymptotic expansion depends on which of the two possibilities arise (Sirovich, 1971 or Jeffreys and Jeffreys, 1956). In evaluating the asymptotic behaviour of the Fourier inversion integral for the response of the NM model by the method of steepest descent problems arose. The function $\Delta(k,s)$ is quadratic in s but is a complicated transcendental function of k. Thus finding the paths of steepest descent in the k plane along which $Im\{s\}$ is constant seemed impossible. Thus deciding between the two possibilities given above would also be impossible. Therefore, at that point it seemed advisable, if the problem was indeed to be finished in a short time, just to evaluate the Fourier integral numerically in order to get some idea of the growth of the unstable waves. Unfortunately the numerical integrations turned out to be quite expensive, due mainly to the large number of evaluations of the integrand required for convergence. For this reason the integral was evaluated only at one point in the stream which was chosen to be the point of velocity maximum. The expected growth of the unstable waves was not seen.

Shortly after this rather discouraging result was obtained the work of the plasma physicists came to my attention through Briggs (1964). The method used there is essentially the same as the method of steepest descent, but the point of view is changed. In this approach the Fourier integral is evaluated first by summing residues. Then causality in the form of the requirement that the integrand in the Laplace inversion integral must be analytic to the right of the Laplace inversion path is used to find a criterion for deciding whether a given saddle point contributes or not. The criterion is that if the paths of steepest descent approach a saddle point from opposite sides of the real k axis the saddle point contributes, otherwise it does not and the asymptotic representation is exponentially small compared to the contribution from the saddle point.

Apparently the criterion given above still requires that paths of steepest descent be drawn and saddle points be determined for each V. However, in a paper by Hall and Heckrotte (1968) a method is given for determining intervals for V within which saddle points contribute and outside of which they do not. It is then only necessary to find the endpoints of these intervals and to test one saddle point on each side. In the same paper it is pointed out that the problem of determining saddle points as a function of V is the same as solving the system of equations

$$\left.\begin{aligned} &\Delta(k,s) = 0, \\ &\Delta_k(k,s) + iV\Delta_s(k,s) = 0, \end{aligned}\right\} \qquad \text{(I.6)}$$

which can be recast as a differential equation in V to be solved numerically. It was found to be easier, however, to solve (I.6) directly using Newton's method. It is still necessary to solve the dispersion relation in order to draw steepest descent paths and to find starting values for Newton's method. This problem is solved by a method due to Delves and Lyness (1967).

Using the conglomeration of methods described briefly above it was possible to calculate the response of the NM model to curl free wind stresses. Of course, the first thing to do was to verify the results with the numerical integrations. The calculations agreed quite well, so further calculations were made using the asymptotic methods. It was found that on the offshore side of the stream the unstable waves are always dominant, but on the inshore side this is not always the case. This is due to the fact that on the inshore side the integrand is small in the interval of instability, compared to its value in the stable regime, whereas on the offshore side it is of the same order in the stable and unstable regimes. This explained the results of the numerical integration.

The collection of results used to solve the problem considered here should in principle be applicable to any initial value problem that can be solved using Fourier-Laplace transforms. Thus any linear system that can be considered infinite in one direction can be handled by this method. The main problem is to solve the dispersion relation. Since in many cases it is impossible even to write a closed form expression for the dispersion relation this can be a very difficult problem. However, since the dispersion relation can be analysed once and for all, and the results then be used for any forcing function, it is possible that it would be feasible to consider such difficult systems. This could require quite extensive numerical work however. In the remainder of this introduction we give a brief outline of Part A of this thesis.

In Chapter II the NM model is described in more detail, and the equations of motion governing it are derived. These equations are solved by Fourier-Laplace transforms subject to the initial condition that at t=0 a general wind stress is applied. The inversion integrals are written out explicitly only for a curl free wind stress. This is done mainly for mathematical convenience. However, the methods developed and used here can be extended to cover more general wind stress models. Further, these calculations should only be regarded as a first step in solving more complicated problems. Finally, the calculations cannot be expected to be very good representations of the response of the Gulf Stream to a general wind stress as the unstable waves that are generated are of a large enough amplitude that a linear model would not really apply.

In Chapter III the results developed by the plasma physicists that are relevant to the problem at hand are presented. These are then extended to cover the case of a traveling disturbance, a problem that has not been considered before in the case of unstable systems.

In Chapter IV the results of Chapter III are applied to the problem of calculating the response of the model presented in Chapter II to curl free wind stresses. It is found that on the coastal side of the stream the unstable waves do not appear until after they have travelled well out of the system. On the offshore side of the stream, however, the unstable waves certainly do dominate the response. A disturbance moving slowly in the direction of the stream is the most efficient at generating the unstable waves. A disturbance moving upstream is much less efficient.

CHAPTER II - Unstable Shelf Waves

Section 1. Introduction

In this chapter we study the generation of low frequency waves in a rotating, laterally sheared flow over a changing bottom topography. In a study of the propagation of such waves NM found that the presence of the lateral shear in the flow gives rise to unstable waves that propagate in the direction of the stream. It is our purpose here to solve the initial boundary value problem for the generation of these waves from an equilibrium configuration in order to study the growth of the unstable waves. The approocah used her is to derive the linearized long wave equations for perturbations to a laterally sheared flow and then solve the equations using Fourier-Laplace transforms for general forcing. The inversion integrals are written out explicitly, however, only for special curl free wind stresses.

Section 2. The Equations

Consider a laterally sheared flow parallel to a long straight coast, running north-south, in a uniformly rotating ocean with the bottom topography varying only in a direction perpendicular to the coast. It is assumed that the flow is depth independent and that the density is a constant, i.e. the flow is barotropic. In studies of more general models that include continuous stratification it is found that the higher baroclinic modes have slower growth rates than the barotropic and first baroclinic modes. Thus it is reasonable to consider a barotropic model. Introduce a right-handed rectangular coordinate system with x eastward, y northward and z vertically upward. The origin is on the coast at the level the free surface would assume if there were no flow. The bottom is at $z=-h(x)$. At time $t=0$ there is an equilibrium state with the flow northward with velocity profile $V_0(x)$. At this time a surface wind stress $\vec{\tau}=(\tau_x,\tau_y)$ is applied. Here the equations governing the response of this system to $\vec{\tau}$ are derived. The bottom topography and observed depth averaged velocity profile representative of the Gulf Stream over the Blake Plateau off South Carolina are shown in Figure II.1.

Let $\bar{u}$, $\bar{v}$ and $\bar{w}$ be the total velocity in the x, y and z direction respectively and u, v and w the perturbation to the equilibrium velocity. Further, let P_0 and η_0 be the equilibrium pressure and surface displacement above $z=0$ and $\bar{p}$ and $\bar{\eta}$ the total pressure and surface displacements. Then

$$\bar{u}=u,\ \bar{v}=V_0+v,\ \bar{w}=w,\ \bar{p}=P_0+p,\ \bar{\eta}=\eta_0+\eta\ ; \tag{II.1}$$

if we put (II.1) into the Navier-Stokes equations for a uniformly rotating system, and by the usual method of linear hydrodynamic stability theory we drop all products of perturbations, then a set of linear equations for the perturbations is obtained. The equilibrium state is geostrophic and hydrostatic, so that

$$fV_0 = g\frac{\partial \eta_0}{\partial x}, \tag{II.2}$$

$$p_0 = \rho g(\eta_0 - z) + p_a, \tag{II.3}$$

where p_a is the atmospheric pressure, assumed uniform.

We suppose that the shelf waves are long compared to the depth so that the vertical velocities and accelerations are all negligible. Then the vertical equation of motion implies that the total pressure is hydrostatic, so that (II.1) and (II.3) give

$$p = \rho g \eta_0. \tag{II.4}$$

Since V_0 depends only on x, (II.2) and (II.3) show that depends only on x and p_0 depends only on x and z. This, along with the long wave hypothesis, gives the following equations of motion in the x and y directions:

$$\frac{\partial u}{\partial t} + V_0\frac{\partial u}{\partial y} - fv = -g\frac{\partial \eta}{\partial x} + \frac{1}{\rho}\frac{\partial \tau^x}{\partial z}, \tag{II.5}$$

$$\frac{\partial v}{\partial t} + V_0\frac{\partial v}{\partial y} + \left(f + \frac{dV_0}{dx}\right)u = -g\frac{\partial \eta}{\partial y} + \frac{1}{\rho}\frac{\partial \tau^y}{\partial z}, \tag{II.6}$$

where $f=2\Omega\sin\phi$ (ϕ=latitude and Ω=angular velocity of the

Earth's rotation) is the Coriolis parameter, here assumed constant. All frictional effects are neglected except for the wind stress at the surface which is modeled as a body force. For a good discussion of the justification for this see Pollard (1970).

The boundary condition at the bottom, z=-h(x), is

$$w+\frac{dh}{dx}u=0 \quad , \quad at \quad z=-h(x). \tag{II.7}$$

This is just a statement of the fact that the velocity normal to the bottom is zero. The kinematic boundary condition at the free surface, $z=\eta(x,y,t)$, is

$$w=\frac{\partial\eta}{\partial t}+V_0\frac{\partial\eta}{\partial y}+u\frac{d\eta_0}{dx} \quad , \quad at \quad z=\eta(x,y,t). \tag{II.8}$$

Now integrate the continuity equation vertically using (II.7) and (II.8). If we further assume that $\bar{\eta}$<<h we get

$$\frac{\partial}{\partial x}(hu)+h\frac{\partial v}{\partial y}=-\left(\frac{\partial\eta}{\partial t}+V_0\frac{\partial\eta}{\partial y}\right). \tag{II.9}$$

Note that the assumption $\bar{\eta}$<<h is not equivalent to the linear hydrodynamic stability procedure as $\bar{\eta}$ is the total surface displacement. However, from (II.2) that

$$\eta_0 \approx \frac{f v_0 L}{g}$$

where L is a characteristic horizontal length scale. From Figure II.1 we see that $L\approx5\times10^6$ cm and $v_0\approx10^2$ cm/sec. Then

$$\eta_0 \approx 50\,cm << 10^5\,cm,$$

which concurs with the approximation $\bar{\eta} \ll h$.

Finally suppose that the right hand side of (II.9) can be ignored, i.e. the motions are horizontally non-divergent. This assumption is justified if the time scale of the motions is long compared to $L/\sqrt{gh} \approx 10$ min. Since the shelf waves have periods of the order of days this assumption is certainly justified. By ignoring the right hand side of (II.9) we are filtering out the surface gravity waves. In light of this assumption a transport stream function, $\psi(x,y,t)$, is introduced such that

$$hu = -\frac{\partial \psi}{\partial y} \quad \text{and} \quad hv = \frac{\partial \psi}{\partial x} \,. \tag{II.10}$$

Introducing (II.10) into (II.5) and (II.6) and intgrating vertically, remembering that $\bar{\eta} \ll h$, we obtain

$$\frac{1}{h}\left[\left(\frac{\partial}{\partial t} + V_0 \frac{\partial}{\partial y}\right)\frac{\partial \psi}{\partial y} + f\frac{\partial \psi}{\partial x}\right] = g\frac{\partial \eta}{\partial x} - \frac{1}{\rho h}\tau^x \,, \tag{II.11}$$

$$\frac{1}{h}\left[\left(\frac{\partial}{\partial t} + V_0 \frac{\partial}{\partial y}\right)\frac{\partial \psi}{\partial x} - \left(f + \frac{dV_0}{dx}\right)\frac{\partial \psi}{\partial y}\right] = -g\frac{\partial \eta}{\partial y} + \frac{1}{\rho h}\tau^y . \tag{II.12}$$

We have assumed that u and v are independent of z, a consequence of the long wave hypothesis.

We can eliminate η by differentiating (II.11) with respect to y and (II.12) with respect to x. Since f is independent of x and y, this gives

$$\left(\frac{\partial}{\partial t} + V_0 \frac{\partial}{\partial y}\right)\left[\frac{\partial}{\partial x}\left(\frac{1}{h}\frac{\partial \psi}{\partial x}\right) + \frac{1}{h}\frac{\partial^2 \psi}{\partial y^2}\right] - \left\{\frac{d}{dx}\left[\frac{f + dV_0/dx}{h}\right]\right\}\frac{\partial \psi}{\partial y}$$
$$= \frac{1}{\rho}\left[\frac{\partial}{\partial x}\left(\frac{1}{h}\tau^y\right) - \frac{1}{h}\frac{\partial \tau^x}{\partial y}\right] . \tag{II.13}$$

This is the equation of motion for the model that we wish to solve. This is the vorticity equation, and the term on the right hand side, essentially the curl of the wind stress, is the source of vorticity. Note that in the absence of curl in the wind stress, however, the slope of the bottom still gives a forcing term.

Before (II.13) can be solved we must specify a form for $h(x)$ and $V_0(x)$. We choose the simple form shown in Figure II.2 which is the simplest that includes all of the features of the Gulf Stream that we wish to include. One major advantage gained from using discontinuous depth and shear profiles is that they give rise to only one mode, whereas using a continuous profile results in an infinite number of modes, as in Buchwald and Adams (1968). For appropriate parameters this is an adequate model of the Gulf Stream over the Blake Plateau. For the configuration shown in Figure II.2 equation (II.3) becomes

$$\left(\frac{\partial}{\partial t} + V_0 \frac{\partial}{\partial y}\right) \nabla^2 \psi = \frac{1}{\rho}\left[\frac{\partial \tau^y}{\partial x} - \frac{\partial \tau^x}{\partial y}\right] \qquad \text{(II.14)}$$

in each of the regions marked 1, 2 and 3. The boundary condition at the coastal edge of region 1 is

$$\psi_1(0,y,t) = 0 \qquad \text{(II.15)}$$

since the coast must be a streamline. Matching conditions at x=L and x=2L are required. There the surface displacements and the mass transport perpendicular to the discontinuity must be continuous. The second of these requires that $\partial\psi/\partial y$ be continuous from (II.10), which means

$$\{\psi(x)\}_{-}^{+}=0 \quad \text{at} \quad x=L \text{ and } x=2L. \tag{II.16}$$

Here

$$\{\psi(x)\}_{-}^{+} = \psi(x+) - \psi(x-).$$

If η is continuous at x=L and x=2L then so is $\partial\eta/\partial y$. Then (II.12) gives

$$\left\{\frac{1}{h}\left[\left(\frac{\partial}{\partial t}+V_0\frac{\partial}{\partial y}\right)\frac{\partial\psi}{\partial x}-\left(f+\frac{dV_0}{dx}\right)\frac{\partial\psi}{\partial y}\right]-\frac{1}{\rho h}\tau^y\right\}_{-}^{+}=0 \quad \text{at} \quad x=L, 2L. \tag{II.17}$$

From (II.14) we see that only one initial condition is needed and it is

$$\psi(x,y,0)=0, \tag{II.18}$$

since at t=0 the perturbations are all zero. Before proceeding we non-dimensionalize the equations as follows:

$$x=Lx^*, \quad y=Ly^*, \quad t=f^{-1}t^*, \quad V_0=v_0V_0^*,$$

$$(\tau^x,\tau^y)=\tau^0(\tau^{x*},\tau^{y*}), \quad h=dh^*,$$

$$\psi=\frac{\tau_0 L}{\rho f}\psi^*, \quad (u,v)=\frac{\tau^0}{df\rho}(u^*,v^*). \tag{II.19}$$

Then equation (II.14) is written

$$\left(\frac{\partial}{\partial t} + \lambda V_0 \frac{\partial}{\partial y}\right) \nabla^2 \psi = \left(\frac{\partial \tau^y}{\partial x} - \frac{\partial \tau^x}{\partial y}\right) \qquad \text{(II.20)}$$

here $\lambda = v_0/Lf$. We have dropped the * above as we will do in the sequel and remember that the variables are now non-dimensionalized. The boundary and matching conditions are

$$\psi(0,y,t) = 0\,, \qquad \text{(II.21)}$$

$$\left\{\psi(1,y,t)\right\}_-^+ = \left\{\psi(2,y,t)\right\}_-^+ = 0, \qquad \text{(II.22)}$$

$$\left\{\frac{1}{h}\left[\left(\frac{\partial}{\partial t} + \lambda V_0 \frac{\partial}{\partial y}\right)\frac{\partial \psi}{\partial x} - \left(1 + \lambda \frac{dV_0}{dx}\right)\frac{\partial \psi}{\partial y}\right] - \frac{1}{h}\tau^y\right\}_-^+ = 0, \text{ at } x=1,2, \qquad \text{(II.23)}$$

$$|\psi(x,y,t)| < M\,, \quad x \geq 0. \qquad \text{(II.24)}$$

Now for the model in Figure II.2 we have

$$V_0(x) = \begin{cases} x & 0 \leq x \leq 1\,, \\ 2-x & 1 \leq x \leq 2\,, \\ 0 & 2 \leq x\,, \end{cases} \qquad \text{(II.25)}$$

and

$$h(x) = \begin{cases} 1 & 0 \leq x < 1\,, \\ \mu - 1 & 1 < x\,, \end{cases} \qquad \text{(II.26)}$$

where $\mu = 1 + D/d > 2$.

Section 3. The Transformed Equations

The problem stated in the last section is an initial boundary value problem for $\psi(x,y,t)$. The domain is $-\infty < y < \infty$, $0 < x < \infty$ and $0 < t < \infty$. Such a problem lends itself to transform methods, where we take a Laplace transform in time and a Fourier transform in y. After we have taken the Fourier-Laplace transform (hereafter denoted by FLT) we are left with an ordinary differential equation in x.

Define the FLT of $\psi(x,y,t)$ as

$$\bar{\Psi}(x,k,s) = \int_0^\infty e^{-st} ds \int_{-\infty}^{\infty} e^{iky} \psi(x,y,t)\, dy \tag{II.27}$$

and apply it to (II.20) and (II.23). This gives

$$(s - i\lambda V_0 k)\left(\frac{\partial^2 \Psi}{\partial y^2} - k^2 \Psi\right) = F(x,k,s) \tag{II.28}$$

$$\left\{ \frac{1}{h}(s - i\lambda V_0 k)\frac{\partial \bar{\Psi}}{\partial x} + i\left(1 + \lambda \frac{dV_0}{dx}\right)\frac{k}{h}\bar{\Psi} - \frac{1}{h}T^y \right\}_-^+ = 0 \quad \text{at } x = 1, 2 \tag{II.29}$$

where $F(x,k,s)$ is the FLT of $(\text{curl}\,\vec{\tau})\cdot k$ and $T^y(x,k,s)$ is the FLT of $\tau^y(x,y,t)$.

We denote the solution of (II.28) in region i by Ψ_i. It is possible to find particular solutions of (II.28) that satisfy

$$\Psi_{1p}(0,k,s) = \Psi_{1p}(1,k,s) = \Psi_{2p}(1,k,s) = \Psi_{2p}(2,k,s) = \Psi_{3p}(2,k,s) = 0, \tag{II.30}$$

and

$$|\Psi_{3p}(x,k,s)| < N \quad , \quad x \geq 2. \tag{II.31}$$

They are given by

$$\Psi_{1p}(x,k,s) = -\frac{1}{k \sinh k}\left[\sinh kx \int_x^1 \frac{F(\xi,k,s)\sinh[k(1-\xi)]}{[s - i\lambda k V_0(\xi)]}\,d\xi\right.$$

$$\left. + \sinh[k(1-x)] \int_0^x \frac{F(\xi,k,s)\sinh k\xi}{[s - i\lambda k V_0(\xi)]}\,d\xi \right], \tag{II.32}$$

$$\Psi_{2p}(x,k,s) = -\frac{1}{k \sinh k}\left[\sinh[k(x-1)] \int_x^2 \frac{F(\xi,k,s)\sinh[k(2-\xi)]}{[s - i\lambda k V_0(\xi)]}\,d\xi\right.$$

$$\left. + \sinh[k(2-x)] \int_1^x \frac{F(\xi,k,s)\sinh[k(\xi-1)]}{[s - i\lambda k V_0(\xi)]}\,d\xi \right], \tag{II.33}$$

$$\Psi_{3p}(x,k,s) = -\frac{\exp[-|k|(x-2)]}{sk} \int_2^x F(\xi,k,s)\sinh[k(\xi-2)]\,d\xi \tag{II.34}$$

$$- \frac{\sinh[k(x-2)]}{sk} \int_x^\infty F(\xi,k,s)\exp[-|k|(\xi-2)]\,d\xi .$$

Note that for (II.34) to satisfy (II.31) $F(x,k,s)$ must be bounded as $x \to \infty$. Now the solutions of (II.28) that are continuous at $x=1$ and $x=2$ are

$$\Psi_1(x,k,s) = A(k,s)\sinh kx + \Psi_{1p}(x,k,s) ,$$

$$\Psi_2(x,k,s) = A(k,s)\sinh kx + B(k,s)\sinh[k(x-1)] + \Psi_{2p}(x,k,s), \tag{II.35}$$

$$\Psi_3(x,k,s) = \exp[-|k|(x-2)]\left[A(k,s)\sinh 2k + B(k,s)\sinh k\right] + \Psi_{3p}(x,k,s).$$

The functions A(k,s) and B(k,s) can be found by applying the matching condtions (II.29) at x=1 and x=2. The equations thus derived are

$$A(k,s)\left\{(\mu-2)(s-i\lambda k)\cosh k + i\left[(\mu-2)+\mu\lambda\right]\sinh k\right\} - B(k,s)(s-i\lambda k)$$
$$= \frac{\mu-2}{k}T^y(1,k,s) + \frac{(s-i\lambda k)}{k}\left[\Psi_{2p_x}(1,k,s) - (\mu-1)\Psi_{1p_x}(1,k,s)\right] , \tag{II.36}$$

$$A(k,s)\left\{se^{2|k|} - i\lambda\sinh 2k\right\} + B(k,s)\left\{se^{|k|} - i\lambda\sinh k\right\}$$
$$= \frac{s}{k}\left\{\Psi_{3p_x}(2,k,s) - \Psi_{2p_x}(1,k,s)\right\} . \tag{II.37}$$

These are of the form

$$\alpha_{11}A + \alpha_{12}B = b_1 ,$$

$$\alpha_{21}A + \alpha_{22}B = b_2 ,$$

and the solutions are

$$A = (b_1\alpha_{22} - b_2\alpha_{12})/\Delta ,$$

$$B = (b_2\alpha_{11} - b_1\alpha_{21})/\Delta ,$$

where

$$\Delta(k,s) = \alpha_{11}\alpha_{22} - \alpha_{21}\alpha_{12}$$
$$= s^2\left\{\mu e^{|k|}\cosh k - 1\right\} - is\left\{\mu\lambda \sinh k \cosh k\right.$$
$$\left. + \mu\lambda e^{|k|}(k\cosh k - \sinh k) - (\mu-2)e^{|k|}\sinh k - \lambda k\right\} \tag{II.38}$$
$$+ \lambda \sinh k\left\{(\mu-2)\sinh k - \mu\lambda(k\cosh k - \sinh k)\right\}.$$

The equation

$$\Delta(k,s) = 0, \tag{II.39}$$

is the dispersion relation as defined in (I.1) with $s=i\omega$. In Figure IV.2 we plot Im{s} as a function of k for real k. Over a certain range of k the Im{s} curves coalesce so that in this range there are two complex solutions of (II.39) that form a compex conjugate pair for is. Thus there is one for which Re{s}>0 and hence the system is unstable.

Section 4. The Inversion Integral

The inversion theorems for Fourier and Laplace transforms give

$$\psi_i(x,y,t) = \frac{1}{4\pi^2 i}\int_{\gamma-i\infty}^{\gamma+i\infty} e^{st}\,ds \int_{-\infty}^{\infty} e^{-iky}\,\Psi_i(x,k,s)\,dk, \tag{II.41}$$

where the Laplace inversion path (LIP), Re{s}=γ, must be to the right of all singularities. Here we will write out these inversion integrals for the wind stress models we wish to consider.

First note that even for the simplest form of $F(x,k,s)$ the integrals in (II.32) and (II.33) are not expressible in terms of elementary functions and that Ψ_{1p} and Ψ_{2p} are multi-valued in the complex k and s planes due to the $(s-ikV_0(\xi))$ in the denominator of the integrals. Thus in order to make the problem of evaluating the inversion integrals as easy as possible let $F(x,k,s)=0$. Thus we consider only curl free wind stresses. There is still a response, as we see from (II.13), due to the discontinuity of the bottom topography. As we pointed out earlier we do not expect to get results from our calculations that can be compared directly with data due to the fact that once the unstable waves have grown to appreciable size the linear model no longer applies. Thus it makes very little sense to try to do calculations for realistic wind stresses. What our calculations should tell us is whether surface wind stresses are efficient in generating the unstable waves and what particular forms of the wind stress are most efficient. The problems involved in calculating the response for wind stress with curl have been looked at and are certainly not insurmountable. It is possible that this could be the topic of a future paper.

In the case of a curl free wind stress the coefficients $A(k,s)$ and $B(k,s)$ are of the form

$$A(k,s) = \frac{(\mu-2)\,T^y(1,k,s)\left[\,s e^{|k|} - i\lambda \sinh k\,\right]}{k\,\Delta(k,s)}\,, \tag{II.42}$$

$$B(k,s) = \frac{(\mu-2)\,T^y(1,k,s)\,[s\,e^{2|k|} - i\lambda \sinh 2k]}{k\,\Delta(k,s)} . \qquad (II.43)$$

Notice that for a curl free wind stress $T^y(x,k,s)$ is independent of x and so we have written it as $T^y(k,s)$. Then from (II.35) and (II.41) we have

$$\psi_1(x,y,t) = \frac{1}{4\pi^2 i}\int_{\gamma-i\infty}^{\gamma+i\infty} e^{st}\,ds \int_{-\infty}^{\infty} \frac{T^y(k,s)\,[s\,e^{|k|} - i\lambda \sinh k]\,\sinh kx}{k\,\Delta(k,s)}\, e^{-iky}\,dk , \qquad (II.44)$$

$$\psi_2(x,y,t) = \frac{1}{4\pi^2 i}\int_{\gamma-i\infty}^{\gamma+i\infty} e^{st}\,ds \int_{-\infty}^{\infty} \frac{T^y(k,s)\,[s\,e^{|k|(2-x)} - i\lambda \sinh k(2-x)]\,\sinh k}{k\,\Delta(k,s)}\, e^{-iky}\,dk , \qquad (II.45)$$

$$\psi_3(x,y,t) = \frac{1}{4\pi^2 i}\int_{\gamma-i\infty}^{\gamma+i\infty} e^{st}\,ds \int_{-\infty}^{\infty} \frac{T^y(k,s)\,e^{-|k|(x-2)}\,\sinh k}{k\,\Delta(k,s)}\, e^{-iky}\,dk ; \qquad (II.46)$$

notice that the integrals in (II.44)-(II.46) will appear whether or not the wind stress is curl free. Thus the results for a curl free wind stress can be considered to be a lower bound for the response to general wind stresses, unless it turns out that the response from the curl of the wind cancels the curl free response.

Finally the two forms of $T^y(k,s)$ for which explicit calculations will be done in Chapter IV are given. The first is an impulsive line source of wind stress at y=0 for which

$$\tau^y(x,y,t) = \delta(y)\,\delta(t), \tag{II.47}$$

and thus

$$T^y(k,s) = 1. \tag{II.48}$$

The response calculated for this case will represent a Green's function from which the response to any other kind of wind stress in principle can be calculated using convolution techniques. The second form of $T^y(k,s)$ is that for a moving line source of wind stress traveling with velocity V^* and having time behaviour $\exp(s^*t)$. Then

$$\tau^y(x,y,t) = \delta(y-V^*t)\,e^{s^*t}\,H(t), \tag{II.49}$$

where H(t) is the Heavyside step function. Then we have

$$T^y(k,s) = (s-s^*-ikV^*)^{-1}. \tag{II.50}$$

We could of course compute the response for this $T^y(k,s)$ using the Green's function found in the first problem, but it is easier to treat this case separately. The wind stress given in (II.49) is a more realistic representation of the wind stress acting on the Gulf Stream than the stationary one given in (II.47) and we will find some interesting results for the moving wind stress. Now we must turn to the problem of evaluating the integrals in (II.44)-(II.46), to which we devote the next chapter.

CHAPTER III - Asymptotics

Section 1. Introduction to the Method for $F(k,s)$ and $\Delta(k,s)$ Entire

In the previous chapter we have expressed the solution of the initial boundary value problem for the unstable shelf waves in terms of integrals of the form

$$\psi(y,t) = \frac{1}{4\pi^2 i}\int_{\gamma-i\infty}^{\gamma+i\infty} e^{st}\,ds \int_{-\infty}^{\infty} \frac{F(k,s)}{\Delta(k,s)}\, e^{-iky}\, dk. \qquad \text{(III.1)}$$

This chapter will be devoted to the problem of evaluating $\psi(y,t)$ asymptotically for large t and arbitrary y. It is to be expected in a system that supports unstable waves that eventually the "most unstable wave" will dominate the response. This is essentially the basic assumption behind the "simple" stability analysis described in the introduction. Here we present a method for determining the total, both stable and unstable, response of the system in order to make this rather vague statement more precise. In the next chapter we apply the method developed here to the unstable shelf wave problem.

As an introduction to the method we outline the approach for the simplest possible case, in which both $F(k,s)$ and $\Delta(k,s)$ are entire functions of k and s. In this form the results are mainly due to Briggs (1964) and Ball and Heckrotte (1968) who investigated such problems in connection with unstable waves in plasmas. In the case of stable waves similar techniques have been used by Adams (1972). In (III.1) we evaluate the k integral first. If $F(k,s)$ is entire in the complex k plane and $|F(k,s)/\Delta(k,s)| \to 0$ as $|k| \to \infty$ in the complex k plane so that Jordan's lemma holds then, for a given s, the value of the Fourier integral is determined entirely by the roots of

$$\Delta(k,s)=0 \tag{III.2}$$

in the complex k plane. We close the contour in the upper or lower k plane according as y<0 or y>0. For y>0 we have by evaluating residues

$$\psi(y,t)=\frac{1}{2\pi i}\int_{\gamma-i\infty}^{\gamma+i\infty} G(y,s)\,e^{st}\,ds\,, \tag{III.3}$$

where

$$G(y,s)=-i\sum_{n}\frac{F(k_+^{(n)},s)}{\Delta_k(k_+^{(n)},s)}\,e^{-ik_+^{(n)}y}\,, \tag{III.4}$$

for any s on the LIP such that $\Delta(k,s)$ has only simple zeroes. The sum extends over all the zeroes of $\Delta(k,s)$, $k_+^{(n)}$, that lie in the lower half k plane. A similar expression holds for y<0 with $k_+^{(n)}$ replaced by $k_-^{(n)}$, where $k_-^{(n)}$ are the zeroes of $\Delta(k,s)$ that lie in the upper half k plane. For y<0 there is no minus sign in front of the sum in (III.4).

It is necessary for causality, i.e. $\psi(y,t)=0$ for $t<0$, that G(y,s) be analytic to the right of the LIP. Thus we must investigate the singularities of G(y,s). If we let s vary the zeroes $k_+^{(n)}$ and $k_-^{(n)}$, which depend on s through (III.2), vary too. It is possible that as s varies a zero $k_+^{(n)}$ or $k_-^{(n)}$ will cross the real k axis. When this happens G(y,s) as defined by (III.4) undergoes a jump as one term on the right side of (III.4) is lost or gained. Thus the images of the real k axis under the mapping (III.2) represent branch lines of G(y,s) in the complex s plane. See Figure III.1. Thus causality requires that the LIP be to the right of all such branch lines. However, G(y,s) can be continued through these branch lines. Suppose G(y,s) is to be evaluated at s which is to the left of a branch line. Choose s_1 on the LIP with $\mathrm{Im}\{s_1\}=\mathrm{Im}\{s_0\}$. For s_1 $\Delta(k,s)$ has zeroes $k_+^{(i)}$ and $k_-^{(j)}$. We let s vary along the line $\mathrm{Im}\{s\}=\mathrm{Im}\{s_0\}$ from s_1 to s_0. As s varies at least one of the $k_+^{(i)}$ or $k_-^{(j)}$ crosses the real k axis since s_0 is to the left of a branch line. When this happens we indent the Fourier contour around the encroaching $k_+^{(i)}$ and $k_-^{(j)}$ so that it is still included or excluded when evaluating residues; see Figure III.2. Thus we define

$$G(y,s)=\frac{1}{2\pi}\int_C \frac{F(k,s)}{\Delta(k,s)}e^{-iky}\,dk\,, \tag{III.5}$$

where C is the indented Fourier contour. The G(y,s) defined in (III.5) agrees with that defined in (III.4) for s to the right of the LIP. Thus it is an analytic continuation of $G(y,s)$ as defined in (III.4), and it no longer has jumps across the branch lines. When we refer to $G(y,s)$ from now on it is to be understood as the analytic continuation defined in (III.5).

The function $G(y,s)$ still has singularities. If two zeroes $k_+^{(i)}$ and $k_-^{(j)}$ merge across the real k axis then it is no longer possible to indent the Fourier contour around either of them. In this case the s at which this merging takes place is a singularity of $G(y,s)$; see Figure III.3. We will now investigate the nature of this singularity. If two zeroes of $\Delta(k,s)$ merge at k_o for $s=s_o$ then we must have

$$\Delta_k(k_o,s_o)=0. \tag{III.6}$$

Expanding $\Delta(k,s)$ about (k_o,s_o) gives

$$\Delta(k,s)=\Delta_s^{(o)}(s-s_o)+\frac{1}{2}\Delta_{kk}^{(o)}(k-k_o)^2+\cdots \tag{III.7}$$

where $\Delta^{(o)}=(k_o,s_o)$, etc. Remember that $\Delta_k^{(o)}=0$ since k_o is a double zero of $\Delta(k,s)$. If $\Delta_s^{(o)}\neq 0$, the two leading terms in (III.7) indicate that

$$k-k_o=a_1(s-s_o)^{1/2}+a_2(s-s_o)+\cdots \tag{III.8}$$

We can find the coefficients in (III.8) by substituting in (III.7) and equating powers of $(s-s_o)^{1/2}$. The first two coefficients are

$$\left.\begin{aligned} a_1 &= -2\,\Delta_s^{(0)}/\Delta_{kk}^{(0)} \ , \\ a_2 &= -\left(\Delta_{ks}^{(0)} + \tfrac{1}{6}\, a_1^2 \Delta_{kkk}^{(0)}\right)/\Delta_{kk}^{(0)} \ , \end{aligned}\right\} \qquad \text{(III.9)}$$

Thus if we denote the two zeroes of $\Delta(k,s)$ near k_0 by k_1 and k_2 we have

$$\begin{aligned} k_1 - k_0 &= a_1(s-s_0)^{1/2} + a_2(s-s_0) + \cdots \\ k_2 - k_0 &= -a_1(s-s_0)^{1/2} + a_2(s-s_0) + \cdots \end{aligned} \qquad \text{(III.10)}$$

If k_1 and k_2 coalesce across the real k axis then only one of them gives a contribution when evaluating the integral in (III.5). Suppose that it is k_1. Then the contribution from the residue at k_1 is expanded about s_0 as

$$-i\,\frac{e^{-ik_0 y}\,F^{(0)}}{a_1\,\Delta_{kk}^{(0)}}\,(s-s_0)^{-1/2} + \cdots$$

Thus if k_1 and k_2 coalesce across the real k axis $G(y,s)$ has a $(s-s_0)^{-1/2}$ singularity at s_0. However, if k_1 and k_2 coalesce from the same side of the real k axis they both contribute to the integral in (III.5). In this case it is not hard to show that the $(s-s_0)^{\frac{n-1}{2}}$, n=0,1,2,...., terms in the expansion about s_0 all cancel, and hence that $G(y,s)$ is analytic at s_0. Thus the only singularities of $G(y,s)$ are those s's that correspond to double zeroes of $\Delta(k,s)$ that coalesce across the real k axis.

We find the asymptotic behaviour for large t of $\psi(y,t)$

by applying Laplaces method (see Carrier, et al, 1966) to the integral in (III.3). In order to apply this method we must have $|G(y,s)|\to 0$ as $|s|\to\infty$ so that Jordan's lemma applies. If

$$\left|\frac{F(k_\pm^{(n)},s)}{\Delta_k(k_\pm^{(n)},s)}\right| \longrightarrow 0 \quad \text{as} \quad |s|\to\infty$$

we can insure that Jordan's lemma holds by taking the limit as $y\to 0$. Then the first term of the asymptotic expansion for $\psi(y,t)$ at $y=0$ is

$$\psi(0,t) \approx -i\frac{1}{\sqrt{\pi t}} \sum \frac{e^{s_0 t}F^{(0)}}{a_1 \Delta_{kk}^{(0)}} , \qquad \text{(III.11)}$$

where the sum extends over all double zeroes of $\Delta(k,s)$, (k_0,s_0), at which k_1 and k_2 coalesce across the k axis. Note that we choose a_1 in (III.11) so that k_1 approaches the real k axis from below. Note that if one of the saddle points (k_0,s_0) has $Re\{s_0\}>0$ then the system is absolutely unstable. This is because there is exponential growth in time in a neighborhood of the origin.

Notice that (III.6) implies that k_0 is a saddle point of the function $s(k)$ defined implicitly by (III.2), i.e. k satisfies

$$S'(k_0)=0. \qquad \text{(III.12)}$$

For this reason we call the k_0's saddle points and the k_0's for which k_1 and k_2 coalesce across the real k axis pinching saddle points. Sometimes we will also refer to the pair

(k_0, s_0) as a saddle point. This nomenclature points out the relationship between the method given here and the method of steepest descent as described in the introduction. In fact the above result can be derived directly from the method of steepest descent. Recall that to use the method of steepest descent the Laplace integral is evaluated first, and then an asymptotic representation of the Fourier integral is obtained by deforming the path of integration into a steepest descent path. If a saddle point is of the pinching type, then the endpoints of the path of integration, $\pm\infty$, lie in different valleys (Sirovich, 1971), and the path of steepest descent must go through the saddle point. On the other hand, if the saddle point is not of the pinching type one of the endpoints lies in a valley, and the other lies on a hill; see Figure III.4.

So far we are limited to finding the asymptotic behaviour of (III.1) at y=0. However, we can get around this limitation in the following way. Let $y=Vt+y_0$ and make the change of variable in (III.1)

$$\left.\begin{aligned} \tilde{s} &= s - ikV \\ k &= k. \end{aligned}\right\} \qquad \text{(III.13)}$$

Then (III.1) becomes

$$\psi(Vt+y_0,t) = \frac{1}{4\pi^2 i}\int_{\gamma-i\infty}^{\gamma+i\infty} e^{\tilde{s}t}\,d\tilde{s}\int_{-\infty}^{\infty}\frac{e^{-iky_0}\tilde{F}(k,\tilde{s})}{\tilde{\Delta}(k,\tilde{s})}\,dk\,, \qquad \text{(III.14)}$$

where

$$\left.\begin{aligned}\tilde{\Delta}(k,\tilde{s}) &= \Delta(k,\tilde{s}+ikV),\\ \tilde{F}(k,\tilde{s}) &= F(k,\tilde{s}+ikV).\end{aligned}\right\} \qquad \text{(III.15)}$$

Then we proceed with (III.14) the same way we did with (III.1). For each V we find the saddle points for $\tilde{\Delta}(k,\tilde{s})$ and determine which of them are of the pinching type. Then we form the sum as in (III.11) with $y_0 \to 0$ for the pinching saddle points. In this way we can find the asymptotic behaviour for any value of y. Note that saddle points are those points at which

$$\tilde{\Delta}_k(k,\tilde{s}) = 0. \qquad \text{(III.16)}$$

But by (III.15) this is equivalent to

$$V = i\frac{\Delta_k}{\Delta_s} = -i\frac{ds}{dk}. \qquad \text{(III.17)}$$

In words this says that an observer moving with velocity V sees a wave with wavenumber k_0 and frequency $-is_0$ that has group velocity V. This is as we expected. Recall the definition of group velocity in (I.3). However, not all such waves are observed but only those that correspond to a pinching saddle point.

The general procedure for determining the asymptotic behaviour of (III.1) for large t in the case considered here is the following. For each V determine the saddle points for $\Delta(k,\tilde{s})$. For a system that supports unstable and/or decaying waves this is not necessarily straight forward. The methods used to solve this problem are discussed in section 5. Then we must determine which of the saddle points are of the pinching type. This is not as bad as it sounds, as there are intervals for V in which the saddle points are pinching and outside of which they are not. There are criteria that can be used to find the endpoints of these intervals, called transition velocities. Finally, for each V the asymptotic behaviour is given as a sum in the form of (III.11).

The case considered here, in which $\Delta(k,s)$ and $F(k,s)$ are entire functions, unfortunately does not cover the problem of unstable shelf waves as can be seen from (II.44)-(II.46). In this case both $F(k,s)$ and $\Delta(k,s)$ have branch points at k=0 due to the presence of $|k|$. This is the problem we investigate in the next section.

Section 2. Extension to $\Delta(k,s)$ and $F(k,s)$ with Branch Points

As pointed out above we must now consider the case in which $\Delta(k,s)$ and/or $F(k,s)$ have branch points at k=0. We will find that the results are the same as before. The results given here are due to Derfler (1970) and were developed to study the growth of instabilities in hot plasmas.

We start with equation (III.3) where now we define

$$G(y,s) = \frac{1}{2\pi}\int_{-\infty}^{\infty} e^{-iky}\,\frac{F(k,s)}{\Delta(k,s)}\,dk. \tag{III.18}$$

Since the branch point at k=0 is due to the presence of $|k|$ in both $F(k,s)$ and $\Delta(k,s)$ we split the integral in (III.18) at k=0. Making the change of variables $k=-k$ in the integral over $(-\infty,0)$, we have

$$G(y,s) = \frac{1}{2\pi}\int_0^{\infty} e^{-iky}\,\frac{F_+(k,s)}{\Delta_+(k,s)}\,dk + \frac{1}{2\pi}\int_0^{\infty} e^{iky}\,\frac{F_-(k,s)}{\Delta_-(k,s)}\,dk, \tag{III.19}$$

$$= G_+(y,s) \qquad + \qquad G_-(y,s)$$

The function $\Delta_+(k,s)$ is the same as $\Delta(k,s)$ with $|k|$ replaced by k, and $\Delta_-(k,s)$ is the same as $\Delta(-k,s)$ with $|k|$ replaced by k. Similarly for $F_+(k,s)$ and $F_-(k,s)$. Now Δ_+, Δ_-, F_+ and F_- are all entire functions. Now expand in partial fractions[1]

$$\begin{aligned}\frac{F_+(k,s)}{\Delta_+(k,s)} &= \sum_n \frac{F_+(k_+^{(n)},s)}{\Delta_{+k}(k_+^{(n)},s)}\,\frac{1}{k-k_+^{(n)}},\\ \frac{F_-(k,s)}{\Delta_-(k,s)} &= \sum_n \frac{F_-(k_-^{(n)},s)}{\Delta_-(k_-^{(n)},s)}\,\frac{1}{k-k_-^{(n)}}\end{aligned} \tag{III.20}$$

---

[1] We can do this if we can find a sequence of contours C_m on which F_+/Δ_+ (or F_-/Δ_-) is bounded such that R_m=closest distance of C_m to the origin becomes infinite as $m\to\infty$, since F_+/Δ_+ and F_-/Δ_- are analytic except at the zeroes of Δ_+ and Δ_-.

where $k_+^{(n)}$ and $k_-^{(n)}$ are the roots of

$$\Delta_+(k,s)=0 \quad \text{and} \quad \Delta_-(k,s)=0, \tag{III.21}$$

respectively, and the sum extends over all such roots.

Thus for $G_+(y,s)$ we have

$$G_+(y,s) = \frac{1}{2\pi} \sum_n \frac{F_+(k_+^{(n)},s)}{\Delta_{+k}(k_+^{(n)},s)} \int_0^\infty \frac{e^{-iky}}{k-k_+^{(n)}}\, dk. \tag{III.22}$$

Note that

$$\int_0^\infty \frac{e^{-iky}}{k-k_+^{(n)}}\, dk = \Psi(1,1;-ik_+^{(n)}y) \tag{III.23}$$

where $\Psi(1,1;z)$ is the confluent hypergeometric function of the second kind with

$$\Psi(1,1;z) = e^{-z}\ln(cz) + \sum_{n=1}^{\infty}\left(1+\frac{1}{2}+\cdots+\frac{1}{n}\right)\frac{z^n}{n!} \quad) \tag{III.24}$$

and $c=e^{\gamma}$ (γ=.5772... is Euler's constant). See Erdelyi, et al (1953) equations 6.5(12) and 6.7.1(13). The function $\Psi(1,1;-ik_+^{(n)}y)$ is a multi-valued function, and as defined in (III.23) is discontinuous along the images in the s-plane of the positive real k axis under the mapping in (III.21). Thus these image curves are branch curves of G (y,s) as defined in (III.22). Again continue G (y,s) through the branch lines by indenting the Fourier contour around any encroaching $k_+^{(n)}$; see Figure III.3. In this way we define an analytic continuation of $G_+(y,s)$ as defined in (III.22) that is not discontinuous across the branch lines. This analytic continuation is defined as in (III.22) with the path of integration in the integrals replaced by the indented paths C_n. We have

$$\int_{C_n} \frac{e^{-iky}}{k-k_+^{(n)}}\,dk = \Psi(1,1;-ik_+^{(n)}y) - 2\pi i\, e^{-ik_+^{(n)}y} \qquad \text{(III.25)}$$

if $k_+^{(n)}$ crosses the postive real k axis from the lower half plane into the upper half plane as s varies along lines Im{s}=constant from right to left; see Figure III.3.

Again $G_+(y,s)$ still has singularities even after the analytic continuation has been carreid out. The singularities are now the saddle points k_o of $\Delta_+(k,s)$ that pinch the <u>positive</u> real k axis. Near k_o there are two solutions k_1 and k_2 of (III.21), just as in (III.10). If only one of k_1 and k_2 cross the positive real k axis then only one term in (III.22) will have the extra term as in (III.25). In this case $G_+(y,s)$ has a $(s-s_o)^{-1/2}$ singularity just as before and the leading term in the asymptotic expansion is as given in (III.11). If k_1 and k_2 both cross the positive real k axis or neither do then we can show that all of the irrational terms in the expansion of $G(y,s)$ about s_o cancel and thus that $G_+(y,s)$ is analytic at $s=s_o$. Notice that there is no problem with a logarithmic singularity at $s=s_o$ unless k =0. This point will be taken up later.

Exactly the same arguments as above apply in considering the contribution from $G_-(y,s)$. Thus the first term in the asymptotic expansion for (III.1) in the case considered here is

$$\psi(0,t) \approx -i\frac{1}{\sqrt{\pi t}}\left[\sum \frac{e^{s_{+0}t}F_+^{(0)}}{a_{+1}\Delta_{+kk}^{(0)}} + \sum \frac{e^{s_{-0}t}F_-^{(0)}}{a_{-1}\Delta_{-kk}^{(0)}}\right]. \tag{III.26}$$

Now the sums extend over the saddle points of Δ_+ and Δ_- that pinch the <u>postive</u> real k axis. We extend the results to non-zero y just as we did in section 1.

Section 3. <u>Transition Velocities</u>

In the last two sections we have found asymptotic expressions for the integral in (III.1) for large t and arbitrary y. In order to evaluate these expressions it is necessary to find the saddle points of $\Delta(k,s)$ that pinch the (postive) real k axis for each value of V. This seems to be a rather formidable task. First we must find the saddle points for each V, then for each saddle point we must find the images of $Im\{s\}=Im\{s_0\}$ to determine if the two zeroes of $\Delta(k,s)$ near k_0 coalesce from opposite sides of the (positive) real k axis. Even given an efficient method of solving $\Delta(k,s)=0$ this could be very time consuming. In this section we introduce a method for streamlining this process. The results given here are due mainly to Hall and Heckrotte

(1968).

As V varies the saddle point $k_o(V)$ also varies. For some interval I, $k_o(V)$ is of the pinching type if $V \in I$ and is not of the pinching type if $V \notin I$. We call the endpoints of any such interval transitions velocities. Notice that all the intervals I must be bounded since otherwise there would be an infinite propagation velocity. There are three fairly simple criteria for determining when a given velocity is a transition velocity. They are:

C1) If, as $V \to V_\infty$, there is a $k_o(V)$ such that $|k_o(V)| \to \infty$, then V_∞ is a transition velocity.

C2) If at $V=V_M$ there is a $k_o(V)$ such that

$$\tilde{\Delta}^{(0)}_{kk} = 0, \tag{III.27}$$

then V_M is a transition velocity. Note that in general this is equivalent to solving the system of equations

$$\left.\begin{aligned} &\tilde{\Delta}(k,\hat{s}) = 0, \\ &\tilde{\Delta}_k(k,\hat{s}) = 0, \\ &\tilde{\Delta}_{kk}(k,\hat{s}) = 0, \end{aligned}\right\} \tag{III.28}$$

which is a set of six real equations ($\tilde{\Delta}$ is a complex valued function) in the five real unknowns k_i, k_r, s_i, s_r and V. Here $k=k_r+ik_i$ and $s=s_r+is_i$. Thus in general there will not be any solutions. However, when there are stable, non-decaying waves, i.e. when there is an interval J such that k real and

$k \in J$ implies that any root of $\Delta(k,s)=0$ is imaginary, then V found from

$$\tilde{\Delta}_k(k,\hat{s}) = \Delta_k(k,\hat{s}+ikV)+iV\Delta_s(k,\hat{s}+ikV)=0 \qquad \text{(III.29)}$$

is automatically real. This is because (III.29) gives

$$V = i\,\frac{\Delta_k(k,\hat{s}+ikV)}{\Delta_s(k,\hat{s}+ikV)} = -i\,\frac{ds}{dk}$$

which is real. Thus the system (III.28) is a set of three equations in three unknowns when the waves are stable and non-decaying. In this case V_M is a maximum or minimum value for V as (III.27) requires that when $V=V_M$

$$\frac{dV}{dk} = 0.$$

Then the point $y=V_M t$ is the leading or trailing edge of the wave.

C3) If for $V=V_I$, there are two saddle points $(k_o^{(a)},\tilde{s}_o^{(a)})$ and $(k_o^{(b)},\tilde{s}_o^{(b)})$ such that $\mathrm{Im}\{\tilde{s}_o^{(a)}\}=\mathrm{Im}\{\tilde{s}_o^{(b)}\}$, then V_I is a transition velocity, Figure III.5 illustrates the interaction of the two saddle points that takes place here. For $V<V_I$, say, both the saddle points A and B contribute with branch I coming from the upper half plane and branch II going into the lower half plane, see Figure III.5(a). For $V=V_I$ the two saddle points "interact" and branch I and II coalesce. See Figure III.5(b). The curve $\mathrm{Im}\{\tilde{s}\}=\mathrm{Im}\{\tilde{s}_o\}$ goes

through B first then A since B lies to the right of A in the complex s plane. For $V>V_I$ only B contributes and now branch I comes in from the lower half plane and branch II goes into the upper half plane, see Figure III.5(c). The branches I and II have exchanged positions. Note that it is only the saddle point with the smaller Re{s} that can be lost in this way. Note also that this criterion only makes sense in a system that supports unstable or decaying waves so that all of the saddle points do not lie along the imaginary s axis.

The procedure then for determining the asymptotic development for (III.1) is to find the saddle points for each V and then use the criteria above to find the transition veocities. Then it is necessary only to check one velocity in each interval to see if the saddle points are pinching or not in the whole interval. Note that we must check both sides of the transition velocities since the criteria above are not sufficient conditions to insure a transition.

Section 4. Moving Disturbances

In sections 1 and 2 we have assumed that F(k,s) has no poles. This corresponds to finding the response to a stationary disturbance that is finite in time and space. Now we extend the results given above to the case in which F(k,s) has a simple pole which is due to a moving and/or oscillating disturbance. Lighthill (1967) has considered the problem of moving disturbances in stable systems and Briggs (1964) has touched on the problem of oscillating disturbances in unstable systems. However, no one has worked out the details of the response of an unstable system to moving oscillating disturbances.

As we see from (II.50) a disturbance moving with velocity V^* and with time dependence $\exp(s^*t)$ gives rise to an integral of the form

$$\psi(Vt+y_0,t) = \frac{1}{4\pi^2 i}\int_{\gamma-i\infty}^{\gamma+i\infty} e^{\tilde{s}t}\,d\tilde{s}\int_{-\infty}^{\infty}\frac{\tilde{F}(k,\tilde{s})\;e^{-iky_0}}{[\tilde{s}-s^*-ik(V^*-V)]\,\tilde{\Delta}(k,\tilde{s})}\,dk. \qquad \text{(III.30)}$$

We know from our previous results that the asymptotic behaviour of (III.30) is governed by the pinching saddle points of the denominator. These are of two types here: 1) the saddle points of $\Delta(k,s)$; and 2) the points $(k_0,\tilde{s}_0)$ such that

$$\left.\begin{aligned} &\tilde{s}_0 - s^* - i k_0 (V^* - V) = 0\,, \\ &\tilde{\Delta}(k_0,\tilde{s}_0) = 0\,. \end{aligned}\right\} \qquad \text{(III.31)}$$

We have already treated the saddle points of $\Delta(k,s)$ in sections 1 and 2, and we need only replace $\tilde{F}(k,\tilde{s})$ by $F(k,s)/[\tilde{s}-s^*-ik(V^*-V)]$ in (III.11). We call this the transient response, ψ_T. Note that if (III.31) is satisfied at a saddle point then this is unbounded. Special consideration can be given to such points but the details are not given here.

We now determine the response due to the points given by (III.31), which we will call the forced response, ψ_F. Given an s near s_0 there are two k's, k_1 and k_2, near k_0 that contribute to the Fourier integral in (III.30). These are given by

$$k_1 - k_0 = -\frac{i}{v^* - v}(\tilde{s} - \tilde{s}_0) \tag{III.32}$$

and

$$k_2 - k_0 = a_1(\tilde{s} - \tilde{s}_0) + a_2(\tilde{s} - \tilde{s}_0)^2 + \cdots . \tag{III.33}$$

We assume here that $\Delta_k(k_0, \tilde{s}_0) \neq 0$, i.e. k_0 is not a saddle point for $\tilde{\Delta}(k, \tilde{s})$, as we mentioned above. From the arguments in section 1 and 2 we know that if k_1 and k_2 coalesce across the (postive) real k axis, then s_0 is singularity of

$$G(y_0, \tilde{s}) = \frac{1}{2\pi} \int_{-\infty}^{\infty} \frac{\tilde{F}(k, \tilde{s})\, e^{-iky}}{[\tilde{s} - s^* - ik(v^* - v)]\, \tilde{\Delta}(k, \tilde{s})}\, dk. \tag{III.34}$$

We must investigate this singularity.

The contribution to G(y,s) from k_1, assuming that y>0 so that we close below and that Im{ k_1 }<0, is

$$\frac{\exp(-ik_1 y_0)\, \tilde{F}(k, \tilde{s})}{(v^* - v)\, \tilde{\Delta}(k, \tilde{s})}$$

and from k_2, under the same assumptions, is

$$\frac{-i \exp(-ik_2 y_0)\, \tilde{F}(k_2, \tilde{s})}{[\tilde{s} - s^* - ik_2(v^* - v)]\, \tilde{\Delta}_k(k_2, \tilde{s})}$$

Now

$$\tilde{\Delta}(k_1,\tilde{s}) = \frac{(V^*-V_0)}{(V^*-V)}\ \Delta_s^{(0)}(s-s_0)$$

where $V = i\Delta_k^{(0)}/\Delta_s^{(0)}$ is the group velccity cf (k_0, s_0). Also

$$[\tilde{s}-s^*-ik_2(V^*-V)] = \frac{V_0-V^*}{(V_0-V)}(s-s_0)+\cdots,$$

since $a_1=-i/(V_0-V)$. Now

$$\tilde{\Delta}_k(k_2,\tilde{s}) = -i\ \Delta_s^{(0)}(V_0-V)$$

so that

$$[\tilde{s}-s^*-ik(V^*-V)]\,\tilde{\Delta}_k(k_2,\tilde{s}) = -i\ \Delta_s^{(0)}(V_0-V^*)(s-s_0)+\cdots.$$

Therefore, the contributions from k_1 and k_2 are expanded abcut s_0 as

$$\frac{\exp(-ik_0y_0)F^{(0)}}{(V^*-V_0)\ \Delta_s^{(0)}}\ \frac{1}{(s-s_0)}+\cdots,$$

and

$$\frac{\exp(-ik_0y_0)F^{(0)}}{(V_0-V^*)\ \Delta_s^{(0)}}\ \frac{1}{(s-s_0)}+\cdots,$$

respectively. The rest of the terms in the expansicn are analytic at s_0. Thus we see that if k_1 and k_2 approach the real k axis from the same side, then the singular terms cancel. On the other hand if they appraoch from cppcsite sides only one contributes and there is no cancelaticn. Note that we have assumed here that $V^*>V$ so that k_1

approaches the real k axis form the lower half plane. If $V^* < V$ then the signs must be reversed. If $F(k,s)$ and/or $\Delta(k,s)$ have branch points as considered in section 2 then the results are extended as they were there.

The results given above show that the leading term in the asymptotic expansion of the forced response is given by

$$\psi_F(Vt,t) \approx \operatorname{sgn}(V^*-V) \sum \frac{F^{(0)} e^{s_0 t}}{(V^*-V^{(0)})\Delta_s^{(0)}} , \qquad \text{(III.35)}$$

where the sum extends over all solutions of (III.31) that are of the pinching type. The total response is $\psi_T + \psi_F$. The criteria given in section 3 can be applied here to determine the transition velocities. Note that $V=V^*$ is a transition velocity since from (III.32) as V^*-V changes sign so does the direction that k_1 moves as s moves toward s_0 from the right. A transition by C2 comes about when the solution of (III.31) is a saddle point. When C3 is applied some rather interesting results arise. This will be pursued further in Chapter IV.

Section 5. Numerical Methods

As we have seen the problem of determining the asymptotic behaviour of the integral in (III.1) reduces to the problem of finding the solutions (k_0, s_0) of

$$\tilde{\Delta}(k,\tilde{s}) = 0 \qquad \text{(III.36)}$$

$$\tilde{\Delta}_k(k,\tilde{s})=0, \tag{III.37}$$

where $\tilde{\Delta}(k,s)$ is defined in (III.15). This system is equivalent to the system

$$\Delta(k,s)=0, \tag{III.36'}$$

$$\Delta_k(k,s)+iV\Delta_s(k,s)=0. \tag{III.37'}$$

After we have solved either of these systems for a given V we must map the lines $\mathrm{Im}\{s\}=\mathrm{Im}\{s_o\}$ into the complex k plane by (III.36) in order to determine whether (k_o, s_o) is a pinching saddle point. This requires that we be able to solve (III.36) for k as afunction of s.

In finding the response to a moving disturbance we are led to the problem of evaluating the aymptotic behavicur of the integral in (III.30). This problem reduces to that of solving (III.36) and (III.37) again and the system (III.31). Solving (III.31) is equivalent to solving the single equation

$$\Delta(k,s^*+ikV^*)=0. \tag{III.38}$$

This equation needs only be solved once for a given s^* and V^*. Call the solution k_1. However, we still need to map the lines $\mathrm{Im}\{\tilde{s}\}=\mathrm{Im}\{s^*+ik_1(V^*-V)\}$ for each V in order tc determine the pinching behaviour of the solutions of

(III.31).

The basic method that we use to solve (III.36') and (III.37') is Newton's method for a system of equations. We make an initial guess, (k_1, s_1), for the solution of the system. Then we calculate a new guess, (k_2, s_2), by

$$k_2 - k_1 = \frac{\Delta_s^{(1)}(\Delta_k^{(1)} + iV\Delta_s^{(1)}) - \Delta^{(1)}(\Delta_{kk}^{(1)} + iV\Delta_{ks}^{(1)})}{\Delta_s^{(1)}\Delta_{kk}^{(1)} + \Delta_{ks}^{(1)}(iV\Delta_s^{(1)} - \Delta_k^{(1)}) - iV\Delta_{ss}^{(1)}\Delta_k^{(1)}},$$

$$s_2 - s_1 = \frac{\Delta^{(1)}(\Delta_{ks}^{(1)} + iV\Delta_{ss}^{(1)}) - \Delta_k^{(1)}(\Delta_k^{(1)} + iV\Delta_s^{(1)})}{\Delta_s^{(1)}\Delta_{kk}^{(1)} + \Delta_{ks}^{(1)}(iV\Delta_s^{(1)} - \Delta_k^{(1)}) - iV\Delta_{ss}^{(1)}\Delta_k^{(1)}}. \qquad \text{(III.39)}$$

These expressions are obtained by expanding (III.36') and (III.37') about the unknown point to first order. Then we assume that (k_2, s_2) is indeed a solution of the system. This leads to a linear set of equations for (k_2, s_2) whose solution is given in (III.39). Continue in this way to generate a sequence of (k, s) pairs. This sequence will converge if the initial guess was close enough to the solution of the system. Once we have solved this system for one value of V we can use this solution as an initial guess for a slightly different V. In this way we can generate all of the branches of $(k_0(V), s_0(V))$ given by (III.36') and (III.37'). All we need is a first guess for each of the branches. These are obtained by solving (III.36') for s_0 with k_0 given, say, and then computing the V_0 for which (III.37') is satisfied. Then (k_0, s_0) can be used as an initial guess for a V close to V_0. If k_0 is in the range of instability, i.e. $s_\circ$ complex, then $V_\circ$ may be complex. In that case the first step is to use (III.39) to find the solution for V with Re{V}=Re{$V_\circ$} and Im{V}=0.

After we have found $(k_\circ(V), s_\circ(V))$ as described above we must apply the criteria given in section 3 to find the transition velocities. To apply C1 and C3 is straight forward. For C1 we just plot Re{$k_\circ(V)$} and Im{$k_\circ(V)$} and look for vertical asymptotes. For C3 we plot Im{$s_\circ(V)$} for each branch. Points of intersection of two branches are transition velocities. For C2 we must finds points where (III.27) is satisfied. Note that this requires no extra computation since when (III.36') and (III.37') are satisfied then the denominators in (III.39) are just

$$\Delta_s^{(0)}\hat{\Delta}_{kk}^{(0)} = \Delta_s^{(0)}(\Delta_{kk}^{(0)} + 2iV\Delta_{ks}^{(0)} - V^2\Delta_{ss}^{(0)}).$$

Thus we can compute $\hat{\Delta}_{kk}^{(0)}$ as we compute $(k_\circ(V), s_\circ(V))$ at no extra expense and thus applying C2 is also easy.

Finally we must determine the pinching behaviour of the saddle points $(k_\circ(V), s_\circ(V))$ on either side of the transition velocities. This requires that we solve (III.36) for k as a function of $\tilde{s}_1$ near a double zero. Newton's method applied to the single equation (III.36) converges slowly, if at all, at such points and even if it does converge deflation must be used to find both solutions. A method due to Delves and Lyness (1967) can be used to solve this problem.

We use the following theorem from the theory of complex variables. If f(z) is analytic in a closed bounded region of the z-plane and has zeroes z_i, i=1,...,n inside C-∂C then

$$S_r = \frac{1}{2\pi i}\int_{\partial C} z^r \frac{f'(z)}{f(z)}\, dz = \sum_{i=1}^{n} z_i^r . \qquad \text{(III.40)}$$

A multiple zero is counted according to its multiplicity in this formula which is just a consequence of Cauchy's theorem. For r=0 the value of the integral in (III.40) is just the number, n, of zeroes within C. Using the s_r for r=1,...,n it is possible to construct a polynomial of degree n that has the same zeroes as the function f(z) inside C by means of the so-called Newton relations. There are powerful techniques for solving polynomials numerically so we can consider the problem solved when we find the polynomial. Anyway, in the problem we are considering we are interested only in cases where there are only two or three zeroes in the region of interest.

In order to determine the pinching behaviour of a saddle point (k_o, s_o) we map the lines Im{s}=Im{s_o} into the complex k plane by (III.36). We choose an s on this line near s_o and apply the above method to find the two k's close to k_o by letting

$$f(k) = \tilde{\Delta}(k, \tilde{s})$$

in (III.40). We choose C to be a small circle around k .

The contour integral in (III.40) is computed numerically. The rapid convergence of numerical contour integrations is discussed by Lyness and Delves (1967) in a companion paper to their one on root finding. Once we have found the two k's near k_o we can use Newton's method on the single equation (III.36) to trace the lines $Im\{s\}=Im\{s_o\}$ away from the saddle point.

Finally we note that in order to solve (III.38) we can use the method of Delves and Lyness.

CHAPTER IV - Discussion and Results

Section 1. Introduction

In NM it is suggested that the unstable shelf waves studied there might be the origin of the meanders in the Gulf Stream and in particular that a fast moving disturbance might be most efficient in generating the unstable waves. We are now in a position to make a first step in checking this hypothesis. In NM two models are considered, one that is applicable to the region in which the Gulf Stream flows over the Blake Plateau and one that is applicable to the region northeast of Cape Hatteras after the Gulf Stream has detached from the continental shelf. Here we consider the first model, which has been described in Chapter II.

Of course, our linear model is not applicable to large amplitude waves and cannot be expected to test the hypothesis in NM in any detail. For example, it would be unrealistic to compute the detailed response of our model to complicated, though realistic, wind stresses and expect the calculated response to resemble the actual behaviour of the Gulf Stream. Hence we have restricted ourselves to considering the simple curl free wind stress models described in section 4 of Chapter II. Using these models alone it is possible, for example, to determine how the efficiency of the generation of the unstable waves varies with the speed and duration of the disturbance.

In order to apply the methods of Chapter III to obtain these results we must first study the dispersion relation. This we do in section 2. In section 3 we calculate the response for an impulsive line source of wind stress, mainly in order to gain experience in using the methods without the additional complications introduced by moving disturbances. In section 4 we turn our attention to the moving distutbance problem.

Section 2. The Dispersion Relation

The actual bottom topography and depth averaged current profile of the Gulf Stream over the Blake Plateau are shown in Figure II.1. The best fit to this by the model shown in Figure II.2 is given by

$\lambda = .22$ and $\mu = 2.8$

with $D = 800$m, $L = 50$km and $f = 10^{-4}\mathrm{sec}^{-1}$. We now study the dispersion relation

$$\Delta(k,s) = 0 \tag{IV.1}$$

where $\Delta(k,s)$ is given in (II.38), for these values of λ and μ.

Before we proceed we note that $\Delta(k,s)$ is of the form studied in section 2 of Chapter III and thus we must consider the two functions

$$\left.\begin{aligned} \Delta_+(k,s) &= s^2 f(k) - isg(k) + h(k), \\ \Delta_-(k,s) &= s^2 f(k) + isg(k) + h(k). \end{aligned}\right\} \qquad \text{(IV.2)}$$

From (III.38) we see that f, g and h are real when k is real and that

$$f(\bar{k}) = \overline{f(k)}, \quad g(\bar{k}) = \overline{g(k)}, \quad h(\bar{k}) = \overline{h(k)}, \qquad \text{(IV.3)}$$

where $\bar{\ }$ denotes the complex conjugate. This allows us to write

$$\Delta_-(k,s) = \overline{\Delta_+(\bar{k},\bar{s})}.$$

From (II.44)-(II.46) we see that $F_+(k,s)$ and $F_-(k,s)$ also satisfy this relation. Thus we have

$$G_-(y,s) = G_+(y,\bar{s})$$

so that

$$\frac{1}{2\pi i}\int_{\gamma-i\infty}^{\gamma+i\infty} G_-(y,s)e^{st}ds = \overline{\left[\frac{1}{2\pi i}\int_{\gamma-i\infty}^{\gamma+i\infty} G_+(y,s)\, e^{st}\, ds\right]}$$

and the total response is just given by

$$2\,\mathrm{Re}\left\{\frac{1}{2\pi i}\int_{\gamma-i\infty}^{\gamma+i\infty} G_+(y,s)\,e^{st}ds\right\}.$$

Hence in the following we consider only $\Delta_+(k,s)$ which here we write as $\Delta(k,s)$.

As we see from the results of Chapter III it is first necessary to solve (IV.1) for s with k taking real values. This gives the branch lines of G(Y,S) in the complex s-plane. Since $\Delta(k,s)$ is quadratic in s this is nct hard to do and the results are given in Figure IV.1 where we plot $\mathrm{Im}\{s\}$ for k real. For most real values of k there are two pure imaginary solutions of (IV.1). However, in a small interval the solutions are complex with solutions s and $-\bar{s}$. This is the "interval of instability" since one of the solutions has positive real part.

Next for each V we must find the saddle points (k_0,s_0) that are solutions of the system (III.36') and (III.37'). Outside of the interval of instability this is straight foward and we do not need the methods described in section III.5. By (IV.2) and (IV.3) we have that

$$i\,\frac{\Delta_k(k,s)}{\Delta_s(k,s)} = i\,\frac{s^2 f'(k) - isg'(k) + h'(k)}{2sf(k) - ig(k)}$$

is real when k is real and s is pure imaginary. Thus when we solve (IV.1) for s_0 with k_0 real and outside the interval of instability, the point (k_0,s_0) is a saddle point for

$$V_0 = i\Delta_k^{(0)}/\Delta_s^{(0)}\ .$$

Then graphically we can invert and get k_0 as a function of V_0. Within the interval of instability we must use Newton's method as described in section III.5. As a starting point we use the real k_0 at which $\mathrm{Re}\{s_0\}$ is a maximum. At this point $V_0 = i\Delta_k^{(0)}/\Delta_s^{(0)}$ is real.[1] In Figure IV.2 we have plotted Re{k} as a function of V for the stable saddle points. In Figure IV.3 we have plotted Re{k}, Im{k}, Re{s} and Im{s} as a function of V for the unstable saddle points.

The saddle points found in this way are the only ones that can be of the pinching type. This is because if any other saddle points are found for some real V they cannot be of the pinching type since neither of the paths of steepest descent through k_0 can have crossed the real k axis.

Once we have found all of the saddle points that can be of the pinching type we must determine which of these really are pinching saddle points. A glance at Figure IV.2 shows us that there certainly must be transition velocities, since otherwise we would have signals traveling at arbitrarily large velocities. This physical criterion is a good check on the mathematical results that we obtain. In order to find the transition velocities we apply the criterion given in section III.3. Recall that we do not expect C2 to apply in the interval of instability and that C3 can only apply there as it requires two saddle points with different Re{s}.

From Figure IV.3(a) we see that by C1 the unstable

---

[1] This is because $ds/dk = -\Delta_k/\Delta_s$ and when Re{s} is a maximum dRe{s}/dk=0. Thus $\mathrm{Im}\{i\Delta_k/\Delta_s\}=0$.

waves only contribute over a finite interval with endpoints given by[2]

$$V=0 \quad \text{and} \quad V=.2195.$$

Thus the system is convectively unstable. We will refer to this interval as the (velocity) interval of instability (dropping the velocity when no confusion will arise). In Figure IV.2 we have marked the points where transitions take place by C2 and C3 by the number of the criterion used to find it. To find transitions by C2 we need only find the maxima and minima in the graph of V as a function of real k. In this way we find a transition at

$$V=.219572,$$

labeled A in Figure IV.2. To find the transitions given by C3 we must plot Im{s} for all the branches of $(k_o(V),s_o(V))$ in the interval of instability and any points of intersection of these curves will be transition velocities. In Figure IV.3(d) we have plotted Im{s} for the unstable saddle points, branch C, and Im{s} for the two sets of stable saddle points, branches A and B. There are two points of intersection at

$$V=.0047 \quad \text{and} \quad V=.2056$$

---

[2] All of the velocities are given in dimensional units in which the velocity of the stream is $\lambda=.22=77$km/day, since in dimensional units $s/k=Lfs^*/k^* \Rightarrow s^*/k^*=\lambda \Rightarrow s/k=v_o$.

labeled B and C respectively in Figure IV.2. In Figure IV.4 we show how the transition takes place for one of these transition velocities. Finally, since we are dealing with $\Delta_+(k,s)$ only a saddle point that arises from a merging across the negative real k axis does not contribute. Thus from Figure IV.2 we see that D and E are also transition points with

$V = .22$ and $V = -.444\cdots$,

respectively. At these velocities $(k_0, s_0) = (0,0)$, a situation that requires special treatment. At these points we see from Figure IV.1 that $(k_0, s_0) = (0,0)$, and from (III.22) or (III.24) it seems that this introduces a logarithmic singularity which would give rise to a response for all V. However, a detailed expansion of G(y,s) about s=0 indicates that the singular terms cancel out so that the two velocities given above are indeed transition velocities. The expansions are quite messy and have not been worked out completely so are not given here.

When we check which intervals contain pinching saddle points we find that besides the interval of instability the sections AF, BD and EC in Figure IV.2 contain pinching saddle points. All of the rest are non-pinching saddle points. This is as we should expect since otherwise infinite signal velocities would have resulted.

One very interesting consequence of the above results is that no wave traveling in the downstream direction travels faster that the maximum speed of the basic flow. Also, waves traveling upstream can travel twice as fast as those going downstream. However, the unstable waves only travel downstream. From Figure IV.3(c), where we have plotted Re{s} as a function of V, we see that the fastest growing wave travels at a speed $V \approx \lambda/2 = .11$. The e-folding time of the fastest growing wave is about 81.3 in dimensionless units or about 9.4 days.

Section 3. Response to a Stationary Disturbance

Here we present the results of calculations made using the above results for the impulsively applied stationary line source of wind stress given in (II.47). This is now straight forward using the results given in Chapter III.

In Figure IV.5 we plot $\psi(1,y,100)$ and $\psi(1,y,200)$ as found using the asymptotic solution given in Chapter III. This corresponds to a snapshot of the response response taken at times t=100 and t=200, i.e. 16 and 32 days after the wind stress was applied, at the center of the stream. The important fact to notice here is that the unstable waves are certainly not dominant. At t=200 the most unstable wave has propagated 1100km, the length of the region in which the model is applicable. This result seems to indicate that the instability is convected out of the system before it grows to significant proportions. Note that no wave travels faster than about .22, so that beyond this point no waves appear. That is why in this and the following figures the curves are cut off at a point corresponding to $V \approx .22$. Actually there should be a smooth exponential decay to zero as shown by an Airy phase analysis, but this was not done here.

However, in Figure IV.6 we plot $\psi(x,4,200)$ for $0 \le x \le 2$, and we see that the response at $x=2$, the offshore edge of the steeam, is much larger than the response at $x=1$, the point of maximum velocity. The profile is similar at all points along the stream. In Figure IV.7 we plot $\psi(2,y,100)$ and $\psi(2,y,200)$, and we see that not only is the response larger than at $x=1$, but also it has a different form. Here the unstable waves are completely dominant. Thus we see that the stationary curl free wind stress generates the unstable waves much more efficiently on the offshore side of the stream than on the inshore side. If we look at (II.44) and (II.45) along with Figures IV.3(a), (c) and (d) the reason for this is clear. In the interval of instability $\mathrm{Im}\{s\} \approx \lambda/2 = .11$, $\mathrm{Re}\{s\} \approx .01$ and $\mathrm{Re}\{k\} \approx 3$. Thus here $\sinh k \approx .5\exp(k)$ so that the integrand in (II.44) is only of order $\mathrm{Re}\{s\} \approx .01$ while the integrand in (II.45) is of order $\mathrm{Im}\{s\} \approx .11$. This argument in fact shows that the "free waves" have this behaviour so that we can expect that for all wind stresses the unstable waves will be generated most effeciently on the offshore side of the stream.

In Figure IV.8 we plot $\psi(x,20,t)$ as a function of t for (a), x=1, and (b), x=2, for $100 \le t \le 350$. Here the difference in the behaviour between x=1 and x=2 is again apparent. Note that when computing $\psi(x,y,t)$ as a function of t for a fixed value of y it is s and not $\tilde{s}$ that determines the response. This is because the exponent in the asymptotic formula is

$$\tilde{s}t=(s-ikV)t=st-iky,$$

and y is a constant.

Finally we estimate the current velocities generated in this case. We are mainly interested in the cross stream velocity, u, as this will tell us how far we can expect the stream to be displaced due to the wave motions. By (II.10) we must find the long shore derivative of ψ in order to find u. From Figure IV.7 we estimate u for x=2 and t=200 at the position of the fastest growing wave to be about 1 km/day for a 1 dyne/cm² wind stress. Since for the fastest growing wave $Im\{s\} \approx .11$ the period is approximately 6.7 days. Hence u as estimated above would result in displacements of about 4 km, which is small compared to the observed Gulf Stream meanders.

Section 4. Moving Disturbances

Now we present results for the moving line source of wind stress as given in (II.49). To calculate the transient response, ψ_T, we proceed exactly as we did for the stationary wind stress except we replace $\tilde{F}(k,\tilde{s})$ by $\tilde{F}(k,\tilde{s})/[\tilde{s}-s^* - ik(V^* - V)]$. To calculate the forced response, ψ_F, it is necessary to solve (III.38) for the values of F and s that are of interest. It is found by solving (III.38) for various values of s^* imaginary and V^* that only real values of k arise. Thus moving and/or oscillating disturbances do not force the unstable waves directly, i.e. through ψ_F. Also, as will be seen later a time decaying disturbance, $Re\{s\}<0$, only gives rise to a time decaying ψ_F.

To begin we will consider the problem in the case for which $s^*=0$. Then since there are no complex solutions of (III.38), solving it is equivalent to finding the intersections of the curves in Figure IV.1 with the line $Im\{s\}=ikV^*$, i.e. we find the wave that has phase velocity V^*. Note that we can also treat the case of s^* pure imaginary this way too. When stated this way the problem is fairly simple. Note first that k=0 is always a solution of (III.38) for $s^*=0$. Again we note that this gives rise to a logarithmic singularity. In this case, with a moving disturbance with no exponential time behaviour, the logarithmic singularity can give rise to a small additicnal response in a finite velccity interval. Again this result is based on a detailed expansion of $G(y,s)$ about $s=0$ in which it is seen that the singular terms cancel outside of certain finite velocity intervals. Next note that for $-.44<V^*<0$ there is only one non-zero solution and that for $0<V^*<.22$ there are always twc non-zero sloutions. Otherwise, $k=0$ is the only solution.

After we have fcund k_o for a given V^* from (III.38) we must determine over what range of V the point (k_o,s_o) obtained from (III.31) is cf the pinching type. First we know that V^* is a transition velocity. Next when $V=V_o$, the group velocity at k_o, the point $(k_o,\tilde{s}_o)$ is a saddle point of $\Delta(k,\tilde{s}+ikV_o)$. If this saddle point is of the pinching type then we have a situation as shown in Figure IV.9. As V goes through V_o, the point $(k_o,\tilde{s}_o)$ changes from pinching to non-pinching. Thus in this case $V=V_o$ is atransition velocity. However, if the saddle point at $(k_o,\tilde{s}_o)$ is not of the pinching type, then we see from Figure IV.10 that $V=V_o$ is not a transition velccity. There must be another transition velocity, since otherwise we would have infinite signal velocities. Note that the criterion that $V=V_o$ is a transition velocity is equivalent to C2 as given in section III.3, since at (k_o,s_o)

$$\left\{\left[\tilde{s}-ik(V^*-V)\right]\tilde{\Delta}(k,\tilde{s})\right\}_{kk}=0$$

when $V=V_o$.

What about C3? Consider the situation in Figure IV.11. Here we have $(k_0, \tilde{s}_0)$ interacting with a saddle point $(k_1, \tilde{s}_1)$ for which $\mathrm{Im}\{\tilde{s}_0\}=\mathrm{Im}\{\tilde{s}_1\}$, at $V=V_I$. As V goes through V_I the point $(k_0, \tilde{s}_0)$ changes from pinching to non-pinching when $\mathrm{Re}\{\tilde{s}_1\}>\mathrm{Re}\{\tilde{s}_0\}$. Otherwise there is no transition at V_I (just change the direction of the arrows through the saddle point k_0 in Figure IV.11). Thus if V_0 is not a transition velocity we should be able to find a transition velocity, V_I, by C3. We see that for the forced response the group velocity of the excited wave is not necessarily the signal velocity.

We now apply the above remarks to the problem of finding the response for particular moving disturbances. First we consider a slow downstream moving disturbance with $V^*=.03$. We choose this value for V^* as it illustrates the remarks above about C3 and as it happens is one of the most efficient disturbance velocities for generating the unstable waves. Solving (III.38) for $V^*=.03$ gives two solutions with

$k_0 = 3.67 \quad , \quad V_0 = -.00038$

$k_0 = 2.61 \quad , \quad V_0 = .254.$

From Figure IV.1 we see that the saddle points for these group velocities are non-pinching. Thus we must apply C3. Again we recall that C3 only applies in the interval of instablility. Hence if we plot

$\mathrm{Im}\{\tilde{s}\} = k_0(V^*-V)$

as a function of V for each of the k_0's above along with

Im{s} for the unstable waves in the interval of instabliity, the points of intersection will be transition velocities. In this way we find transition velocities at

$V = .00082$ for $k_0 = 3.67$

$V = .182$ for $k_0 = 2.61$

Thus for the forced response we have the following situation: for $V<.00081663$ and $V>.1815881$ only the transient response is observed, for $.00081663<V<.03$ the forced response has wavenumber $k_0=3.67$ and for $.03<V<.1815881$ it has wavenumber $k_0=2.61$.

In Figure IV.12 we plot $\psi(x,y,100)$ and $\psi(x,y,200)$ for $V=.03$. In (a) and (b) we plot ψ_T and ψ_F, respectively, for $x=2$. We see that behind the disturbance the transient and forced responses are of about the same magnitude. However, in front of the disturbance the transient response dominates since here the unstable waves are important. In (c) and (d) we plot ψ_T and ψ_F, respectively, for $x=1$. Here we see that though the response is still much smaller than at $x=2$ the unstable waves are now dominant, as they were not in the case of the stationary disturbance. This is because the phase speed, $-is/k$, of the unstable waves is very close (in the compex plane) to the velocity of the disturbance so that $(s-ikV)^{-1}$ is very large in the asymptotic formula. Thus the unstable waves are amplified. A comparison of Figures IV.12 (a) and IV.7 shows that the amplification factor is about 40. Hence we see that a slow downstream moving disturbance is very efficient at generating the unstable waves. In fact we find that the maximun amplification is produced by a disturbance moving with $V^*=.03902$.

In contrast to the last example we now consider a fast upstream moving disturbance with $V^*=-.1$. In this case there is only one solution to (III.38) with

$k_0 = 1.45 \quad , V_0 = .141$.

Since the saddle point for this V_0 is a pinching one V_0 is a transition velocity. Thus for $-.1<V<.141$ there is a forced response with wavenumber $k=1.45$ and outside this interval there is only the transient response. In Figure IV.13 we plot $\psi_T(2,y,100)$ and $\psi_T(2,y,200)$. We ignore the forced response since, as in the last example, it is small compared to the transient response in the region of wave growth. Here we see that although the unstable waves are amplified, the amplification is only about one-fifth that in the previous case. The discontinuities in the plots of $\psi_T(x,y,t)$ occur at $V=V_0$ which, as was pointed out in Chapter III, is a point at which the asymptotic formulas do not apply. We will see below that introducing damping into the wind stress removes the discontinuities.

Now we consider the above examples in the case that the disturbances are decaying in time with $s^*=-.06$. This corresponds to an e-folding time of about two days which is a reasonable time scale for weather systems. Now when solving (III.38) both the k_o's and V_o's obtained are complex, so that now in both cases the transition velocities must be found using C3. The k_o's, V_o's and transition velocities for $V^*=.03$ are now

$$k_o=3.67-i2.0 \quad \text{and} \quad V_o=-.98\times10^{-4}+i(.65\times10^{-4}) \quad \text{with} \quad V_I=.205$$

$$k_o=2.64+i(.32) \quad \text{and} \quad V_o=.209+i(.0085) \quad \text{with} \quad V_I=.001$$

and for $V^*=-.1$ are

$$k_o=1.45+i(.025) \quad \text{and} \quad V_o=.141+i(.0037) \quad \text{with} \quad V_I=.137.$$

It is important to note that the transition velocities are such that $\mathrm{Re}\{s^*+ik(V^*-V)\}<0$ for all V's for which there is a forced response. In Figure IV.14 we show $\psi_T(2,y,t)$ and $\psi_F(2,y,t)$ for $V^*=.03$ in this case. We see that here the amplification of the unstable waves is not as great as with the non-decaying disturbance since the transient response is only about one-half of what it is in that case. The forced response now decays from the transition velocity. Hence we can see the significance of the transition velocity as the signal velocity. In Figure IV.15 we plot $\psi_T(x,y,t)$ for $V^*=-.1$. We see that in this case the decay of the disturbance has no effect on the transient response, other than smoothing out the discontinuities. Again the forced response is significant only near the transition velocity, and even here it is completely negligible.

Section 5. Discussion

In this section we will discuss the application of the results presented above to the problem of meanders in the Gulf Stream. As has been pointed out in NM the wavelength of the unstable waves is about 140 km and the pericd abcut 10 days, which corresponds well to the wave-like characteristics of the meanders in the Gulf Stream (see Hansen, 1970). Thus it is reasonable to consider the wind generation problem.

All of the results given above indicate that the unstable waves are generated on the off shore side of the velocity maximum by any kind of wind, since the curl free component studied here would contribute in any case. The displacements of the stream that can be expected to result from these waves can be estimated from estimates of the cross stream velocity by multiplying the maximum cross stream velocity by one-half the period of the waves. This was done above for the staticnary wind strss. For the wind stress moving with $V^*=.03$ (10 km/day) the response calculated is about 40 times that for the stationary disturbance and thus so are the displacements. The displacements for the upstream moving disturbance with $V^*=-.1$ are about 8 times those for the stationary disturbance. Thus displacements of the order of 150 km can be accounted for as unstable waves generated by moving disturbances.

A result that could be important to the expermimental problem of observing unstable shelf waves propagating along the Gulf Stream is contained in the results given above. The method used for detecting shelf waves has been to analyse tide gauge records taken along the coast. Non-barometric responses are attributed to shelf waves propagating along the coast (see Mysak and Hamon, 1969). Our results indicate that the unstable waves have small amplitudes on the inshore side of the stream, and that in some cases they are of about the same amplitude as the stable waves. Thus it is questionable that the unstable waves could be observed in this way.

Note that though our results have been derived for curl free wind stresses it is expected that the results for wind stress with curl would agree at least qualitatively because of the structure of the "free waves". Before considering the problem of more realistic wind stresses it would be more important to try to look at a more realistic model. For example we have completely ignored the stratification and vertical shear in the stream. Finally, though, we point out again that the methods developed here apply only for linear models that cannot hope to cope accurately with finite amplitude phenomena such as the meanders in the Gulf Stream.

CHAPTER V - Conclusion

In Part A of this thesis we have studied the problem of the generation of unstable shelf waves by the wind in a barotropic model that could apply to the Gulf Stream over the Blake Plateau. This was done in order to test the hypothesis that the meanders observed in the Gulf Stream might originate as unstable shelf waves that extract energy from the lateral shear of the stream and are generated by the wind. The propagation of such waves was studied in NM where it was found that the unstable shelf waves have properties similar to the wavelike properties of the meanders. Here we have studied the generation of these waves in order to find under what conditions the wind generates them most efficiently.

In order to solve this problem we solved the initial boundary value problem for the response of the model to an applied wind stress by means of Fourier-Laplace transforms. This leads us to the problem of evaluating the asymptotic behaviour for large t of Fourier-Laplace inversion integrals for systems that support unstable waves. This problem has been worked out by plasma physicists studying the interaction of plasmas with electron streams for the case of stationary forcing functions. An observer moving at velocity V will see the wave $\exp(s_o - ik_o y)$ if (k_o, s_o) is a double zero of $\Delta(k,s+ikv)$ ($\Delta(k,s)=0$ is the dispersion relation), such that the steepest descent paths through k approach k_o from opposite sides of the (positive) real k axis. Such a k_o is called a pinching saddle point. Criteria can be found to determine transition velocities at which saddle points change from pinching to non-pinching.

These results are easily extended to the problem of determining the asymptotic response for a moving forcing function. The response is the sum of two terms, the forced response and the transient response. The transient response is determined exactly as the response for a stationary forcing function. The forced response is a wave whose phase velocity, $-is/k$, is the same as the velocity of the forcing function. It appears only in a finite range of velocities the endpoints of which may or may not be the group velocity of the forced wave.

We have applied the above techniques to the problem of the generation of unstable shelf waves by the wind for simple curl free wind stresses. The results indicate that moving wind systems can be very efficient in generating the unstable waves. A slow downstream moving system is the most efficient at generating the unstable waves, though its efficiency is affected quite considerably by the duration of the disturbance. A fast upstream moving wind system is less efficient at generating the unstable waves, but the efficiency here is almost completely independent of the duration of the disturbance. It is found in general for the curl free wind stresses that the unstable waves are much larger on the offshore edge of the stream than anywhere else. The results described above could be useful in interpreting Gulf Stream meander data since now we can obtain a relationship between the velocity and time scale of a weather system, and its efficiency at generating the unstable waves.

In solving the problem of the generation of the unstable shelf waves by the wind we have made many simplifying assumptions. The stratification and vertical shear in the Gulf Stream have been ignored. The model studied is linear so that it cannot describe the finite amplitude meanders accurately. The wind stresses that we have considered are curl free when almost all wind systems in the real world have non-zero curl. However, we have solved the problem we set out to do which was to go beyond the stability analysis that is usually done and to determine how much faith can be put in their results. Our results indicate that care should be exercised in applying general stability analysis to geophysical systems and that if possible it should be augmented by at least determining whether the system is convectively or absolutely unstable. Further as we have seen it is possible for the instability to be of importance only in a part of the system. Besides this we have obtained results that can possibly be of use in interpreting meander data.

The work presented here shows how methods developed in one field can be used profitably in another. We have solved a problem in geophysical fluid dynamics, not attempted before, by methods developed in plasma physics. This work at least indicates a direction that instability studies of more realistic models in geophysical fluid dynamics could take, since the methods gathered together here are sufficiently general that they could be applied to a large class of such models. Further, the results are of interest in themselves as they indicate that certain wind systems, in particular those moving slowly in the direction of the stream, are very efficient at generating the unstable waves, at least on the offshore side of the stream.

FIGURES FOR PART A

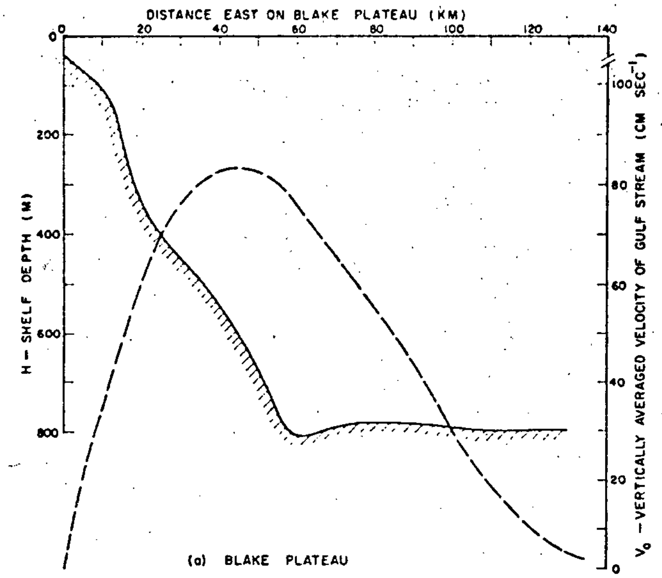

FIGURE II.1

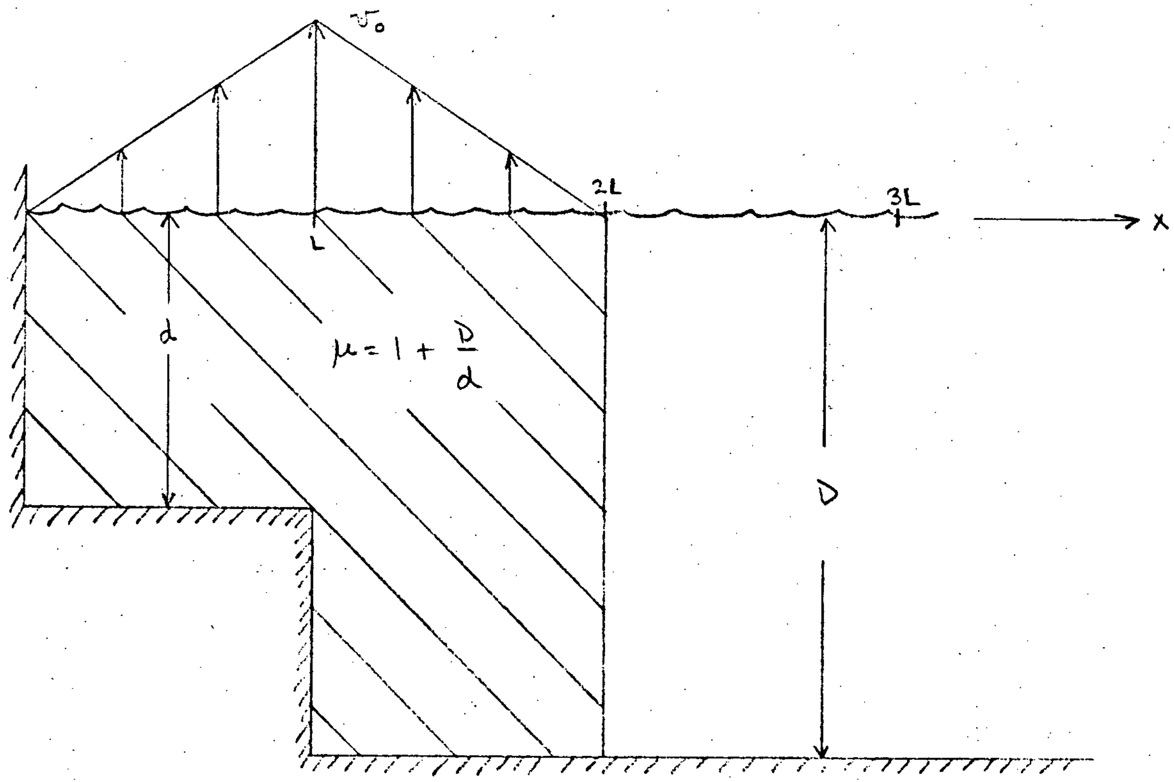

FIGURE II.2

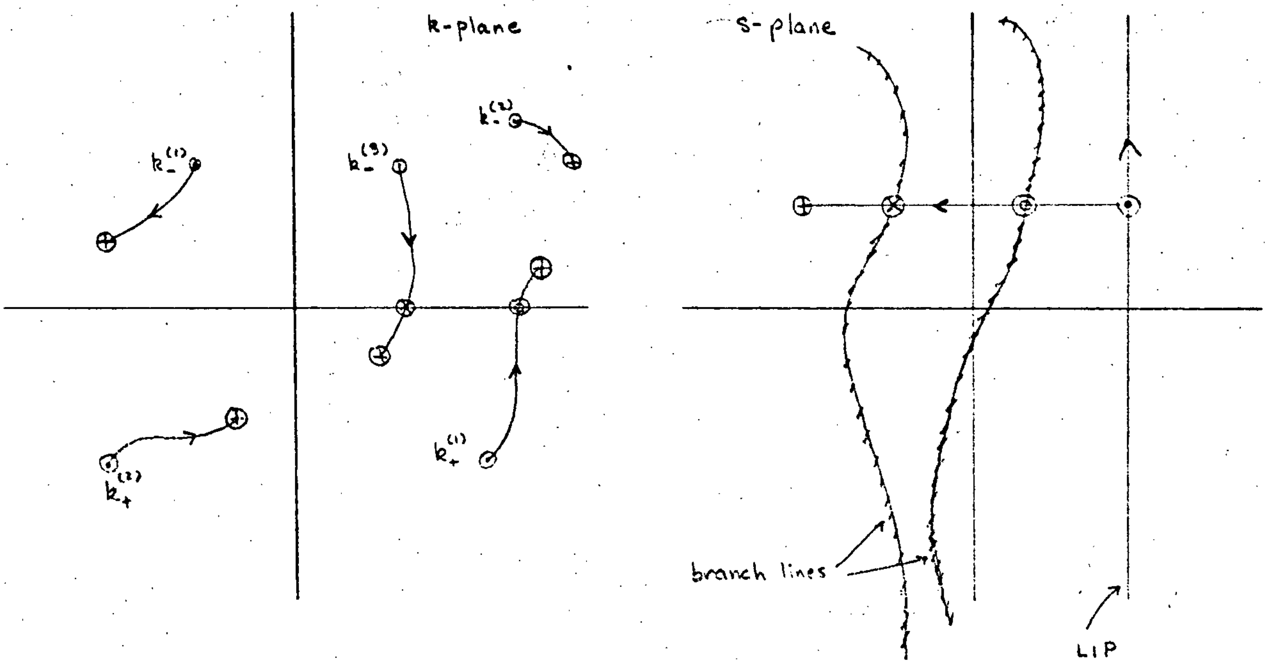

FIGURE III.1

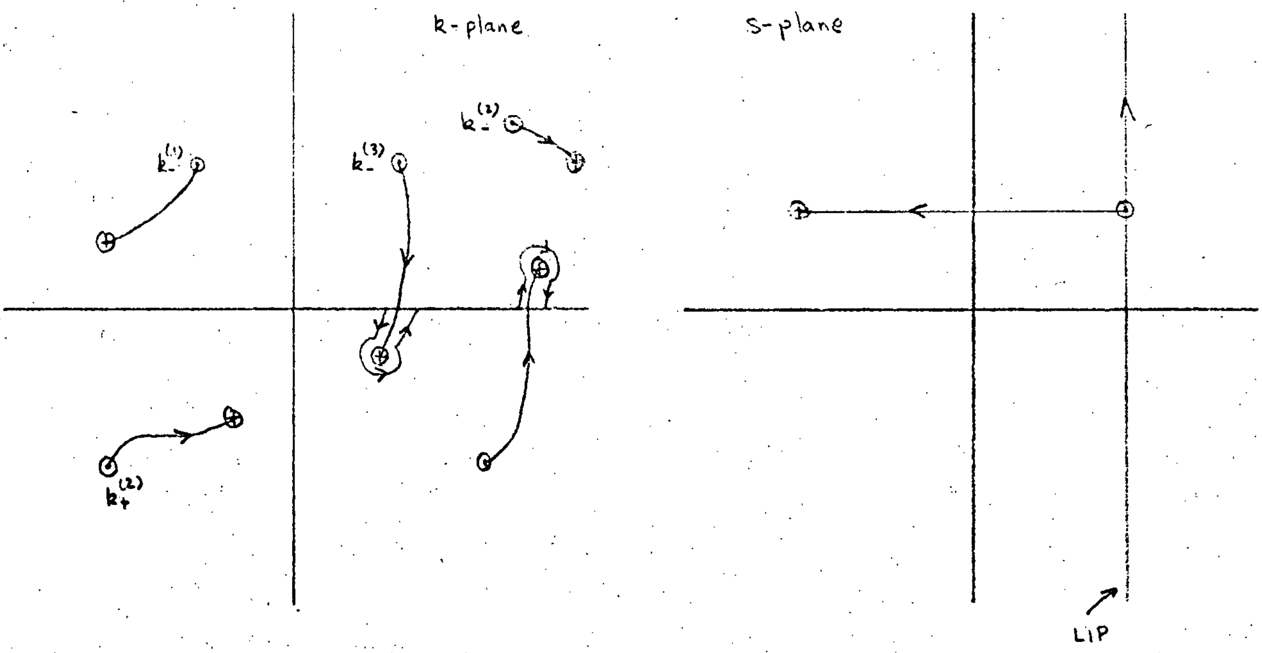

FIGURE III.2

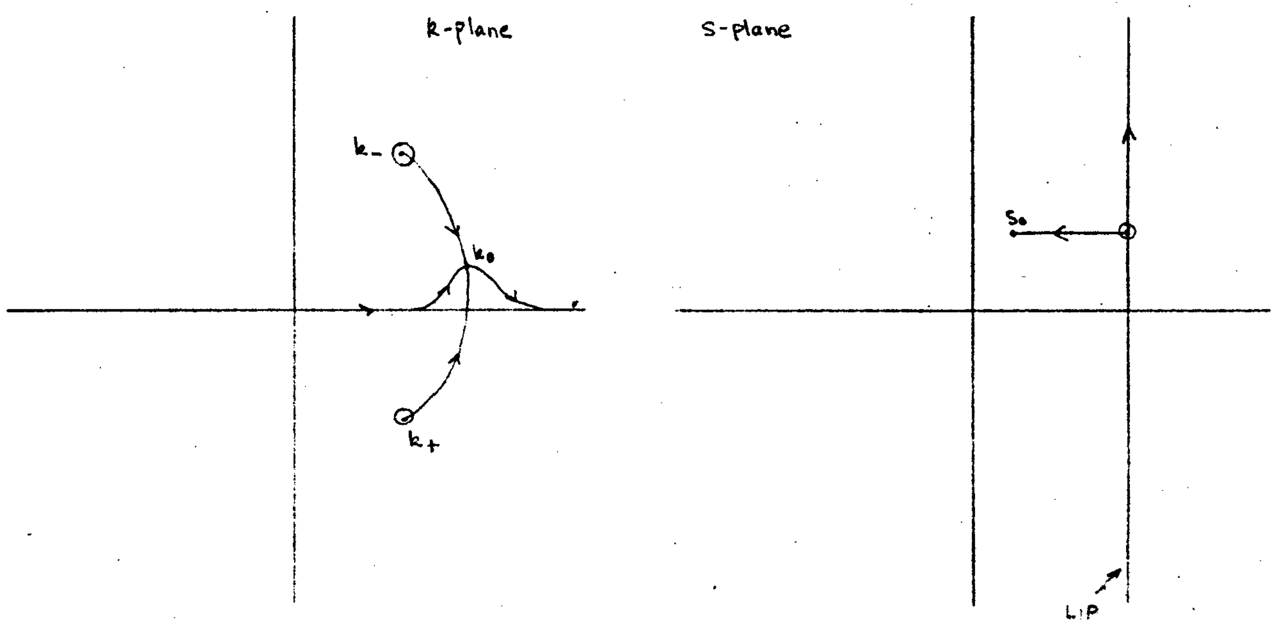

FIGURE III.3

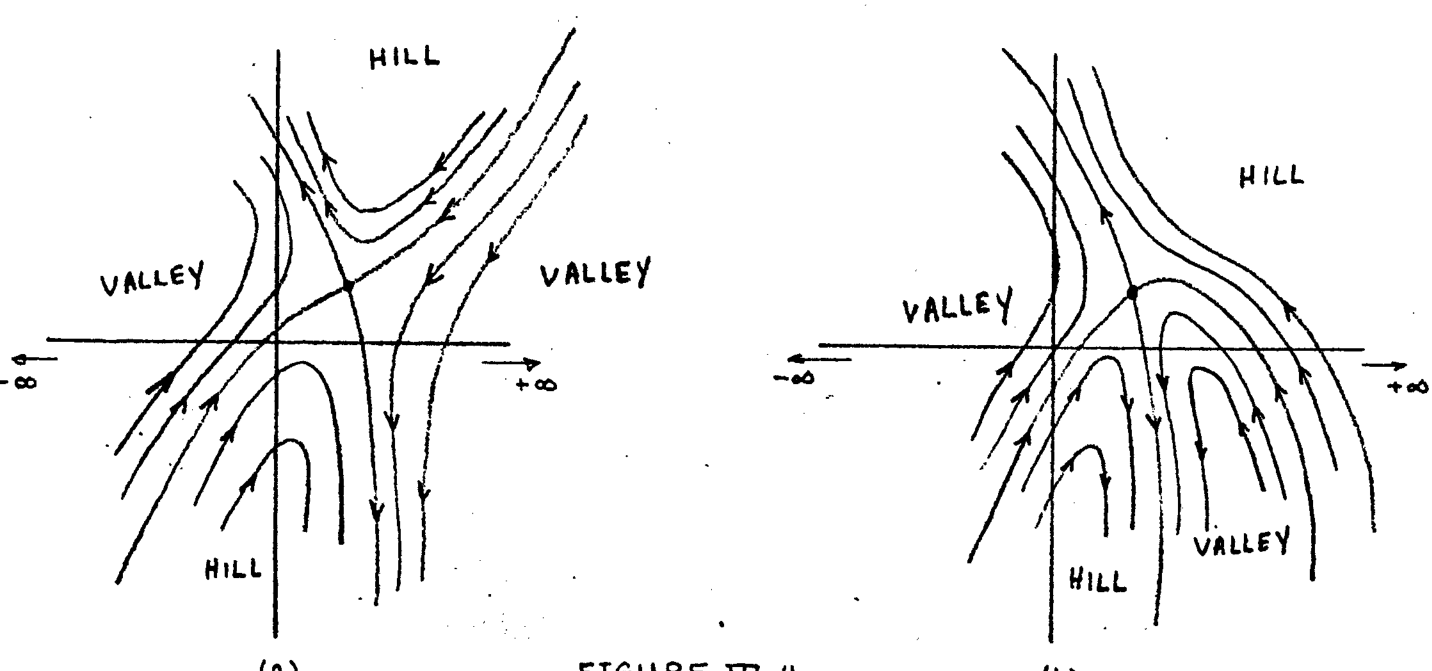

FIGURE III.4

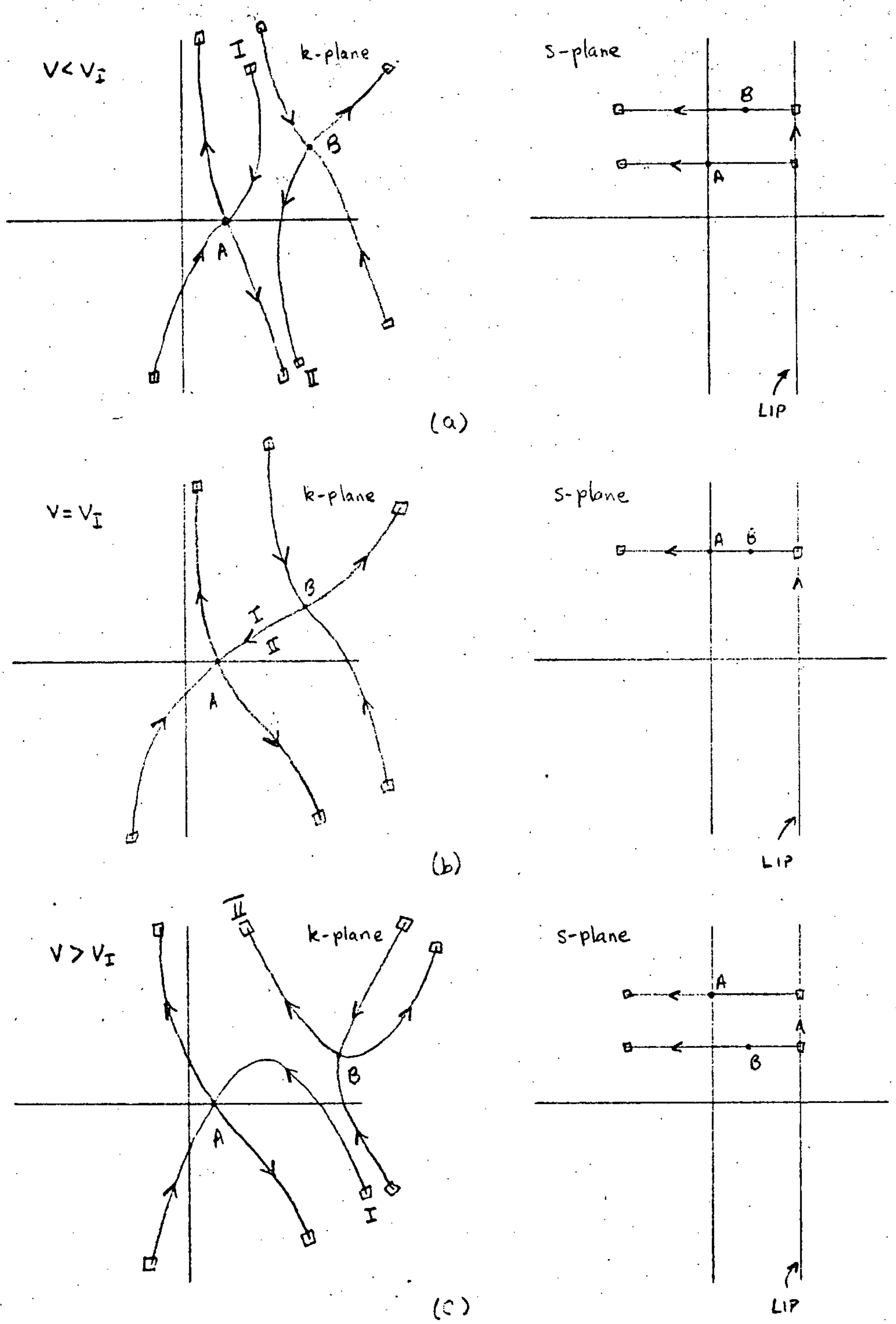
V< V_I
k-plane
I
II
A
B
s-plane
LIP
(a)
V=V_I
k-plane
I
II
A
B
s-plane
LIP
(b)
V>V_I
k-plane
II
I
A
B
s-plane
LIP
(c)

FIGURE III.5

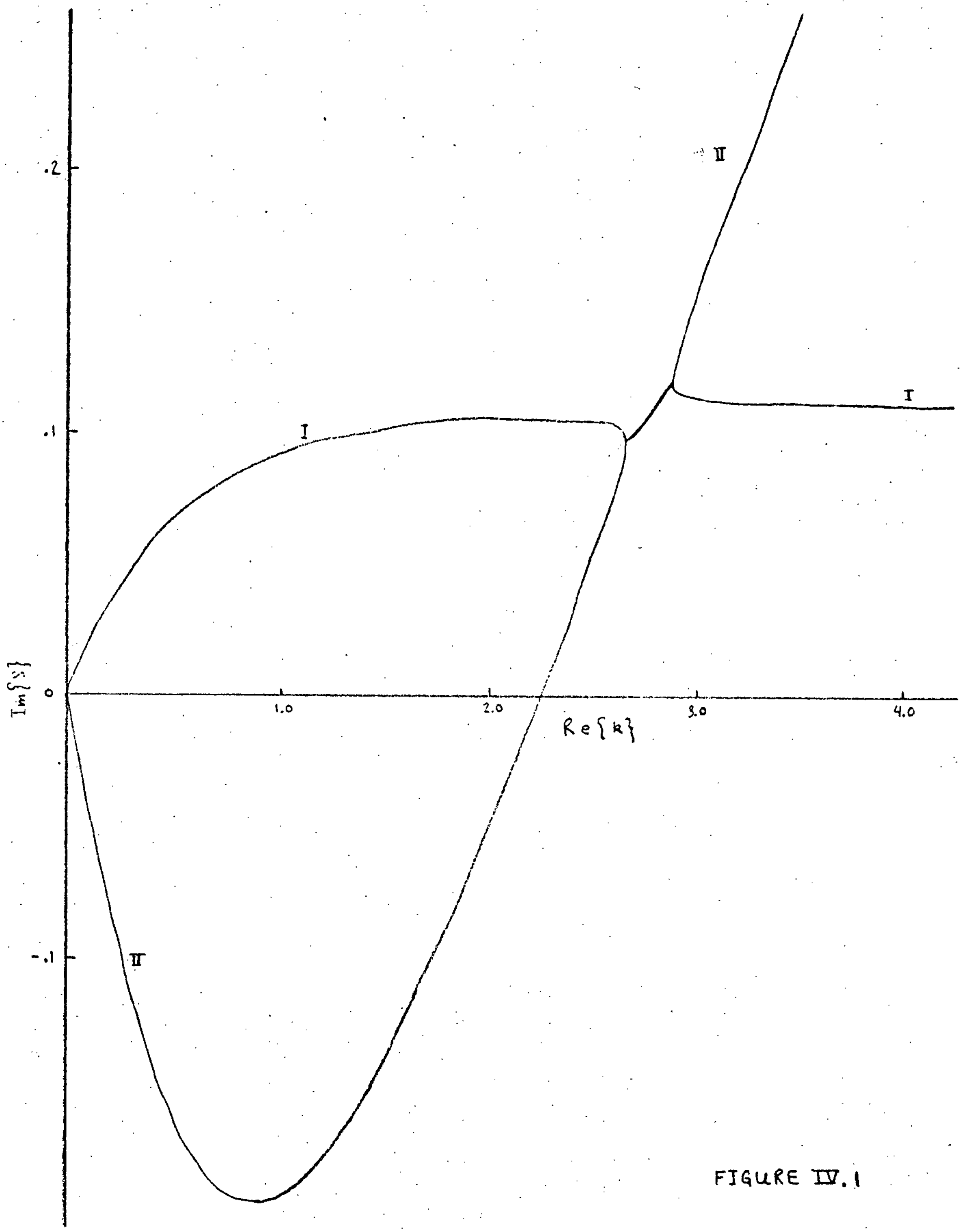

FIGURE IV.1

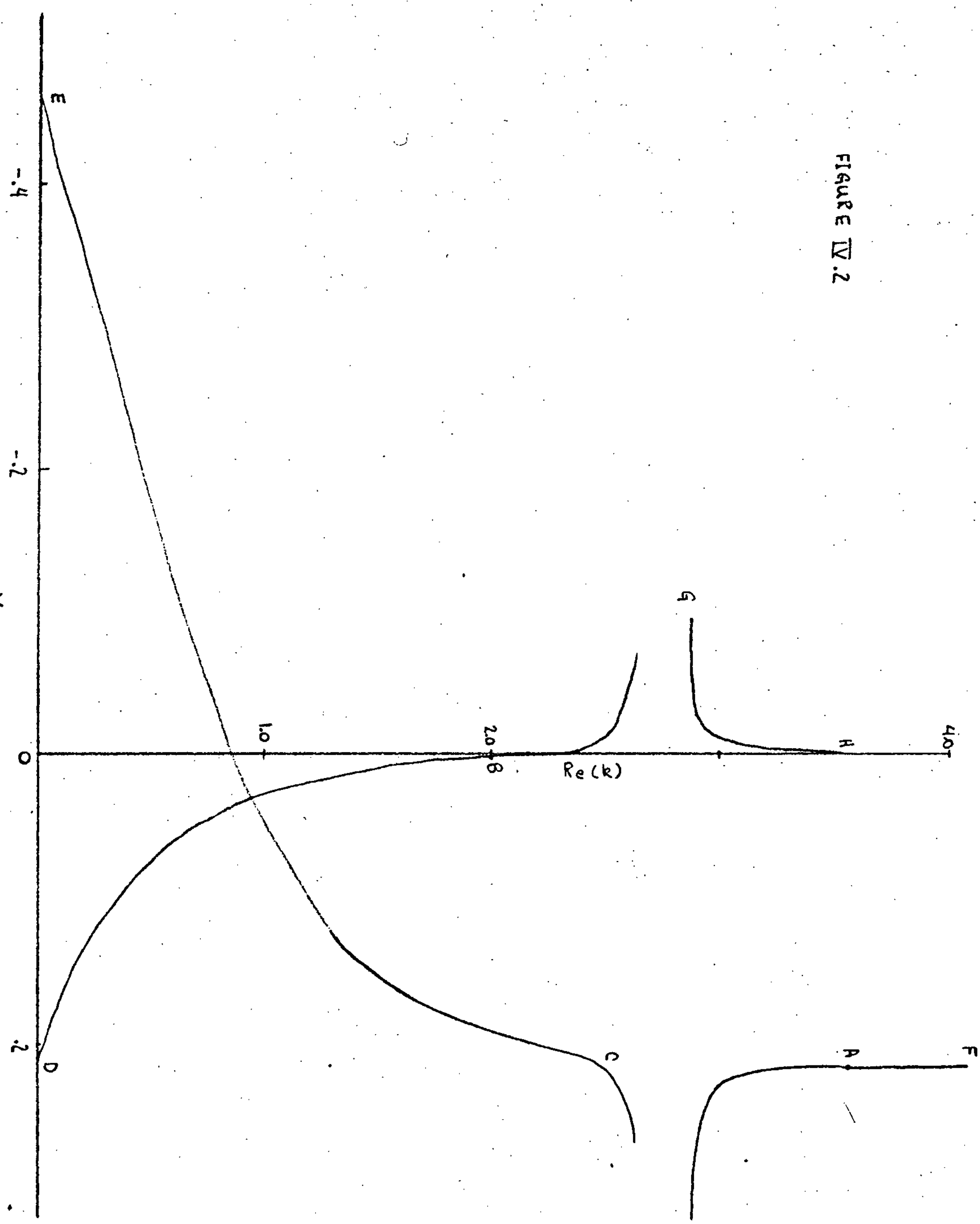

FIGURE IV.2

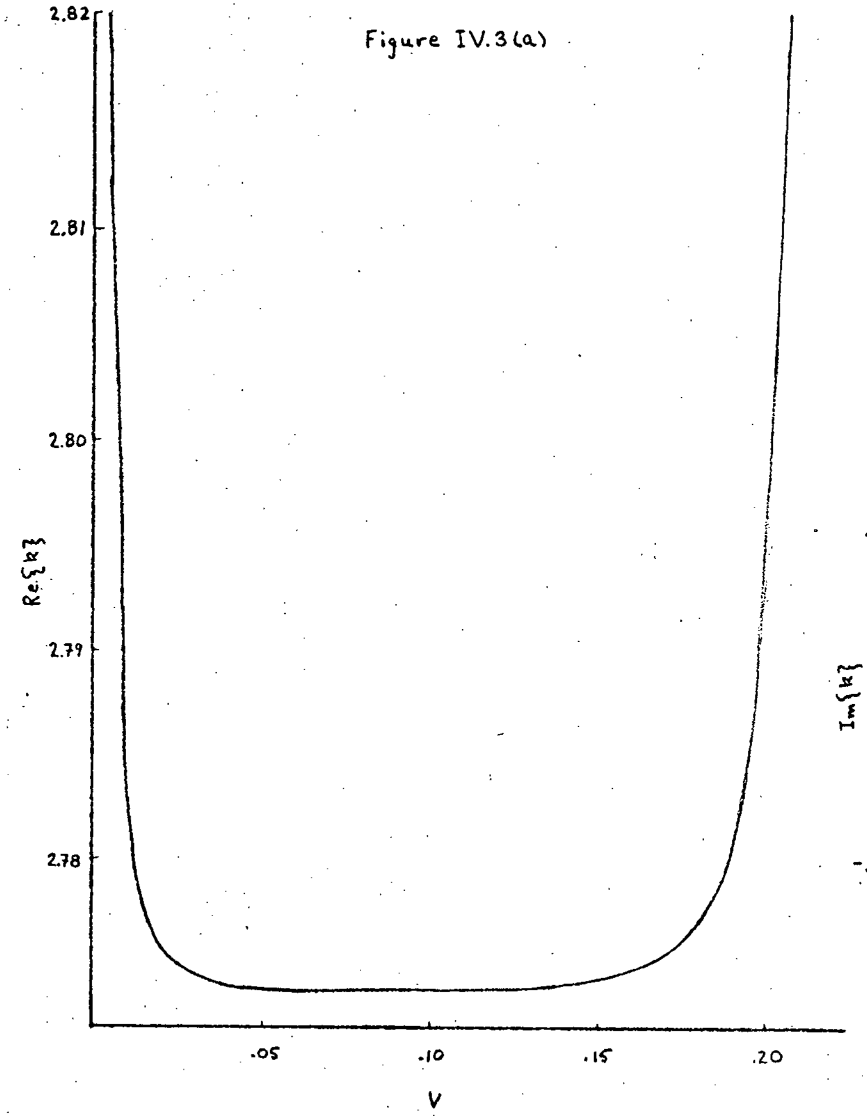
Figure IV.3(a)
Re{k}
2.82
2.81
2.80
2.79
2.78
.05
.10
.15
.20
V

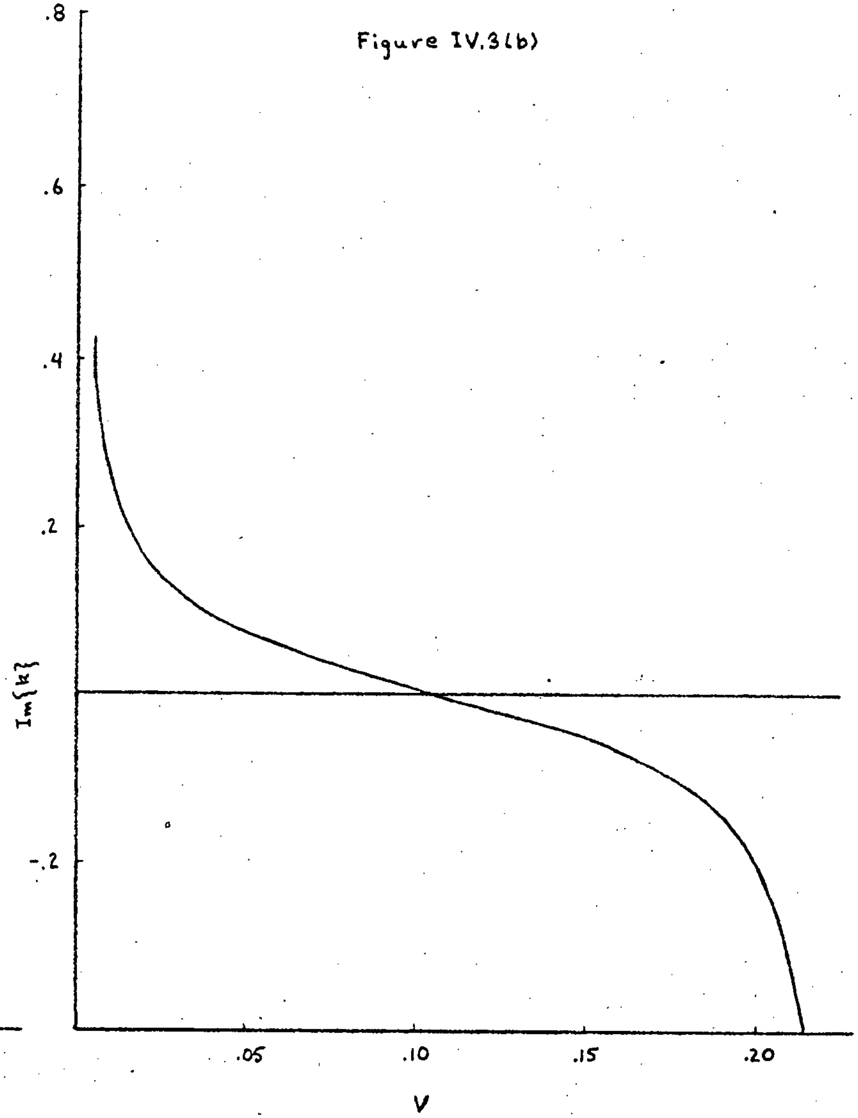
Figure IV.3(b)
Im{k}
.8
.6
.4
.2
-.2
.05
.10
.15
.20
V

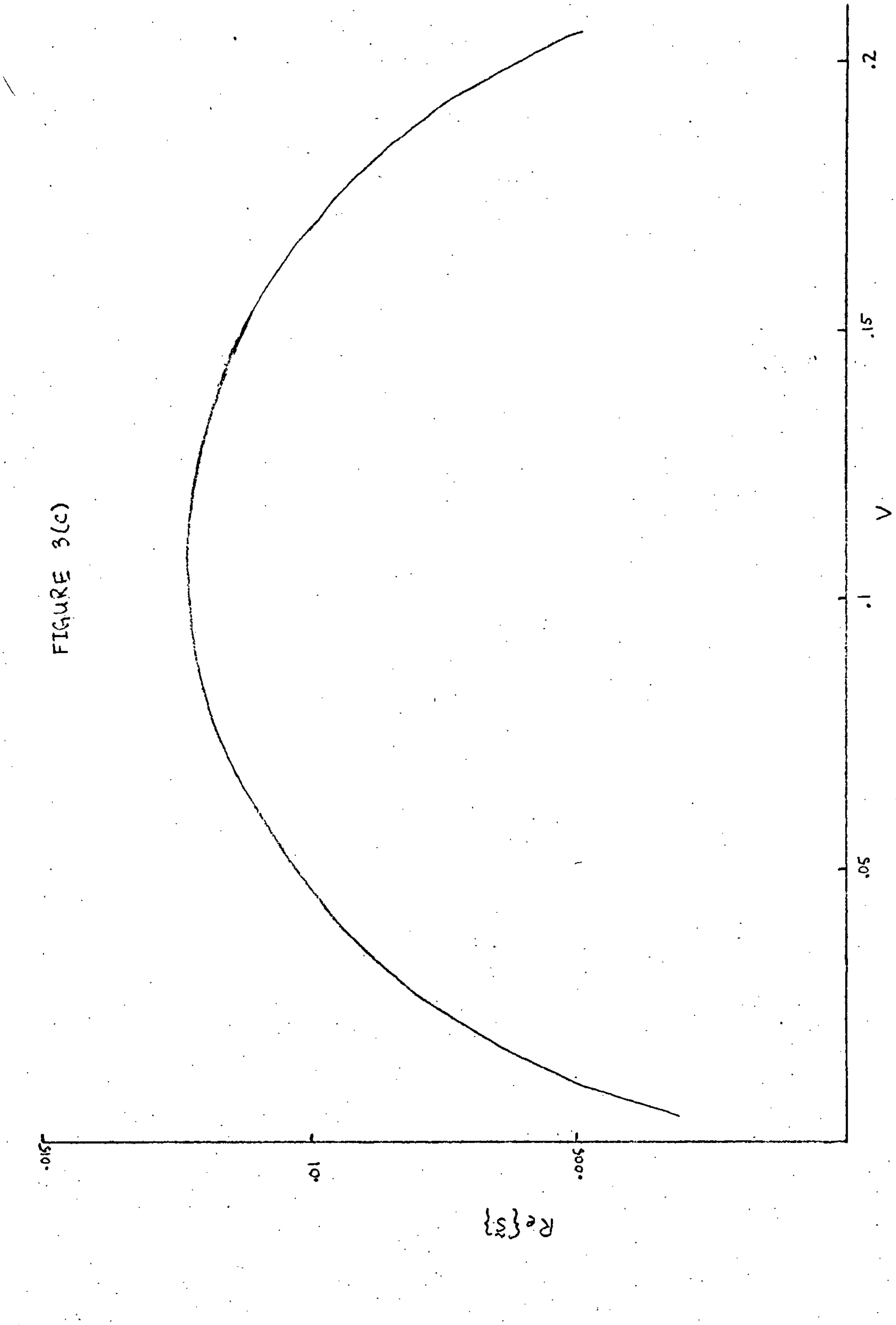

FIGURE 3(C)

FIGURE IV.3(d)

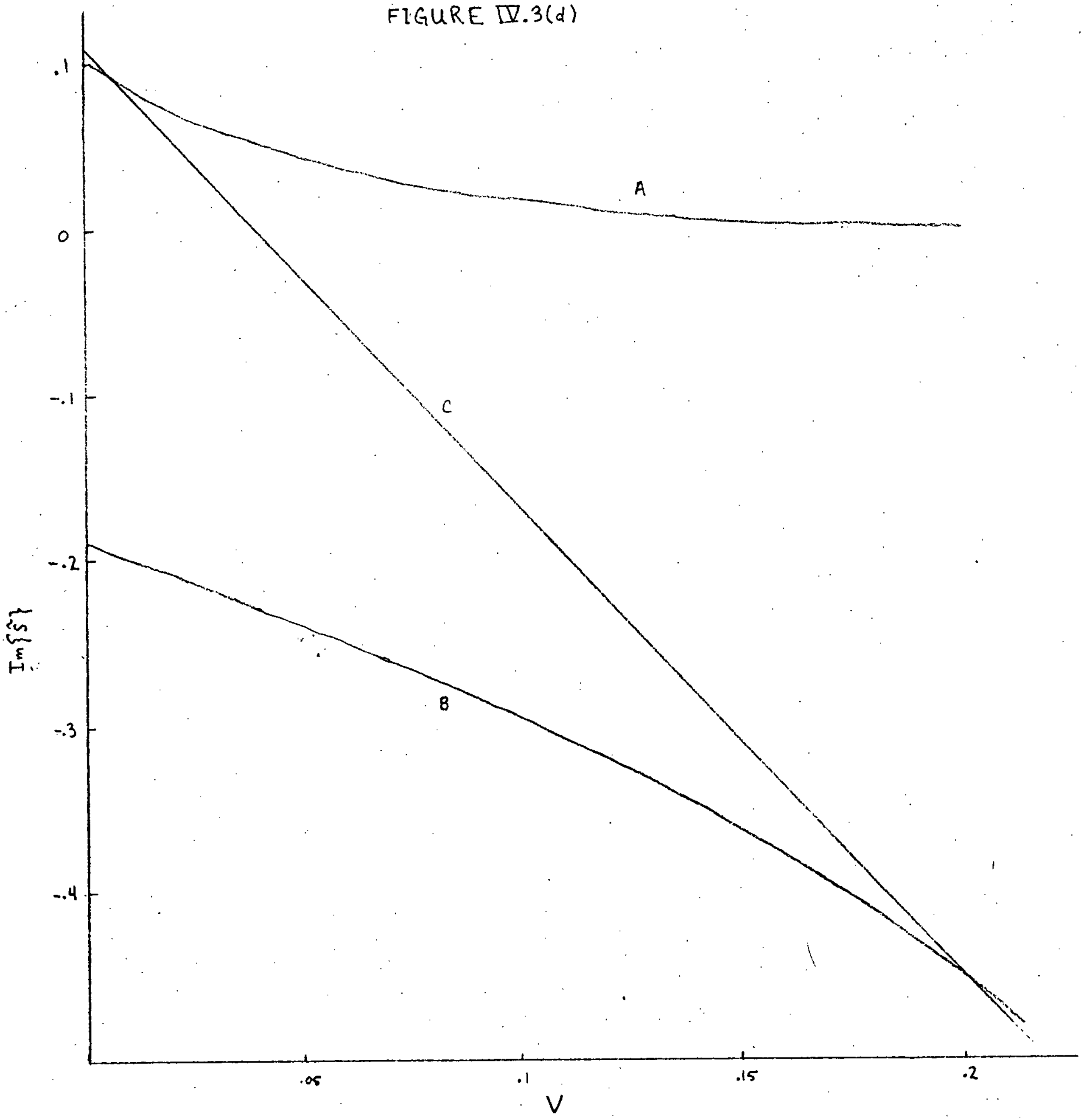

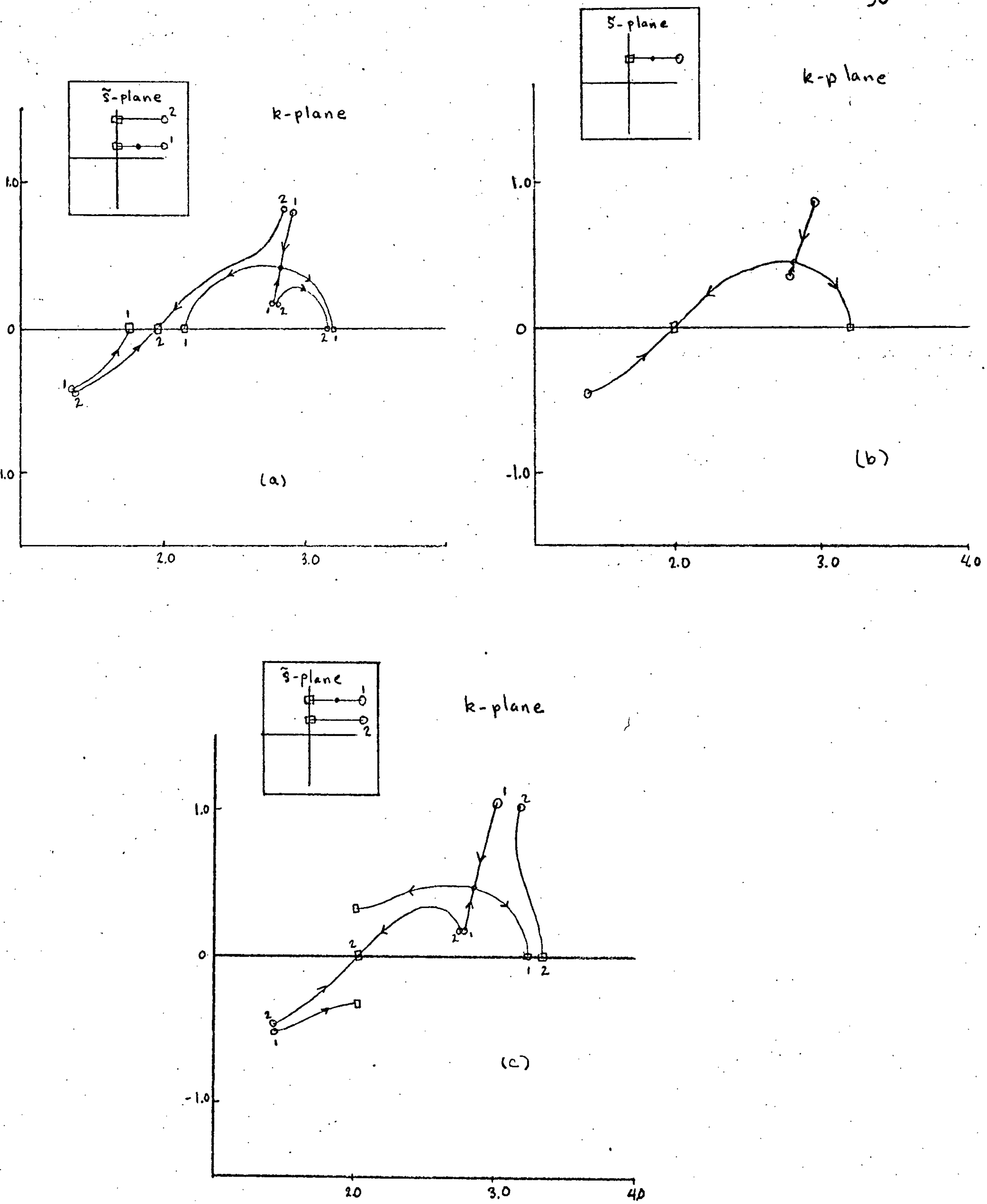
s̃-plane
k-plane
2
1
1.0
0
-1.0
2.0
3.0
(a)
s̃-plane
k-plane
1.0
0
-1.0
2.0
3.0
4.0
(b)
s̃-plane
k-plane
1.0
0
-1.0
2.0
3.0
4.0
(c)

FIGURE IV.4

Figure IV.5

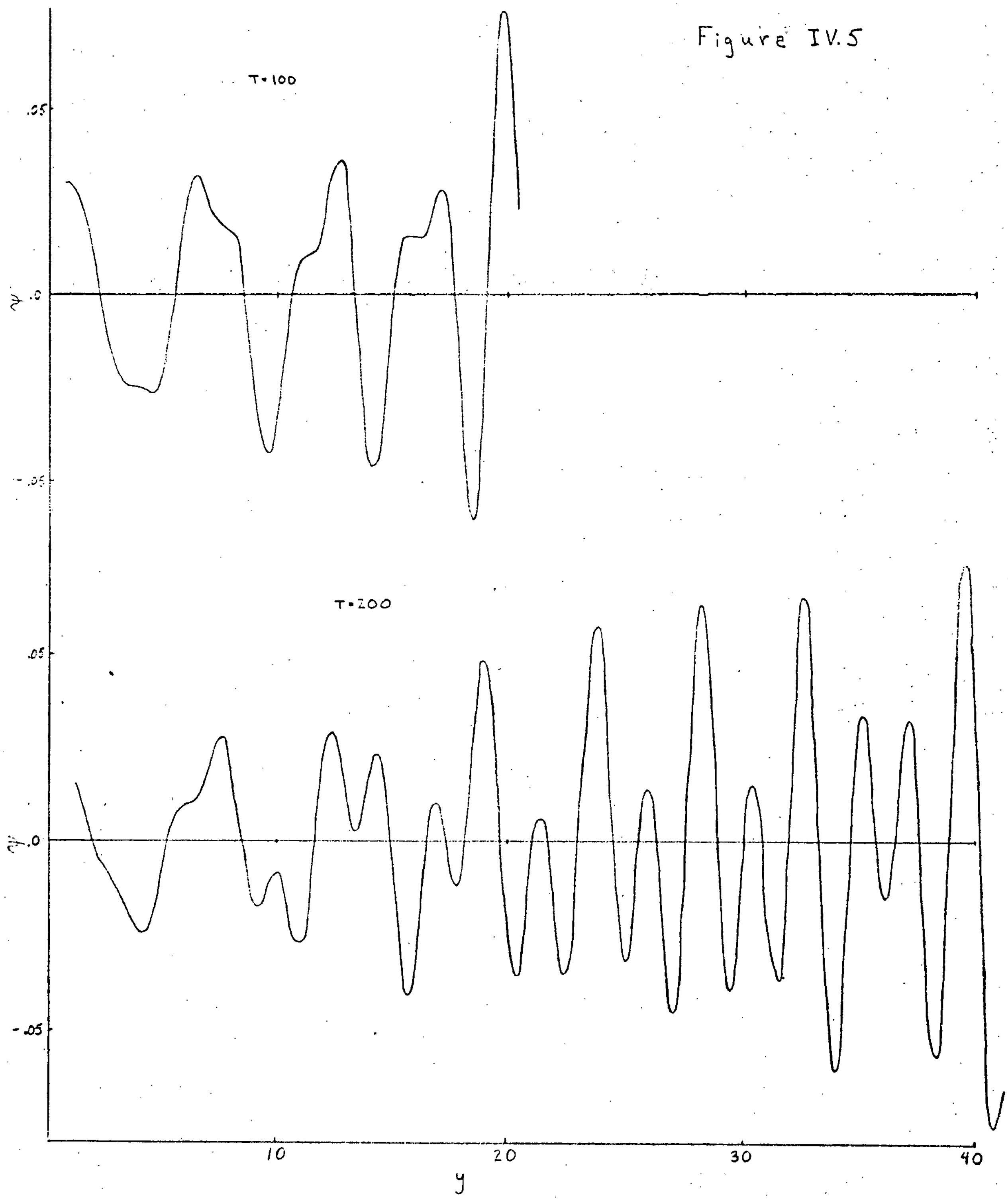

FIGURE IV.6

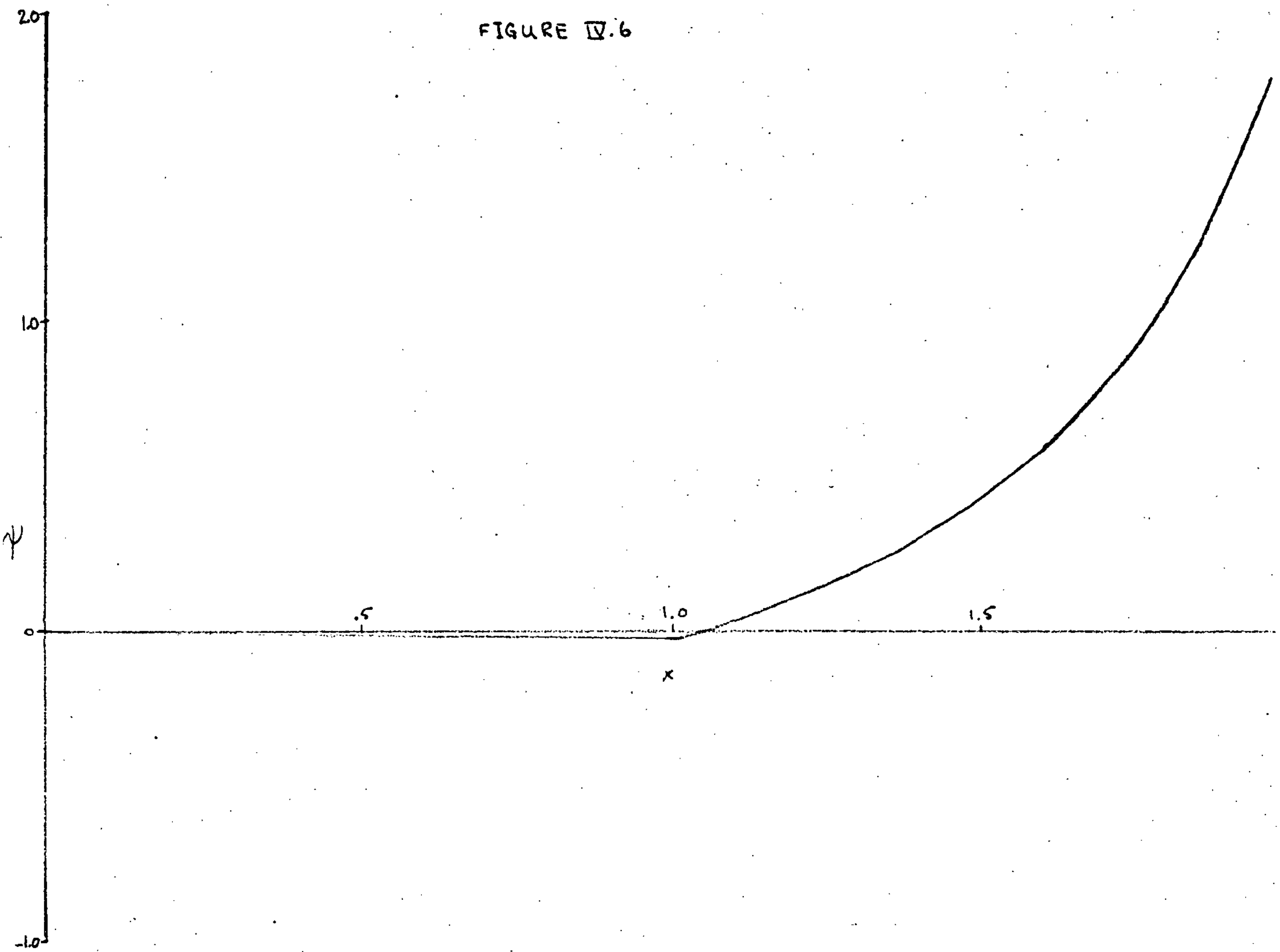

Figure IV.7

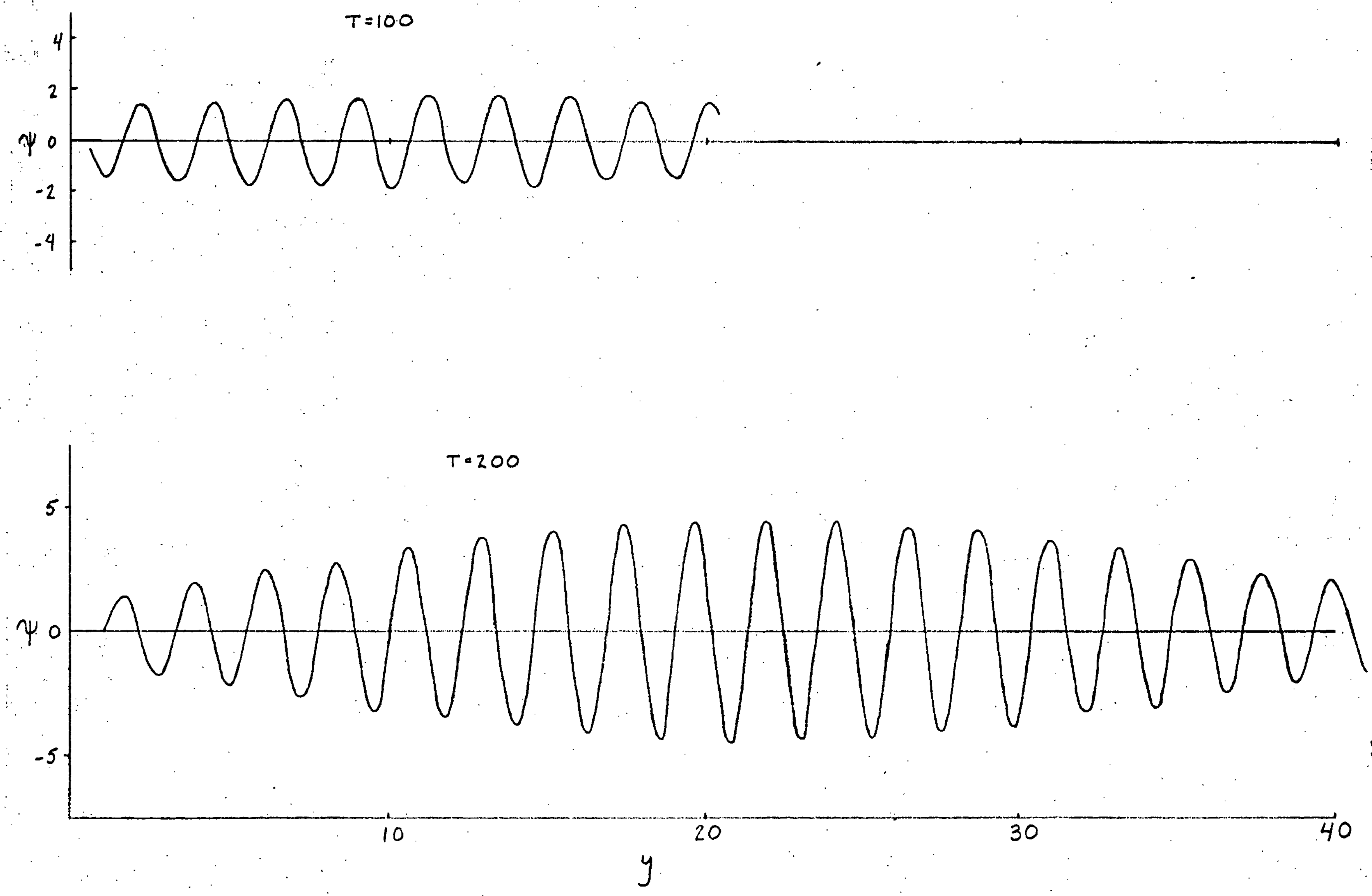

Figure IV.8

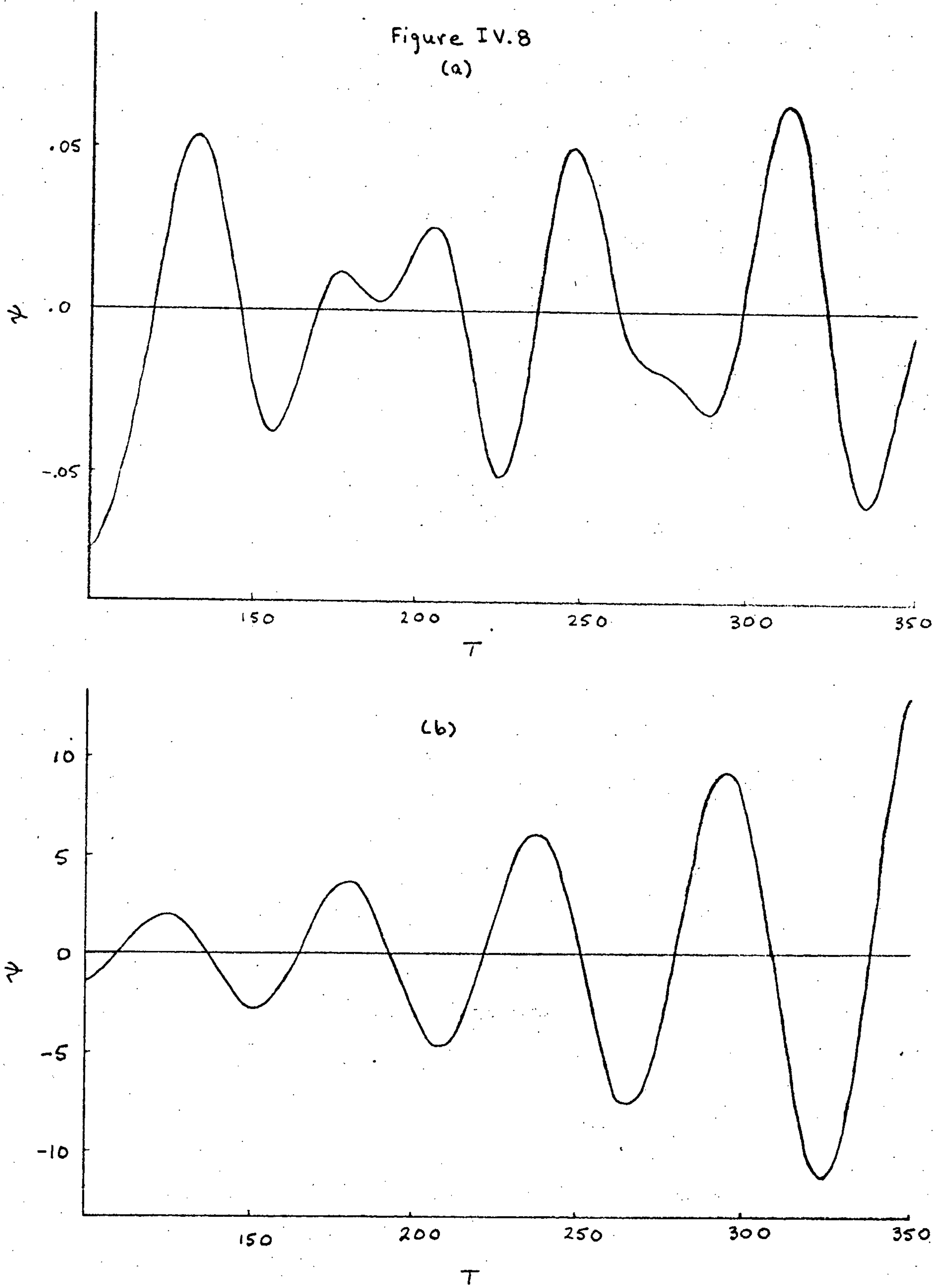

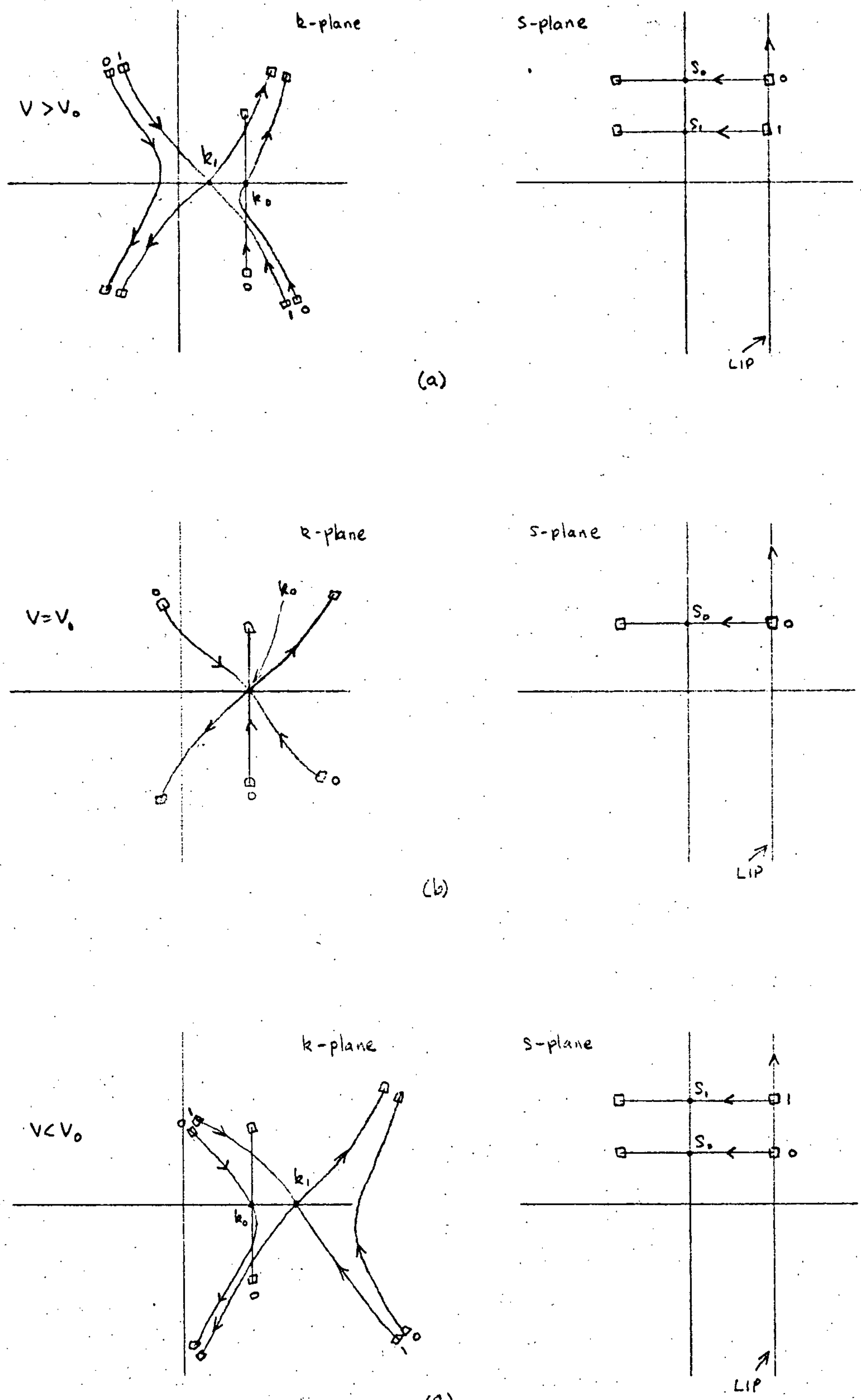
k-plane
s-plane
V > V₀
k₁
k₀
S₀
S₁
LIP
(a)
k-plane
s-plane
V=V₀
k₀
S₀
LIP
(b)
k-plane
s-plane
V<V₀
k₁
k₀
S₁
S₀
LIP
(c)

FIGURE IV. 9

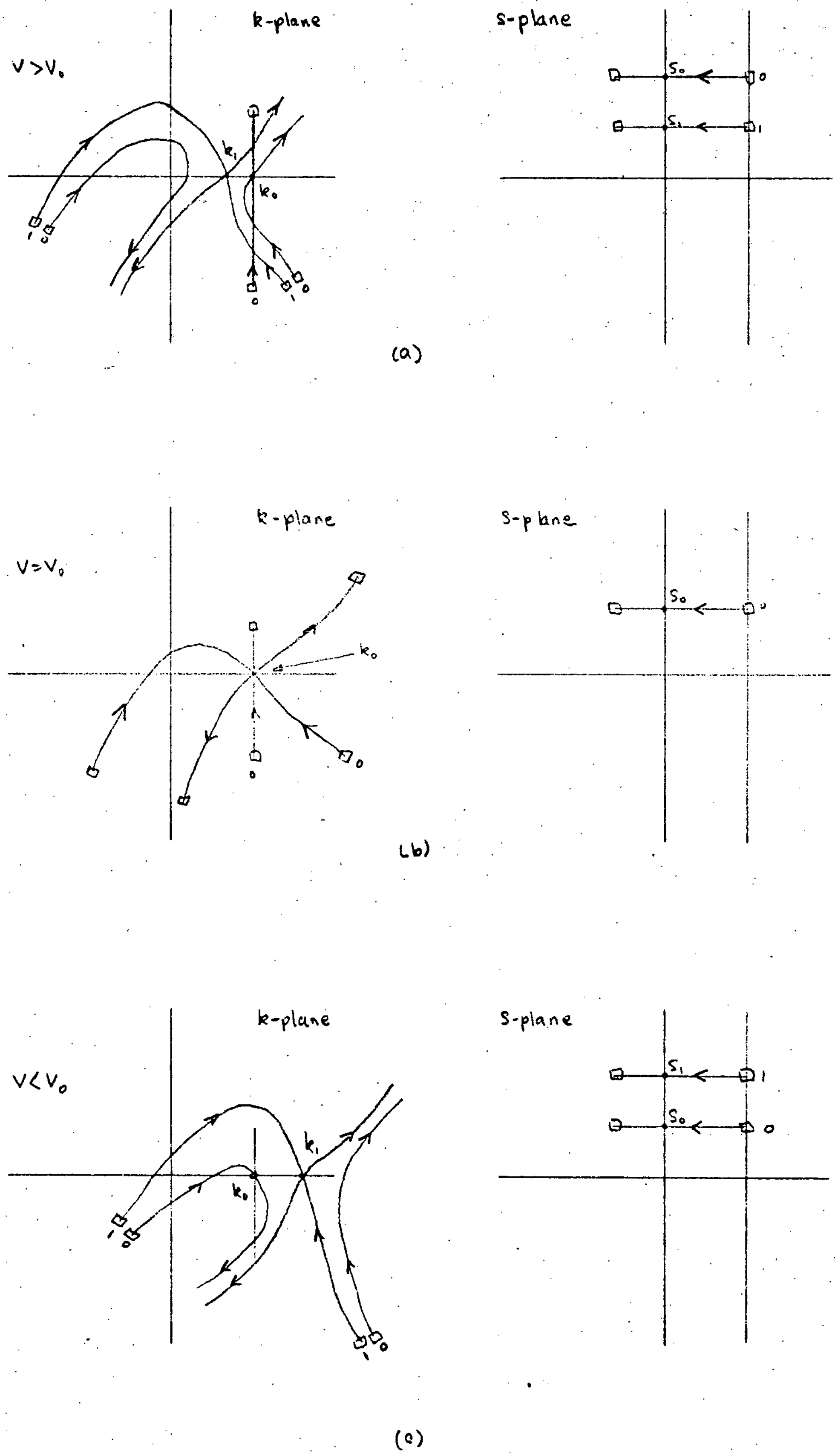

FIGURE IV. 10

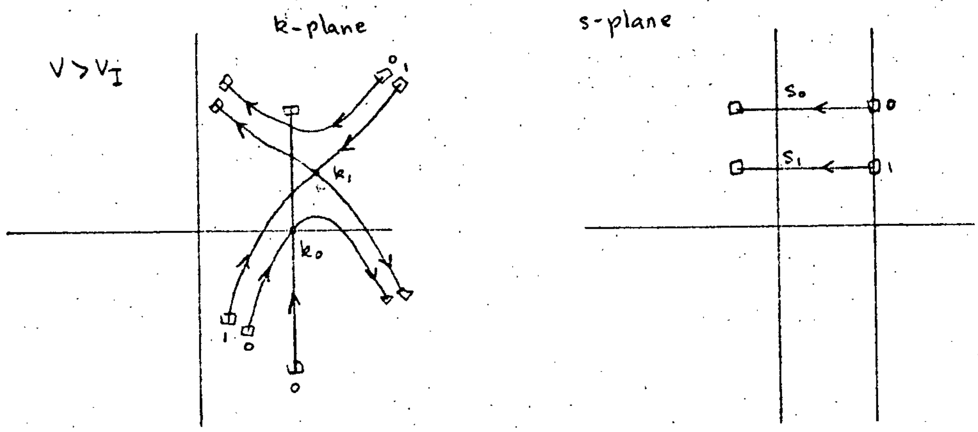

(a)

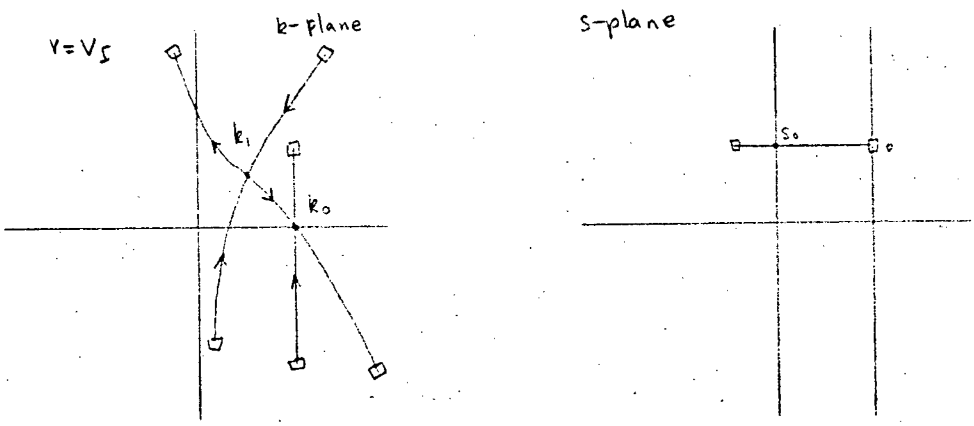

(b)

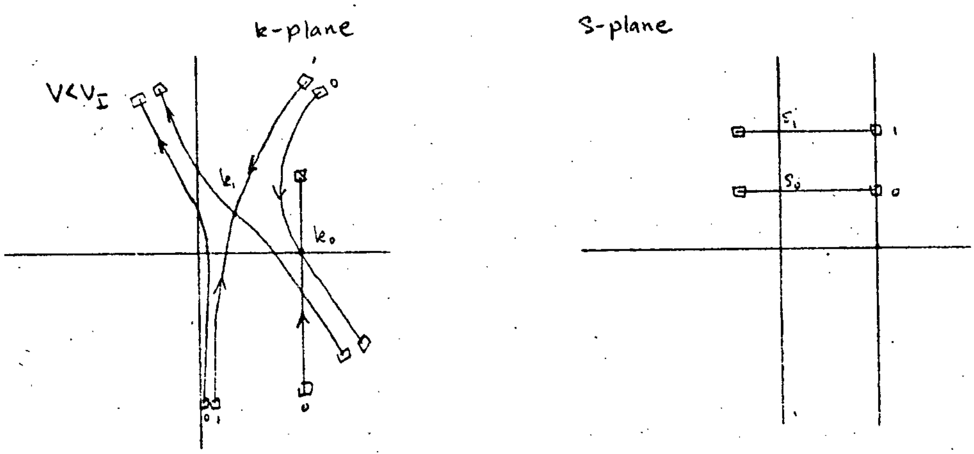

(c)

FIGURE IV. 11

Figure IV.12 (a)

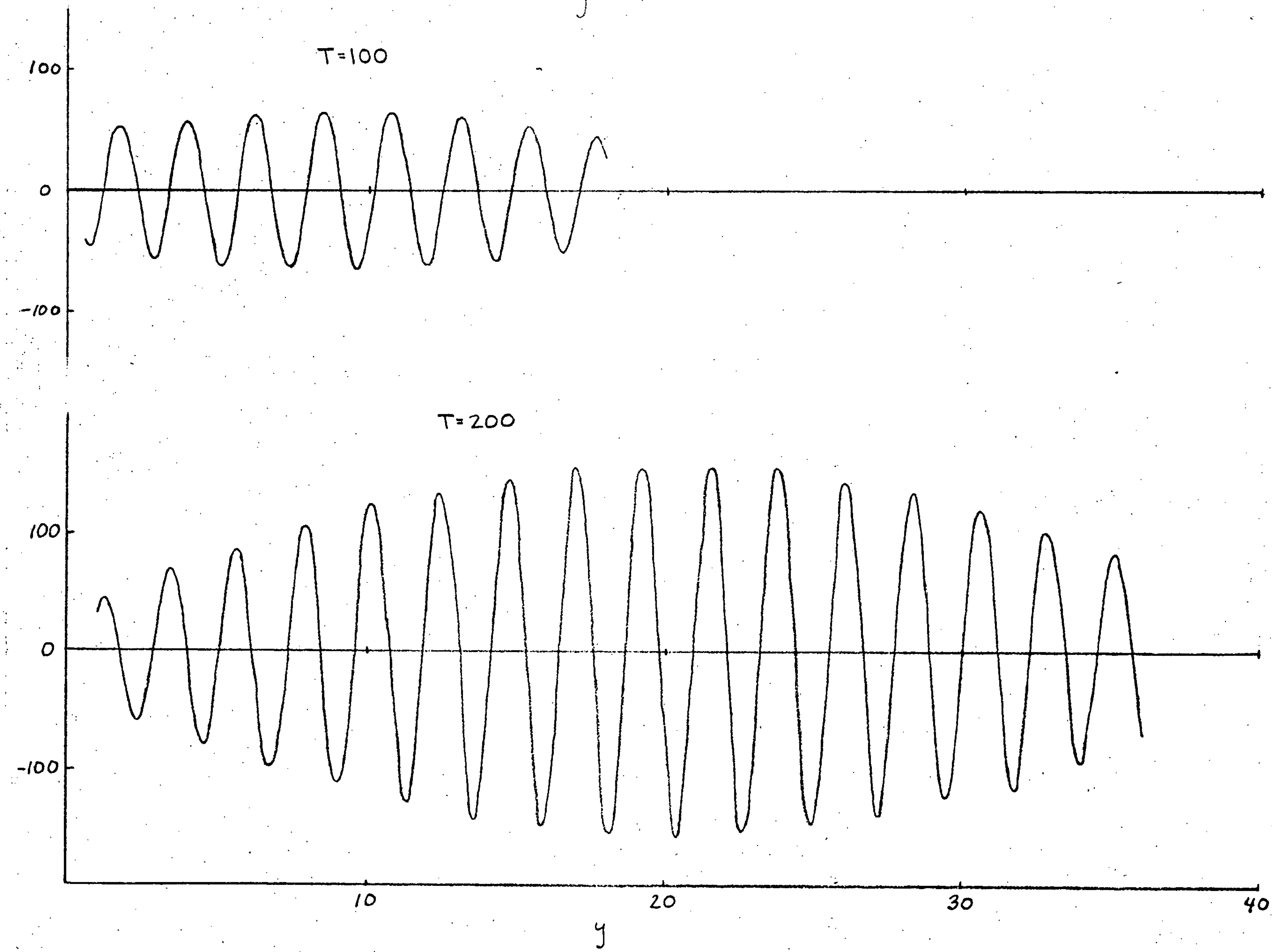

Figure IV.12(b)

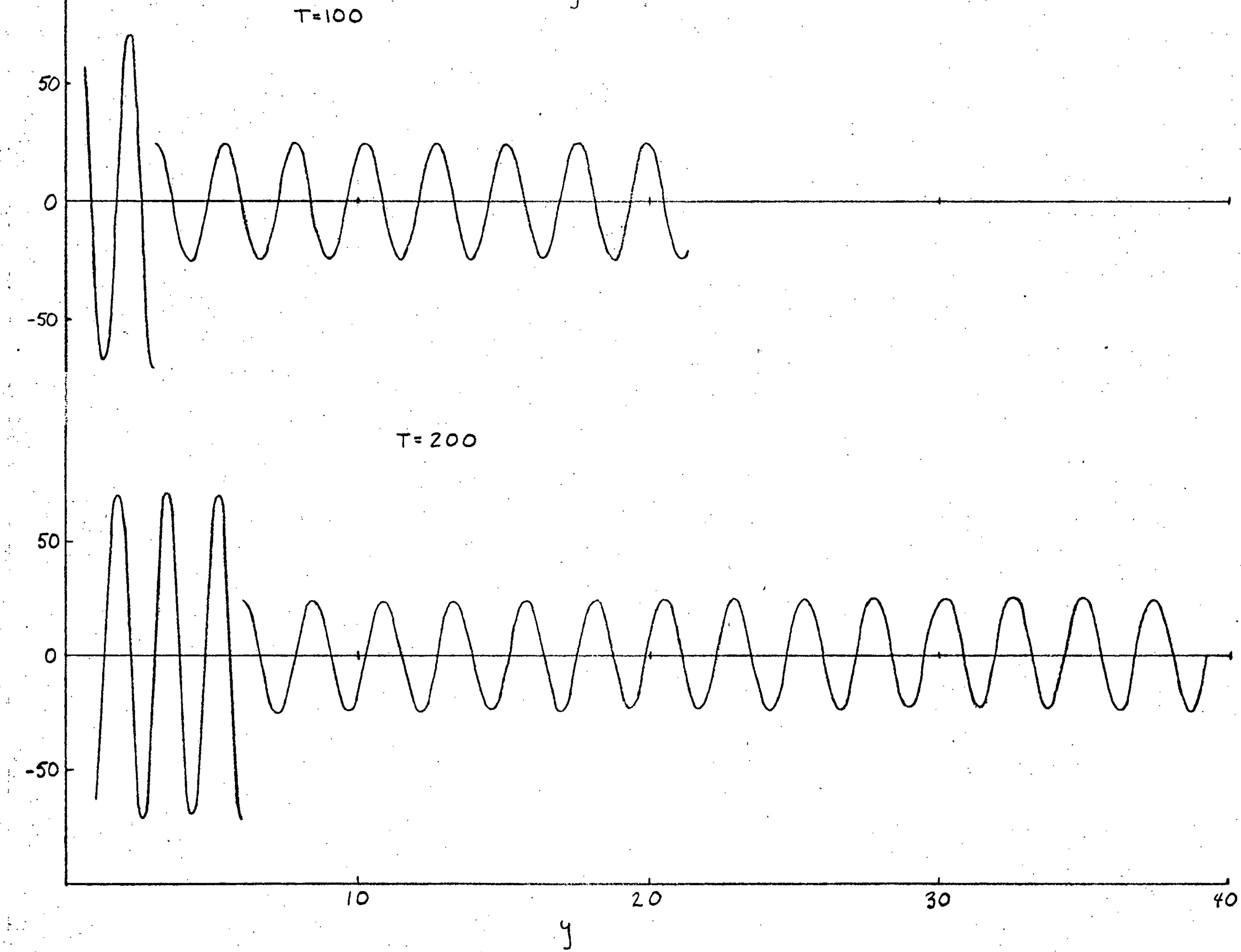

Figure IV.12(c)

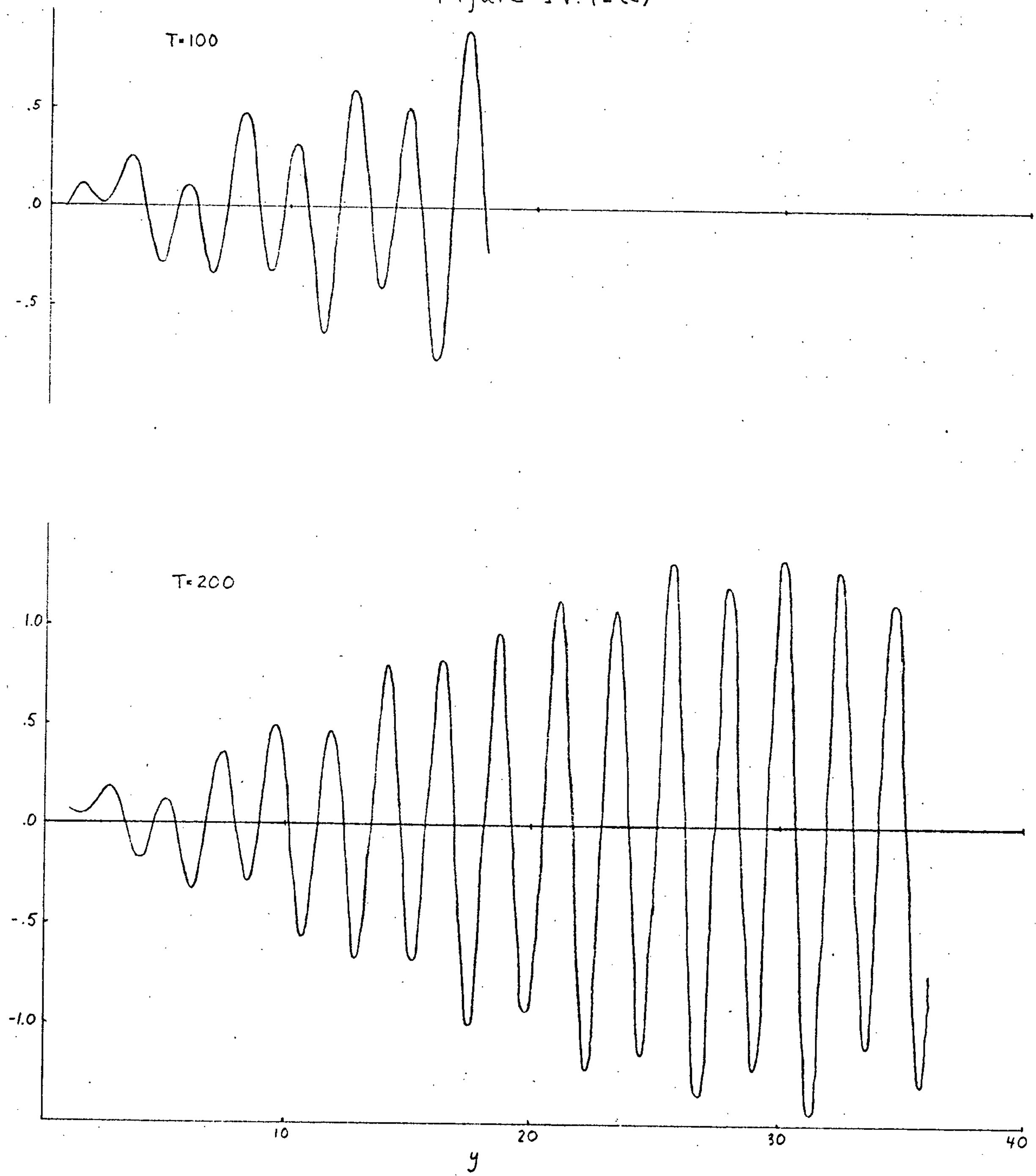

Figure IV.13

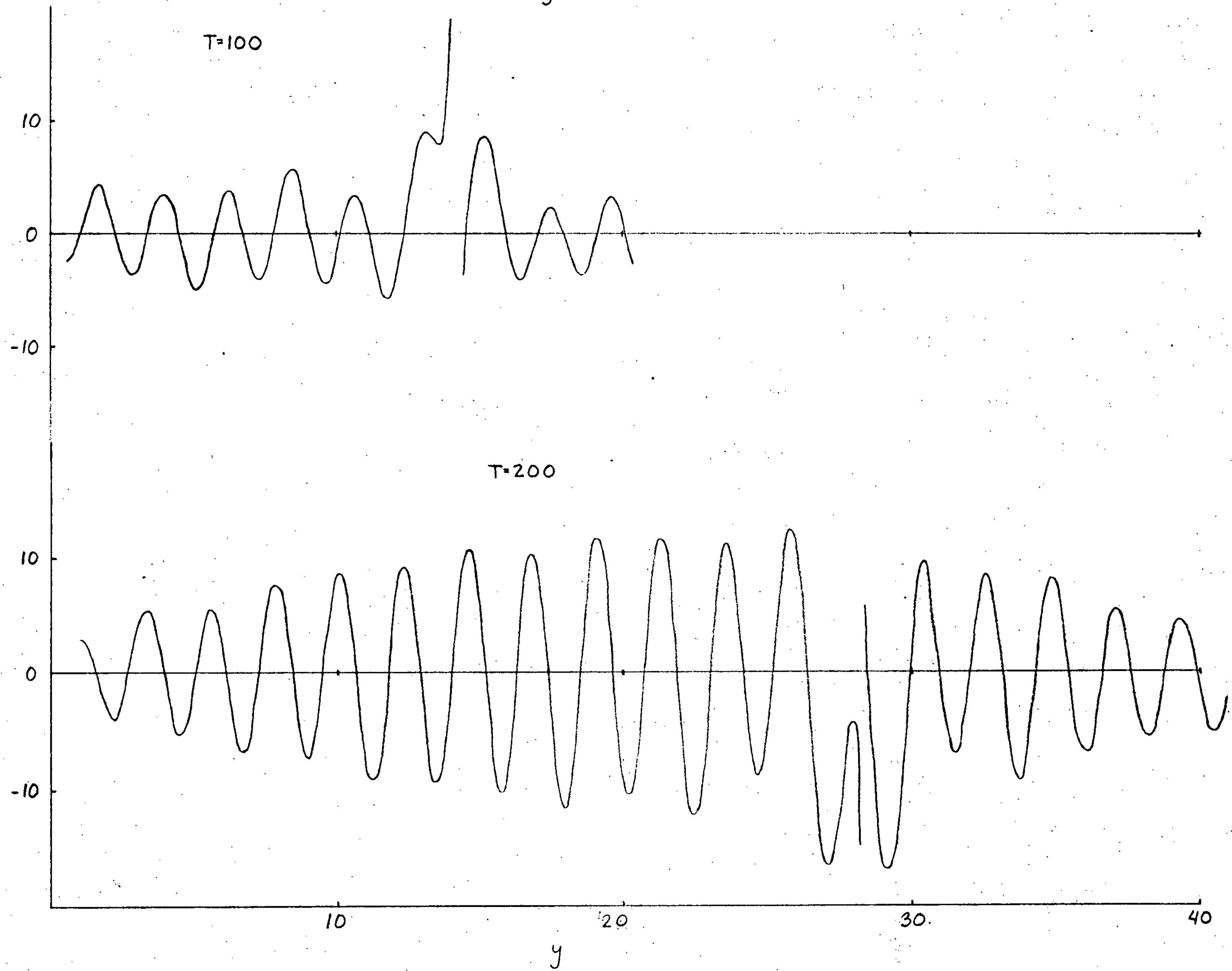

Figure IV.14(a)

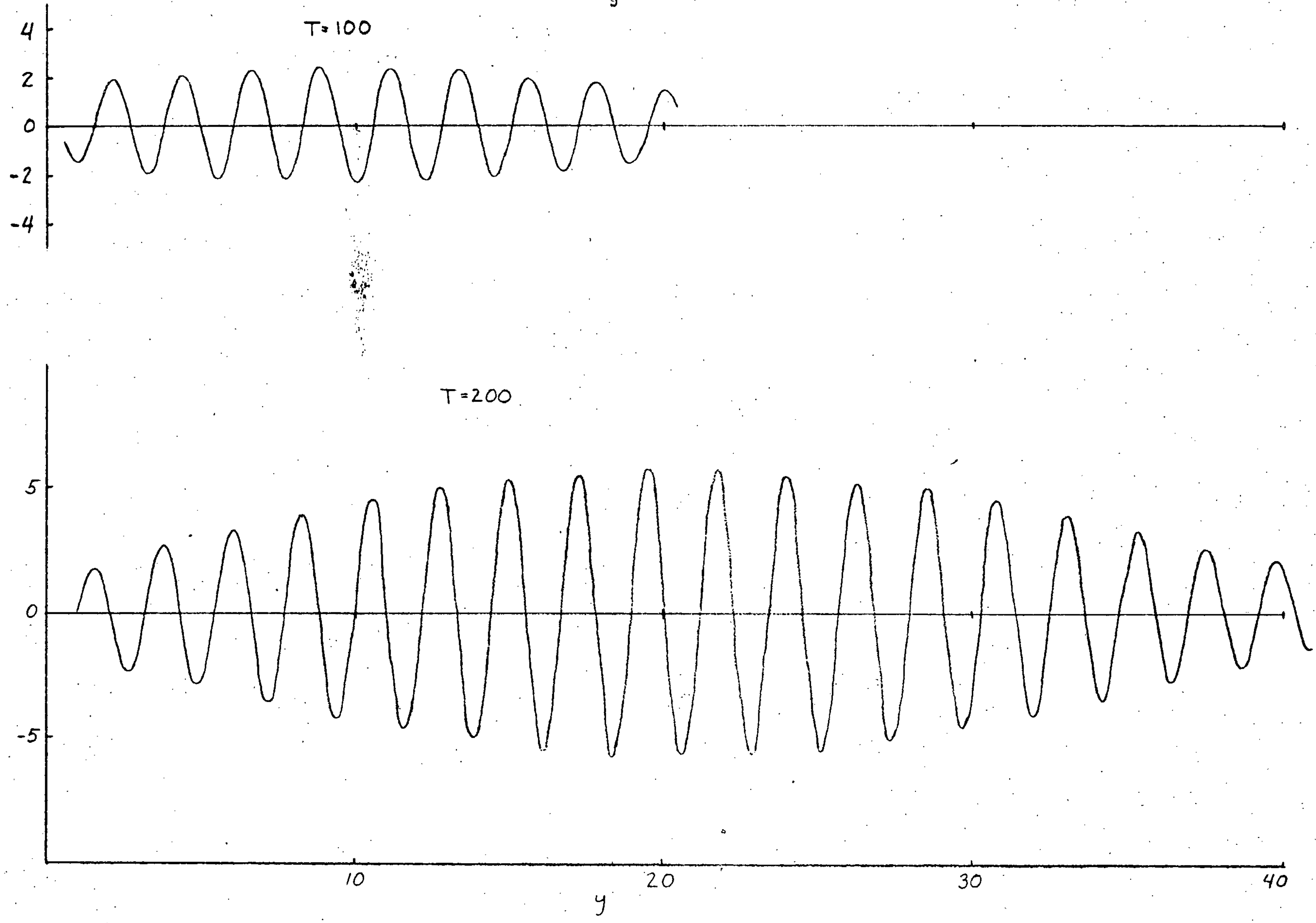

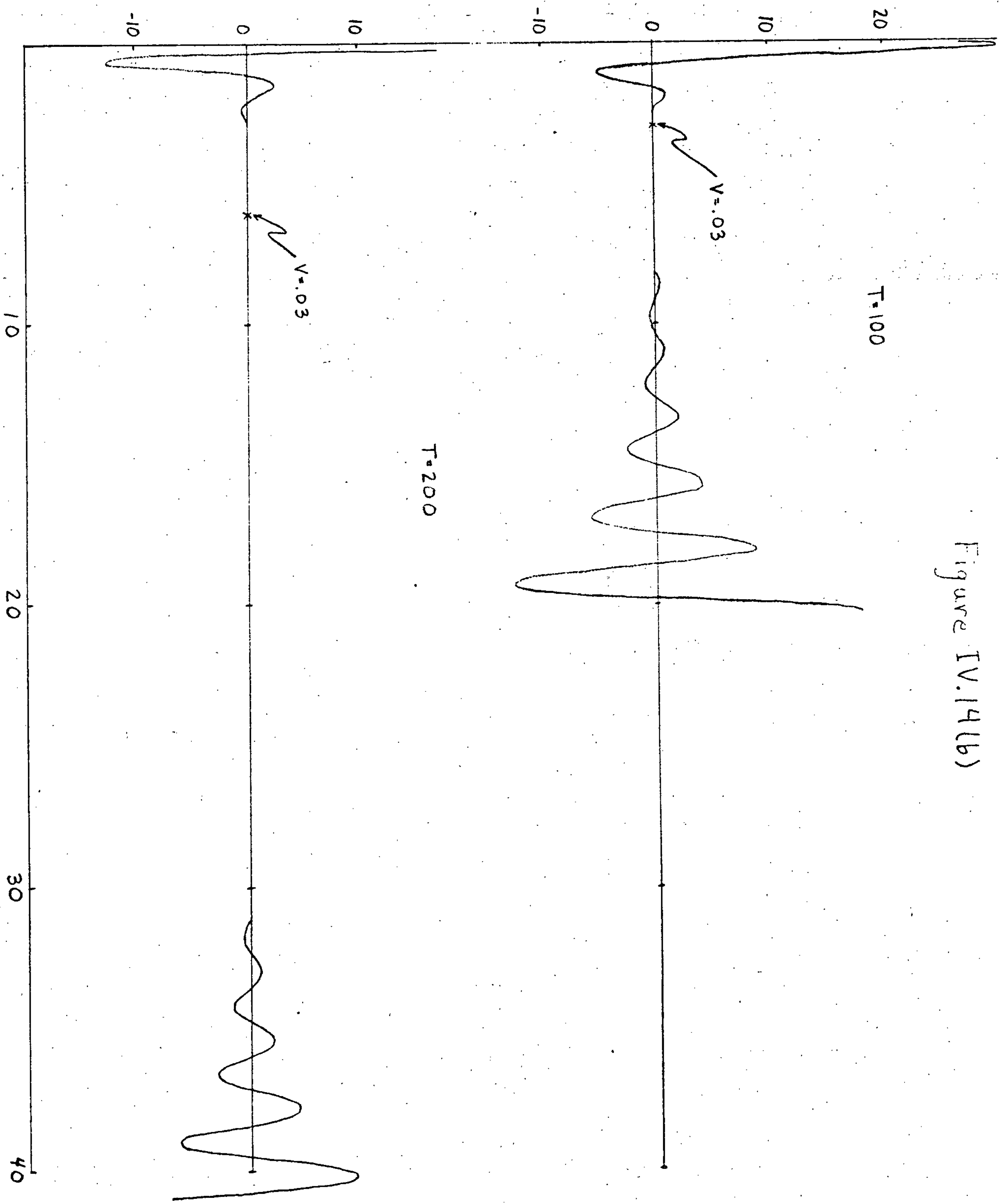

Figure IV.14(b)

Figure IV.15

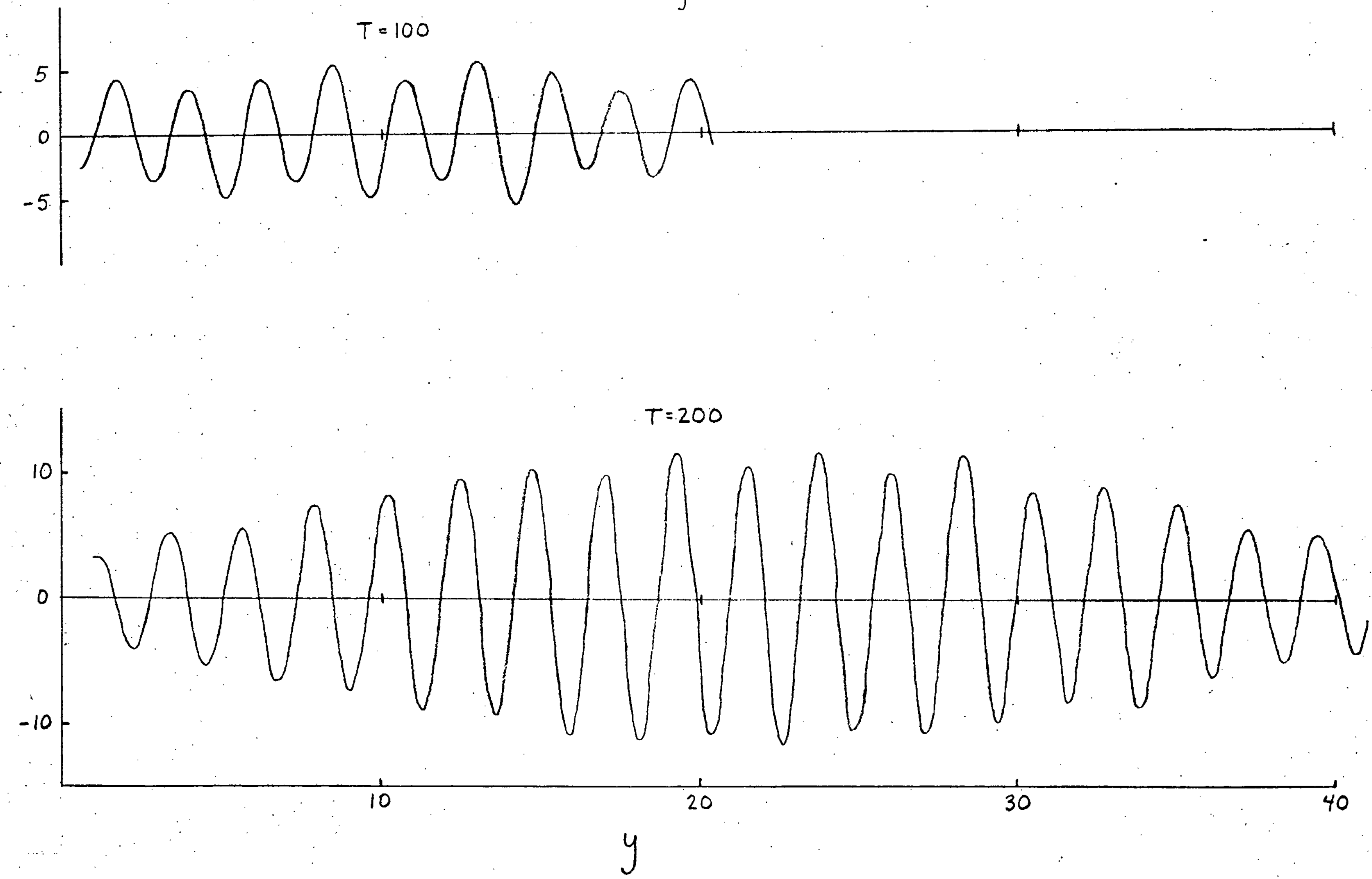

REFERENCES FOR PART A

Adams, J. K., 1972: Ph. D. Thesis. University of New South Wales.

Adams, J. K. and V. T. Buchwald, 1969: The generation of continental shelf waves. J. Fluid Mech., 35, 815-826.

Betchov, R. and W. O. Criminale, 1967: Stability of Fluid Flows. New York, Academic Press.

Briggs, R. J., 1964: Electron-Stream Interaction with Plasmas. Cambridge, Mass., MIT Press.

Buchwald, V. T. and J. K. Adams, 1968: The propagation of continental shelf waves. Proc. Roy. Soc. A., 305, 235-250.

Chandrasekhar, S., 1961: Hydrodynamic and Hydromagnetic Stability Theory. Oxford, Oxford Univ. Press.

Criminale, W. O. and L. S. G. Kovasžnay, 1962: the growth of localized disturbances in a laminar boundary layer. J. Fluid Mech., 14, 59-80.

Delves, L. M. and J. N. Lyness, 1967: A numerical method for locating the zeroes of an analytic function. Math. Comp., 21, 543-560.

Derfler, H., 1967: Growing wave and instability criteria for hot plasmas. Proc. 8th Int. Conf. On Phen. In Ionized Gases, Vienna, Springer-Verlag, 294.

Hall, L. S. and W. Heckrotte, 1968: Instabilities: Convective vs. Absolute. Phys. Rev., 166 (1), 120-128.

Hansen, D. V., 1970: Gulf Stream meanders between Cape Hatteras and the Grand Banks. Deep-Sea Res., 17, 495-511.

Haurwitz, D. and H. A. Panofsky, 1950: Stability and meandering of the Gulf Stream. Trans. Am. Geophys. Union, 31, 723-731.

Jacobs, S. J., 1971: Ageostrophic stability of divergent jets. J. Atmos. Sci., 28, 954-961.

Jeffreys, H. and B. S. Jeffreys, 1956: Methods of

Mathematical Physics. Cambridge Univ.press.

Lighthill, M., 1965: Group velocity. J. Inst. Mats. Aplics., _1_, 1-28.

______________, 1967: On waves generated in dispersive systems by travelling forcing effects, with applications to the dynamics of rotating fluids. J. Fluid Mech., _27_, 725-752.

Lin, C. C., 1955: The Theory of Hydrodynamic Stability, Cambridge Univ. Press.

Lipps, F. B., 1963: Stability of jets in a divergent barotropic fluid. J. Atmos. Sci., _20_, 120-129.

Lyness, J. N. and L. M. Delves, 1967: On numerical contour integration round a closed contour. Math Comp., _21_, 561-577.

Munk, W. H., 1950: On the wind-driven ocean circulation. J. Met., _7_, 79-93.

Mysak, L. A., 1967a: On the theory of continental shelf waves. J. Mar. Res., _25_, 205-227.

______________, 1967b: On the very low frequency spectrum of the sea level on a continental shelf. J. Geophys. Res., _72_(12), 3043-3047.

Mysak, L. A. and B. V. Hamon, 1969: Low-frequency sea level behaviour and continental shelf waves off North Carolina. J. Geophys. Res., _74_(6), 1397-1405.

Niiler, P. P. and L. A. Mysak, 1971: Barotropic waves along an eastern continental shelf. Geophys Fluid Dyn., _2_, 273-288.

Reid, W. H., 1967: The stability of fluid flows. From _Basic Developments in Fluid Dynamics_, ed. Maurice Holt, New York, Academic Press, 249-307.

Robinson, A. R., 1964: Continental shelf waves and the response of sea-level to weather systems. J. Geophys. Res., _69_, 367-368.

Orlanski, I., 1969: The influence of bottom topography on the stability of jets in a barotropic fluid. J. Atmos. Sci., _26_, 1216-1232.

Pedlosky, J., 1964a: The stability of currents in the atmosphere and the ocean: Part I. J. Atmos. Sci., 21, 201-219.

_____________, 1964b: The stability of currents in the atmosphere and the ocean: Part II. J. Atmos. Sci., 21, 342-353.

Pollard, R. T., 1970: On the generation of inertial waves in the ocean. Deep-Sea Res., 17, 795-812.

Sirovich, L., 1971: Techniques of Asymptotic Analysis. Berlin, Springer-Verlag.

Stern, M. E., 1961: The stability of thermoclinic jets. Tellus, 13, 503-508.

Stewart, R. W., 1964: The influence of friction on inertial models of oceanic circulation. Studies in Oceanography, ed. Kozo Yoshida, Univ. Of Washington Press, 3-9.

Stommel, H., 1948: The westward intensification of wind-driven ocean currents. Trans. Am. Geophys. Union, 29, 202-206.

_____________, 1966: The Gulf Stream, 2nd Edition, Berkeley, Univ. Calif. Press.

PART B

Transverse Upwelling in a Long Narrow Lake with Applications to Babine Lake

CHAPTER I - Introduction

Upwelling can be important to the biological processes in any body of water. In particular it can be a limiting factor in the productive capacity of a nutrient poor lake. Thus it is important to understand the processes responsible for the generation of the thermocline motions that would be associated with upwelling in lakes.

It is well established that longitudinal thermocline motions (longitudinal internal seiches) are generated in lakes and inlets by winds parallel to the long axis of the lake or inlet (see Heaps and Ramsbottom (1966), Farmer (1972)). Csanady (1973) has also found that transverse internal seiches are generated by winds in large oblong lakes. His work indicates that winds perpendicular to the long axis of the lake are most efficient in generating these motions, especially for narrow lakes. However, in long narrow glacial lakes the topography around the lake usually confines the winds to blow parallel to the axis of the lake. Thus we wish to know whether such winds can generate siginficant transverse thermocline motions. Csanady's work does show that long axis winds do generate transverse motions that grow with time but no numerical results are given.

Here we investigate the response of a long narrow lake to arbitrary winds and compare the theoretical results to observations made at Babine Lake in northern British Columbia. We also compare our results to those given by Csanady for Lake Michigan. The model that we use is much the same as the infinitely long two layer Channel model used by Csanady. The main difference being that we include the effects of horizontal turbulence whereas Csanady's model is comletely inviscid.

In the next section we describe the model in more detail and present the equations of motion for arbitrary wind stress. Next we present the solutions for two different impulsively applied wind stresses, a long axis wind and a cross channel wind, both uniform in space and time. We find that the inclusion of eddy viscosity improves the convergence of the series representing the solutions so that it is practical to sum them. Next we present calculated results for a model Babine Lake and a model Lake Michigan. Finally we compare the results from the model with data taken at Babine Lake by the author.

CHAPTER II - Formulation

We consider a rotating infinitely long two layer channel with a flat bottom. Horizontal turbulence is modeled through a constant coefficient of eddy viscosity, A, that is assumed to be the same in both layers. We ignore vertical stresses, except for the wind stress at the surface. Thus both bottom friction and interfacial friction are ignored. O'Brien and Hurlburt (1972) have found that these are negligible in their numerical models of ocean upwelling. The linearized equations of motion for this model are

$$u_{1t} - fv_1 = -g(h_1+h_2)_x + Au_{1xx} + \tau^{sx}/\rho_1 H_1 , \qquad (1a)$$

$$v_{1t} + fu_1 = Av_{1xx} + \tau^{sy}/\rho_1 H_1 , \qquad (1b)$$

$$h_{1t} + H_1 u_{1x} = 0 , \qquad (1c)$$

$$u_{2t} - fv_2 = -g(h_1+h_2)_x + g' h_{1x} + Au_{2xx} , \qquad (1d)$$

$$v_{2t} + fu_2 = Av_{2xx} , \qquad (1e)$$

$$h_{2t} + H_2 u_{2x} = 0. \qquad (1f)$$

The subscripts 1 and 2 refer to the upper and lower layers, respectively, and $g'=g(\rho_2-\rho_1)/\rho_2$. The Coriolis parameter, f, is assumed constant. The geometry is shown in Figure 1, where H_i are the equilibrium depths of the layers, assumed constant and the h_i are the perturbed depths.

These equations include the assumptions that the bottom is flat and that the channel is infinitley long. This last assumption allows us to assume no y dependence if the wind stress is uniform along the lake. Csanady has discussed the justification for these assumptions. Briefly, the infinite channel approximation is valid for times less than the time required for internal waves to travel the length of the lake. In ignoring variations in bottom topography we are neglecting singularities in the equations of motion that result from the depth going to zero at the side. For a lake with steep sides and a shallow thermocline the possible effects of neglecting this singularity will be confined to a narrow layer at the sides.

In linearizing the equations we have also neglected the effect of any curvature that the lake might have. However, it is possible to estimate the importance of the curvature by comparing v_1/R with f. Here R is the radius of curvature. After we have computed v_1 using the linear model above we will make this comparison to make sure that we were justified in neglecting curvature.

Finally, it has been assumed that the motion is depth independent and horizontal in each layer separately. Thus the wind stress acts as a body force in the upper layer and is only coupled to the lower layer by means of hydrostatic equilibrium.

The system of equations (1) is solved subject to the boundary conditions

$$u_i(0,t) = v_i(0,t) = u_i(L,t) = v_i(L,t) = 0, \tag{2}$$

and the initial conditions

$$\left.\begin{aligned} u_i(x,0) &= v_i(x,0) = 0, \\ h_i(x,0) &= H_i. \end{aligned}\right\} \tag{3}$$

CHAPTER III - The Solutions

The system (1) is solved by expanding in Fourier series in x. This is equivalent to expanding in terms of the internal and gravity wave modes. From the boundary conditions (2) we see that the expansions will be of the form

$$u_i(x,t) = \sum_{n=1}^{\infty} u_{in}(t) \sin\frac{n\pi x}{L}, \tag{4a}$$

$$v_i(x,t) = \sum_{n=1}^{\infty} v_{in}(t) \sin\frac{n\pi x}{L}, \tag{4b}$$

and then we must have

$$h_i(x,t) = H_i + \sum_{n=1}^{\infty} h_{in}(t) \cos\frac{n\pi x}{L}. \tag{4c}$$

Substituting these expressions into (1) gives a system of first order ordinary differential equations in t. They are then solved subject to the initial conditions

$$u_{in}(0) = v_{in}(0) = h_{in}(0) = 0. \tag{5}$$

We now present solutions obtained in this way for a uniform long axis wind and a uniform cross channel wind.

Section A. Long Axis Wind

For the long axis wind we have for the wind stress

$$\tau^{sx}(x,t) = 0, \tag{6a}$$

$$\tau^{sy}(x,t) = \tau_0 \begin{cases} 1 & t > 0 \\ 0 & t \leq 0 \end{cases} . \tag{6b}$$

Then $\tau^{sx}(x,t)$ can be expanded in a Fourier series as

$$\tau^{sy}(x,t) = \frac{4\tau_0}{\pi} \sum_{n=1}^{\infty} \frac{1}{(2n+1)} \sin\left(\frac{2n+1}{L}\pi x\right). \tag{7}$$

Thus we see immediately that for uniform wind only odd modes will be excited.

The Fourier coefficients for the upper layer for this wind stress are

$$h_{1n}(t) = -\frac{\tau_0 f L^3}{24 A \rho_1 H_1 g'}\left(\frac{96}{\pi^4 n^4}\right)\left[1 + \sum_{i=1}^{3}\left(b_{Ii}\exp(s_{Ii}t) + b_{Ei}\exp(s_{Ei}t)\right)\right], \tag{8}$$

$$v_{1n}(t) = \frac{\tau_0 L^2}{2 A \rho_1 H_1}\left(\frac{8}{n^3\pi^3}\right)\left[1 - \frac{fL^2}{g' H_1 \pi}\sum_{i=1}^{3}\left(c_{Ii}\exp(s_{Ii}t) + c_{Ei}\exp(s_{Ei}t)\right)\right], \tag{9}$$

$$u_{1n}(t) = \frac{4\tau_0 f L^2}{\rho_1 H_1^2 g' \pi}\frac{1}{n^3}\sum_{i=1}^{3}\left[d_{Ii}\exp(s_{Ii}t) + d_{Ei}\exp(s_{Ei}t)\right], \tag{10}$$

for odd n. They are all zero for n even. The expressions for the lower layer are similar but are not given here. The subscripts I and E refer to the baroclinic and barotropic modes, respectively. The coefficients in the above expressions are given by

$$d_{Ii} = \frac{\delta_I^2 (1-\delta_E^2)}{(\delta_I^2 - \delta_E^2)(s_{Ii} - s_{Ij})(s_{Ik} - s_{Ii})} , \tag{11}$$

$$c_{Ii} = \frac{d_{Ii}}{(s_{Ii} + A n^2 \pi^2 L^{-2})} , \tag{12}$$

$$b_{Ii} = s_{Ij} s_{Ik} d_{Ii} , \tag{13}$$

where j and k are the cyclic permutations of i. Identical expressions hold for the barotropic mode with the positions of I and E interchanged.

The exponents, s, in (8)-(10) satisfy the cubic equation

$$s^3 + A n^2 \pi^2 L^{-2} s^2 + \left[A^2 n^4 \pi^4 L^{-4} + f^2 (1 + n^2 \lambda^2)\right] s + f^2 n^2 \pi^2 L^{-2} \lambda^2 A = 0, \tag{14}$$

where for the s_I, $\lambda = \lambda_I$ and for the s_E, $\lambda = \lambda_E$ with

$$\lambda_I^2 = \gamma_I^2 \pi^2 L^{-2} \left[2/(1+\sqrt{1-4\epsilon^2})\right] , \quad \lambda_E^2 = \gamma_E^2 \pi^2 L^{-2} \left[(1+\sqrt{1-4\epsilon^2})/2\right] , \tag{15}$$

and

$$\gamma_I^2 = g' H_1 f^{-2} \left[H_2/(H_1+H_2)\right] , \quad \gamma_E^2 = g(H_1+H_2) f^{-2} . \tag{16}$$

The length scales γ_I and γ_E are the baroclinic and barotropic Rossby radii of curvature, respectively, as defined by O'Brien (1973). Further

$$\delta_I^2 = \left[(1+\sqrt{1-4\epsilon^2})/2\right](H_1+H_2)/H_2 , \quad \delta_I^2 = \left[2/(1+\sqrt{1-4\epsilon^2})\right] g' H_1 / g(H_1+H_2) . \tag{17}$$

where

$$\epsilon = \gamma_I/\gamma_E. \tag{18}$$

Note that the coupling between the baroclinic and the barotropic modes, which is measured by ϵ, is small if $\gamma_I \ll \gamma_E$. This is always the case, since both in the oceans and in lakes $g' \ll g$. Further the barotropic mode is less important than the baroclinic since $\delta_E^2 \ll \delta_I^2$ for the same reason.

Using (14) it is possible to show that

$$s_1 = -A\pi^2 L^{-2}(n^2 - K), \tag{19}$$

where in situations that are not dominated by friction,

$$K \approx (\lambda^2 + n^2)^{-1}. \tag{20}$$

These are the situations of interest to us. For small n, the other two solutions of (14) are a complex conjugate pair with

$$\mathrm{Re}\{s_2\} = \mathrm{Re}\{s_3\} = -\tfrac{1}{2}A\pi^2 L^{-2}(n^2 + K), \tag{21}$$

and

$$\mathrm{Im}\{s_2\} = \mathrm{Im}\{s_3\} \approx f(1+\lambda^2 n^2)^{1/2} - A^2 f^{-1}\pi^4 L^{-2} n^4 (3+\lambda^2 n^2)(1+\lambda^2 n^2)^{-3/2}. \tag{22}$$

We will see later that the second term in (22) is small for n small enough. Thus we see that at least the first few modes have frequencies close to those given by the inviscid theory (see Csanady). When n becomes large, of course, the second term dominates and then (22) no longer holds. When this happens all of the solutions of (11) become real and instead of (21) and (22) we have

$$s_2 = -A\pi^2 L^{-2}(n^2 + S^2)\,, \tag{23}$$

$$s_3 \approx -L^2 A^{-1} \pi^{-2} f^2 (n^{-2} + \lambda^2)\,, \tag{24}$$

where $s = -s_3 - K$. The transition comes when $n = n_c$ where n_c is given by

$$n_c \approx 2\lambda f L^2 / A\pi^2 \quad , \quad \lambda > 1 \tag{25}$$

or

$$n_c \approx \sqrt{2}\, f L^2 / A\pi^2 \quad , \quad \lambda < 1. \tag{26}$$

The important thing to note is that all of the modes have a time decaying component and a steady state component (in some cases the steady state component is zero) and that up to a certain value of n, the higher the mode number the faster the decay. Of course, after all the roots turn real s_3 no longer increases with n, but we will see that the contributions from such terms are negligible. The steady state components can be summed exactly and the sums with the decaying components converge very rapidly. Thus it is practical to sum the series numerically.

The sums of the steady state part of the solutions are

$$h_1(x) - H_1 = -\frac{\tau_0 f L^3}{24 A \rho_1 H_1 g'} \left[4(x/L)^3 - 6(x/L)^2 + 1 \right], \tag{27}$$

$$v_1(x) = \frac{\tau_0 L^2}{2 A \rho_1 H_1} (x/L) \left[1 - (x/L) \right], \tag{28}$$

$$u_1(x) = 0. \tag{29}$$

These are the asymptotic distributions for $t \to \infty$ of the solutions in (8)-(10). They may be obtained from (1) directly assuming steady state (and that $h_1(x)=0$ at $x=L/2$). Notice that there is no coastal jet contained in these steady state solutions, as is to be expected, since the coastal jet is a time dependent phenomenon, as has been pointed out by O'Brien and Hurlburt (1972) in the case of coastal upwelling

Section B. Cross Channel Wind

For the cross channel wind stress we have

$$\tau^{sx}(x,t) = \tau_0 \begin{cases} 1 & t > 0, \\ 0 & t \leq 0, \end{cases} \tag{30a}$$

$$\tau^{sy}(x,t) = 0. \tag{30b}$$

Then τ^{sx} is expanded as in (7) for τ^{sy} in the previous case. The coefficients now are

$$h_{1n}(t) = -\frac{\tau_o L}{2g'\rho_1 H_1}\left(\frac{8}{\pi^2 n^2}\right)\left[1 + \sum_{i=1}^{3}\left(b_{Ii}\, e^{S_{Ii}t} + b_{Ei}\, e^{S_{Ei}t}\right)\right] \tag{31}$$

$$v_{1n}(t) = -\frac{4\tau_o L^2}{\rho_1 H_1^2 g' \pi^3}\,\frac{1}{n^3}\sum_{i=1}^{3}\left[\frac{S_{Ii} b_{Ii}}{S_{Ii} + A\pi^2 n^2 L^{-2}}\, e^{S_{Ii}t} + \frac{S_{Ei} b_{Ei}}{S_{Ei} + A\pi^2 n^2 L^{-2}}\, e^{S_{Ei}t}\right], \tag{32}$$

$$u_{1n}(t) = \frac{4\tau_o L^2}{\rho_1 H_1^2 g' \pi^3}\,\frac{1}{n^3}\sum_{i=1}^{3}\left[S_{Ii} b_{Ii}\, e^{S_{Ii}t} + S_{Ei} b_{Ei}\, e^{S_{Ei}t}\right], \tag{33}$$

where we have

$$b_{Ii} = -\frac{f^2 n^2 \pi^2 \lambda_I^2 \left(S_{Ii} + A n^2 \pi^2 L^{-2}\right)}{S_{Ii}(S_{Ii} - S_{Ij})(S_{Ik} - S_{Ii})}\;\frac{\delta_I^2 (1 - \delta_E^2)}{(\delta_I^2 - \delta_E^2)} \tag{34}$$

Again an identical expression holds for the b_{Ei} with I and E interchanged. Here the steady state responses are

$$h_1(x) - H_1 = -(\tau_o L / 2\rho_1 H_1 g')\left[1 - 2(x/L)\right], \tag{35}$$

$$v_1(x) = u_1(x) = 0, \tag{36}$$

and we see that the thickening of the upper layer on the downwind side of the lake is forced directly by the cross channel wind. Whereas for the long shore wind the thickening on the side of the lake to the right of the wind (in the Nothern Hemisphere) is forced indirectly by the wind through the Coriolis force due to the earth's rotation.

Note that the series in (31)-(33) would not converge at all rapidly if it were not for the decrease in decay time with mode number. This illustrates the difficulties encountered in trying to sum these series in the inviscid case.

CHAPTER IV - Computed Results

We now present numerical results obtained for the above model in two different situations. The first is for a model Babine Lake and the second is for the model Lake Michigan considered by Csanady. The relevant parameters for the two models are given in Table I.

Table I

Parameter	Babine Lake	Lake Michigan
H_1	10 m	15 m
H_2	190 m	60 m
L	2 km	120 km
g'	1 cm/sec^2	2 cm/sec^2
f	10^{-4} sec^{-1}	10^{-4} sec^{-1}
γ_I	3.1 km	4.9 km
γ_E	450 km	920 km

Note that no values are given in this table for A. This is because we know very little about the value of A for lakes except that it certainly should be smaller than oceanic values since the largest horizontal length scales are smaller. Thus for Babine Lake results are presented for a range of values of A. It is found that for $A<10^4$ cm^2/sec the results are almost independent of A. For Lake Michigan we present results for only one representative A.

In order to calculate the response of the model we must sum the series in (4) with the coefficients given in (8)-(10) for long axis wind and (31)-(33) for cross channel winds. As has been pointed out before this will present no problems for times longer than the decay times of the higher modes. This is not the case for the inviscid problem where the coefficients in the series do not decay in time. Thus introducing eddy viscosity is at least a computational convenience in that it greatly improves the convergence of the series. This is especially true for the cross channel wind where the coefficients decrease only as $(1+\lambda^2 n^2)^{-1}$ for the inviscid model (see Csanady (1973)).

Section A. Babine Lake

We will present results for $A=10^5$, 10^4 and 10^3 cm²/sec. Using the values in Table I we have

$$\lambda_I^2 = 23.75 \quad , \quad \lambda_E^2 = 5\times 10^5 ,$$

$$\delta_I^2 = 1.053 \quad , \quad \delta_E^2 = 5\times 10^{-5} .$$

Thus we see immediately that the barotropic modes are negligible compared to the baroclinic, since . Thus we only consider the baroclinic mode in the discussion below.

Before we present the solutions we will first point out the relevant time scales for the motion. From equations (19) and (21) we have, since $\lambda_I^2 > 1$

$$s_1 \approx -A\pi^2 n^2 / L^2$$

$$Re\{s_2\} = Re\{s_3\} \approx -A\pi^2 n^2 / 2L^2$$

up to $n=n_c$. From (25) n_c is given by

$$n_c \approx 39(10^5/A)$$

For $n>n$ (23) and (24) give

$$s_2 \approx -A\pi^2 n^2/L^2$$

$$s_3 \approx -f^2 L^2 \lambda^2/A\pi^2$$

for $n<n_c$ then, the important time scale is

$$T_n \approx 11(10^5/An^2)\ \text{hr.}$$

For $n>n_c$ we must also consider the time scale for the s_3 component, which is

$$T \approx .003(10^{-5}A)\ \text{hr.}$$

Thus we see that the contributions from the s_3 components for $n>n_c$ are unimportant for any times longer than one hour and, therefore, the T_n are the important time scales. For $A=10^5$ cm²/sec, $T_1=11$ hr and for $A=10^3$ cm²/sec, $T_1=1100$ hr sc that for $A=10^5$ cm²/sec the system will reach equilibrium after only about one day. Whereas for $A=10^3$ cm²/sec equilibrium is reached only after more than two or three months. However, even for $A=10^3$ cm²/sec, $T_{32}=1.1$ hr sc that even then not too many terms are needed to approximate the sums. Finally, the frequencies of the oscillating modes are

$$\sigma_n \approx f(1+\lambda_I^2 n^2)^{1/2} \approx f\lambda_I n.$$

The first mode has a period of about 3.6 hr.

The results obtained for a long axis south wind are shown in Figures 2-6. In Figures 2 and 3 we show the depth anomaly of the upper layer and the long shore velocity in the upper layer after a 1 dyne/cm^2 wind stress has been applied for 22 hrs. Note that there is little difference between the profiles for $A=10^3$ and $A=10^4$ cm^2/sec, except in a narrow viscous boundary layer. The depth profile is unimodal, as is to be expected for a narrow lake. The difference in the depth of the interface across the lake is 12 m. As A 0 these profiles approach those for the inviscid problem. In Figures 4 and 5 the maximum values of the depth anomaly and the long shore velocity are plotted as functions of time for a 1 dyne/cm^2 wind stress. The depth anomaly oscillates slightly at the frequency of the first internal mode but the velocity does not. Again we note that there is little difference between $A=10^3$ and $A=10^4$ cm^2/sec. In fact the curves for $A=10^3$ and $A=10^4$ cm^2/sec for v are indistinguishible. Internal oscillations at the frequency of the first internal mode dominate the cross stream velocity as is seen in Figure 6. Note that the lake is too narrow for inertialoscillations.

In Figures 7 and 8 we show some results for a cross channel wind. Here we see that the internal oscillations dominate the depth anomaly response, as seen in Figure 7. Again the depth profile is unimodal and almost completely independent of A. One impcrtant difference between the response to a cross channel wind and long axis wind is that the response to the former is much faster. The maximum displacements are reached within the first internal wave period for the cross channel wind. The displacements fcr a long axis wind grow almost linearly in time. So that for short periods the cross channel response dominates, but as is seen by comparing Figures 4 and 7 the response due to a long axis wind eventually domiates, in contrast tc what Csanady suggests.

Section B. Lake Michigan

For the case of a wide lake we expect the results to be quite different. Csanady has found that for the inviscid case the first few modes are almost of equal importance so that the response is expected to be multi-modal instead of unimodal as for a narrow lake. This agrees with observations made at Lake Michigan (see Csanady (1973)).

We will present results only for $A=10^6$ cm^2/sec as this is as large as we expect A to be (it is abcut the lowest value used for the ocean) and it is found that again the results are pretty much independent of A for $A<10^6$ cm^2/sec. From Table I we find

$\lambda_I^2 = 1/60$, $\lambda_E^2 = 250/48$,

$\delta_I^2 = 1.25 \quad , \quad \delta_E^2 = 4\times10^{-4}.$

Thus again the baroclinic mode dominates, i.e., $\delta_E^2 \ll \delta_I^2$. However, now $\lambda_I^2 < 1$ so that we are in a different regime. Here we have

$$s_1 \approx -A\pi^2 n^4 \lambda_I^2 / L^2$$

$$Re\{s_2\} = Re\{s_3\} \approx -A\pi^2 n^2 / L^2$$

until $n^2 > 1/\lambda_I^2$, i.e., for $n \le 7$. For $n > 7$ we have again

$$s_1 \approx -A\pi^2 n^2 / L^2$$

$$Re\{s_2\} = Re\{s_3\} \approx -A\pi^2 n^2 / 2L^2$$

The time scales of the first few modes go as

$$T_n \approx 10^4 n^{-4} \text{ day}$$

Thus the response time for the first mode is about 30 years. Further

$$n_c \approx 2000,$$

and the time scale for the s_3 mode for $n > n_c$ is about 7 mins. The important time scales for $n > 7$ then go as

$$T_n \approx 4\times10^3 n^{-2} \text{ hr}$$

for $n \simeq 63$, $T_n = 1$ hr. So that again summation of the series is tractable; however, here more terms are required to obtain satisfactory accuracy for times of the order of hours. The frequencies of the first few modes are almost inertial, i.e., with periods of about 18 hrs.

In Figures 9-11 we show some results obtained for the model Lake Michigan. In Figure 9 we show the depth anomaly as a function of x for times of one, two and three days for a wind stress of 1 dyne/cm². We see that again the response is very fast with the maximum response being reached within the first inertial period. The profile is multi-modal as we expected. However, the full structure does not develop within the first oscillation. Note that the maximum displacement away from the sides is of the order of 1 m. In Figure 10 we show the depth anomaly for a long axis wind with a 1 dyne/cm² stress for times of 10, 20 and 30 days. We see that only the first and third modes are in evidence and that only for rather long times does the response to a long axis wind dominate the response to a cross channel wind. In Figure 11 we show the long shore velocity as a function of x for a 1 dyne/cm² long axis wind. We note that the coastal jet is present here.

The results described above indicate that a steady wind stress in an infinitely long channel model is not sufficient to account for the observed displacements in Lake Michigan which are of the order of 10 m (see Csanady (1973)). These larger displacements cannot be explanied as a response of the infinitely long channel to a long term long axis wind since the observed displacements definitely have a multi-modal structure. Anyway, such long term winds would certainly require inclusion of end effects. Two possibilities that could be considered within a linear model are that either the responses are a resonance effect or that end effects are important. Either of these possibilities requires that a closed basin model be considered.

CHAPTER V - Comparison with Observations for Babine Lake

Here we present some observations made at Babine Lake by the author and compare them with the theoretical results given above. During 21-25 August, 1973 a series of temperature transects was made at Babine Lake. Three transects were made at different locations twice a day, once in the morning and once in late afternoon or early evening. See Figure 12 for map of Babine Lake and locations of transects. During this period wind data were being recorded by instruments placed by D. Farmer of the Marine Sciences Branch. The instrumentation was placed as part of a larger program of study being conducted by Farmer in conjunction with the Fisheries Research Board at Babine Lake. The purpose of doing the transects was to determine whether there were significant transverse displacements of the thermocline that could be correlated with winds.

On two separate occasions there were significant tilts in the thermocline. These occurred on the afternoon run of 21 August and the morning run of 24 August, see Figure 13. On the 21st there was a large displacement at two stations but none was observed on the other. The maximum displacement across the lake was 6 m. On the 24th displacements were observed on all transects with a displacement of about 4 m across the lake. In both cases the displacements were unimodal as predicted by the model.

It was found that the tilting observed on the 21st was observed just after a 5 hr period of rather strong north winds, beginning at about 11:00 PST, see Figure 14. Note that the winds are in the right direction to give the observed tilts. On the transect where there was no tilting observed cross channel winds were almost as large as the long shore wind. This could explain the lack of observed displacemants. At the other two transects the wind stress had an average value of about 1 dyne/cm² for the 5 hr period. Going to Figure 3 we see that we get a displacement of about 3 m in this case.

The tilting of the isotherms observed on the 24th follows a period of about 2 days of mild intermittent long shore north winds with a short period of stronger long shore winds occurring just before the measurements were taken, see Figure 15. The average value of the wind stress for this period was about .1 dyne/cm². Figure 3 gives a displacement of about 3 m across the lake for this case.

Even though the theoretical results agree fairly well with the observations we will estimate the effect of neglecting the curvature of the lake to determine whether we are justified by the success of the agreement. As can be seen from Figure 11 there is appreciable curvature in the area where the measurements were taken. The radius of curvature here is about 5 km. As stated earlier we can estimate the importance of the curvature by comparing v_1/R with f. Now for both cases described above Figure 4 indicates that $v_1 < .5$ m/sec. Thus $v_1/R < 10^{-4}$ sec^{-1}, and we see that inertial effects certainly do not dominate but that they might modify the flow somewhat. Finally we mention that end effects are probably not important since it requires about 60 hrs for an internal wave to travel the length of the lake.

CHAPTER VI - Conclusion

In part B of this thesis we have presented a model that describes the generation of transverse motions of the interface in an infinitely long two layer lake by uniform wind of arbitrary direction. We have included the effects of horizontal eddy viscosity. The main consequence of its inclusion seems to be that the convergence of the series solutions for the model is greatly improved and makes numerical summation practicable.

A comparison of the computed results with data from Lake Michigan indicates that a cross channel wind generates the multi-modal structure observed there, but that the magnitude of the displacements are larger by a factor of 10 than those predicted by the theory. Long axis winds do not even generate motions of the observed form. It seems that a model including end effects and/or non-linear effects is required.

Applying the theory to a narrower lake gives better results. Observations made by the author at Babine Lake show that in a long narrow lake significant interface displacements are generated by long shore winds. The model predicts displacements that agree both in magnitude and form with those observed.

FIGURES FOR PART B

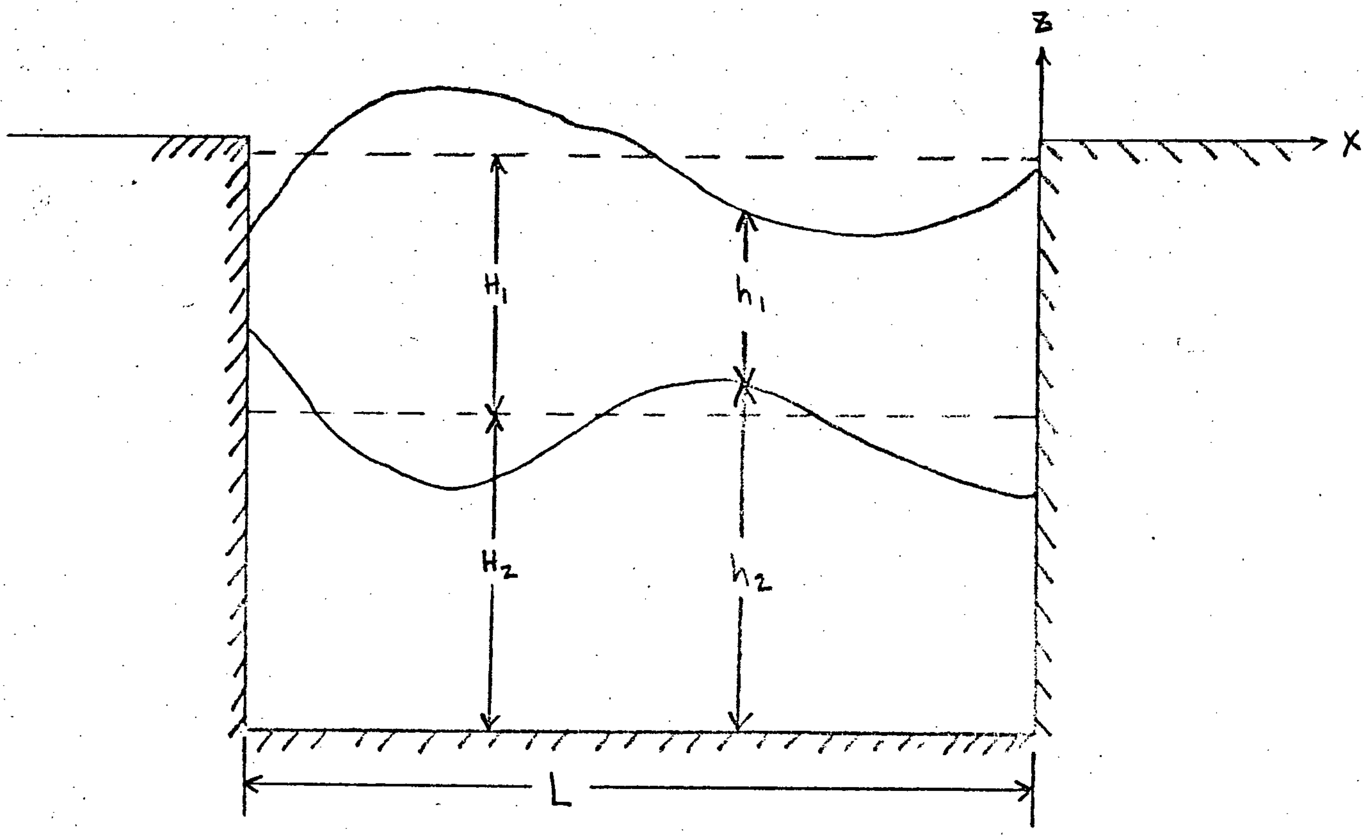

Figure 1

Figure 2

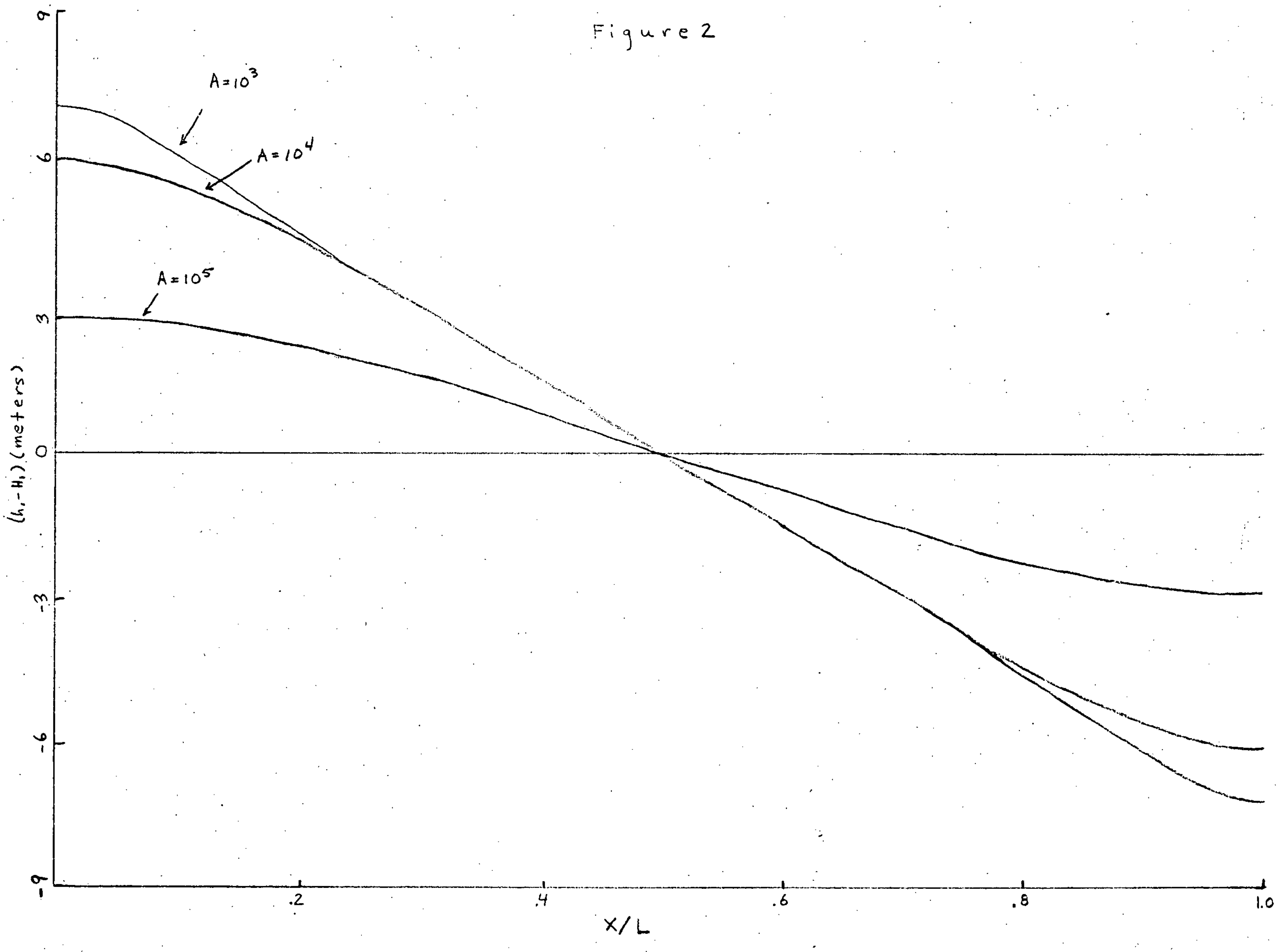

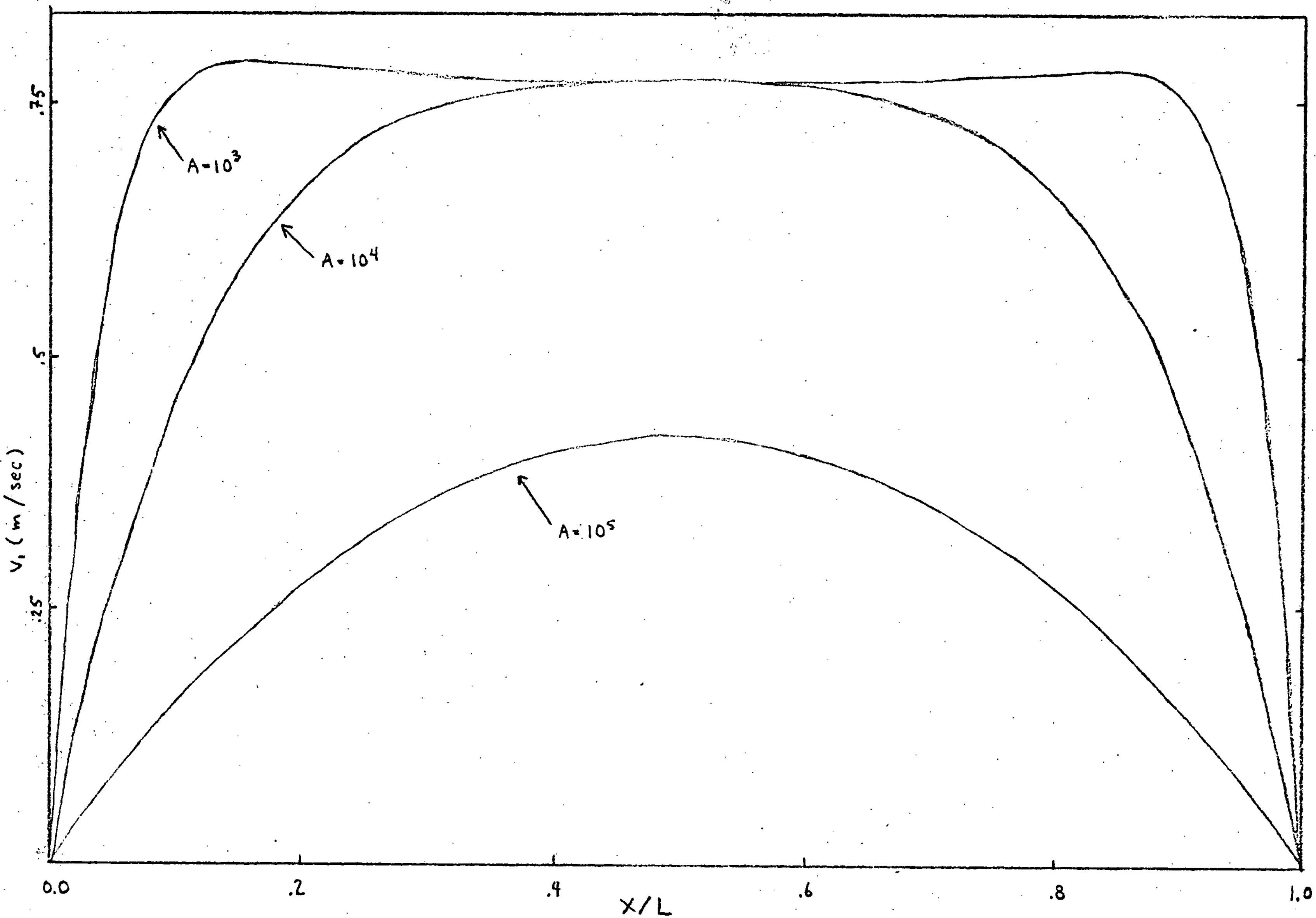

Figure 3

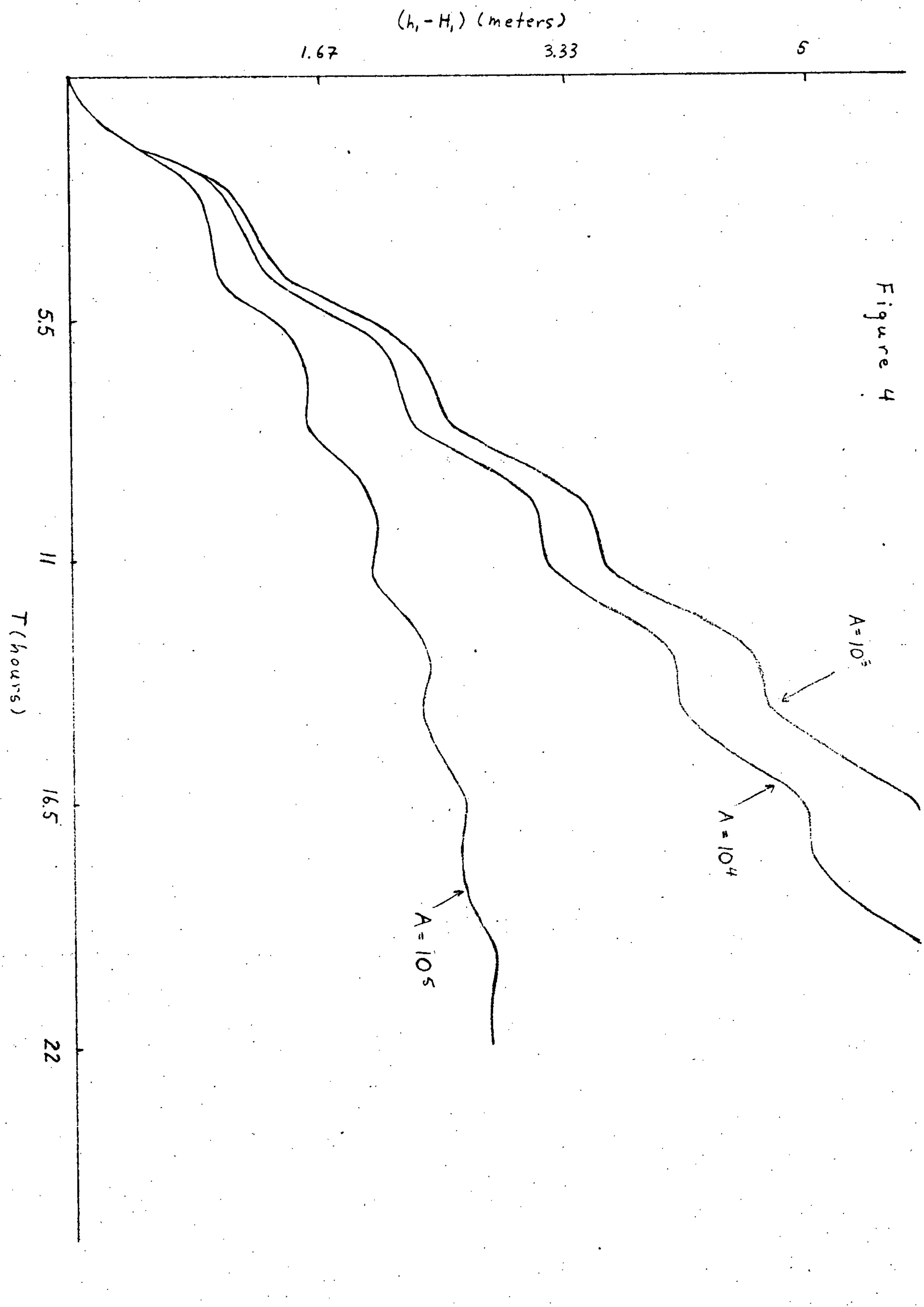

Figure 4

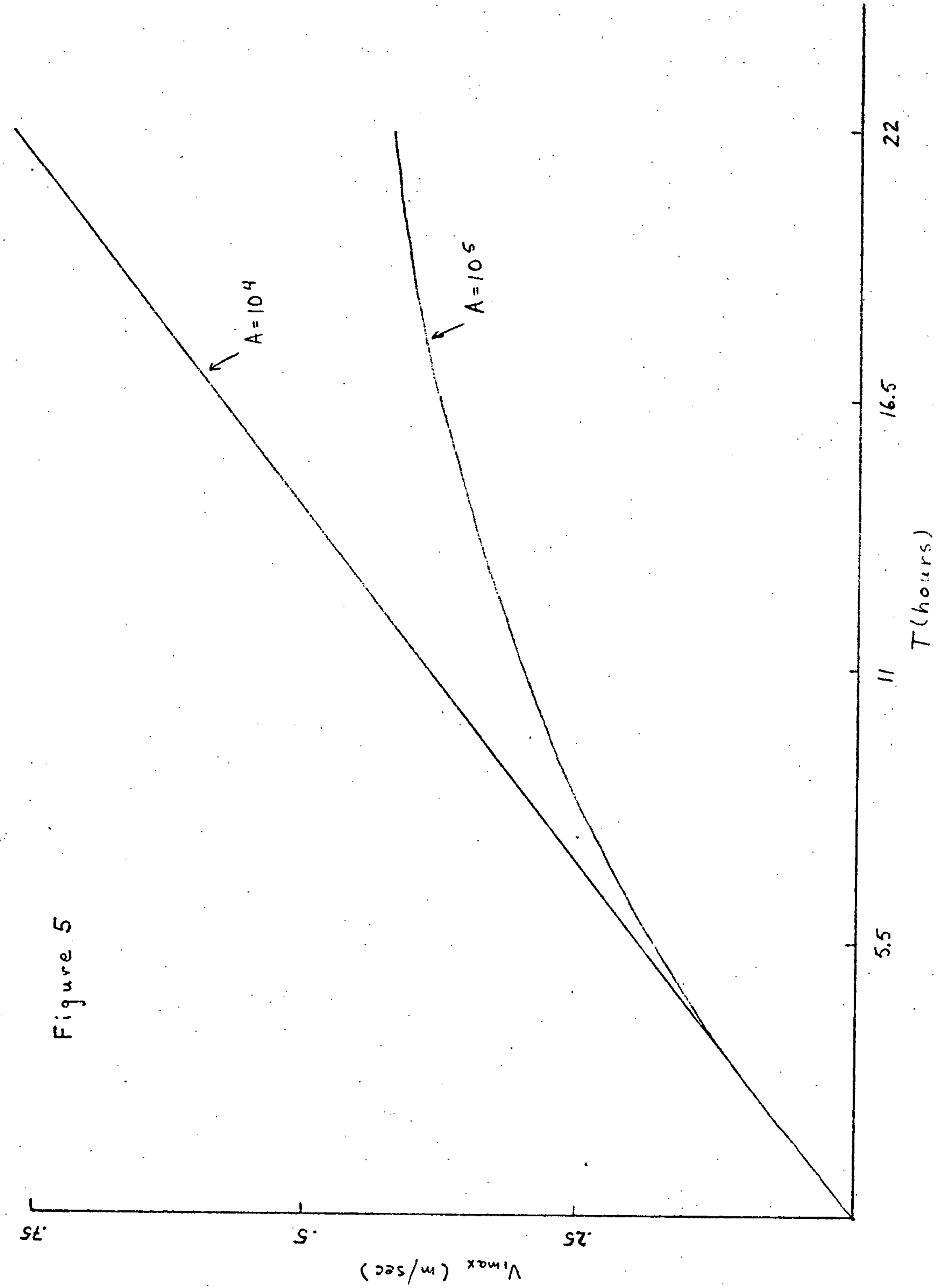

Figure 5

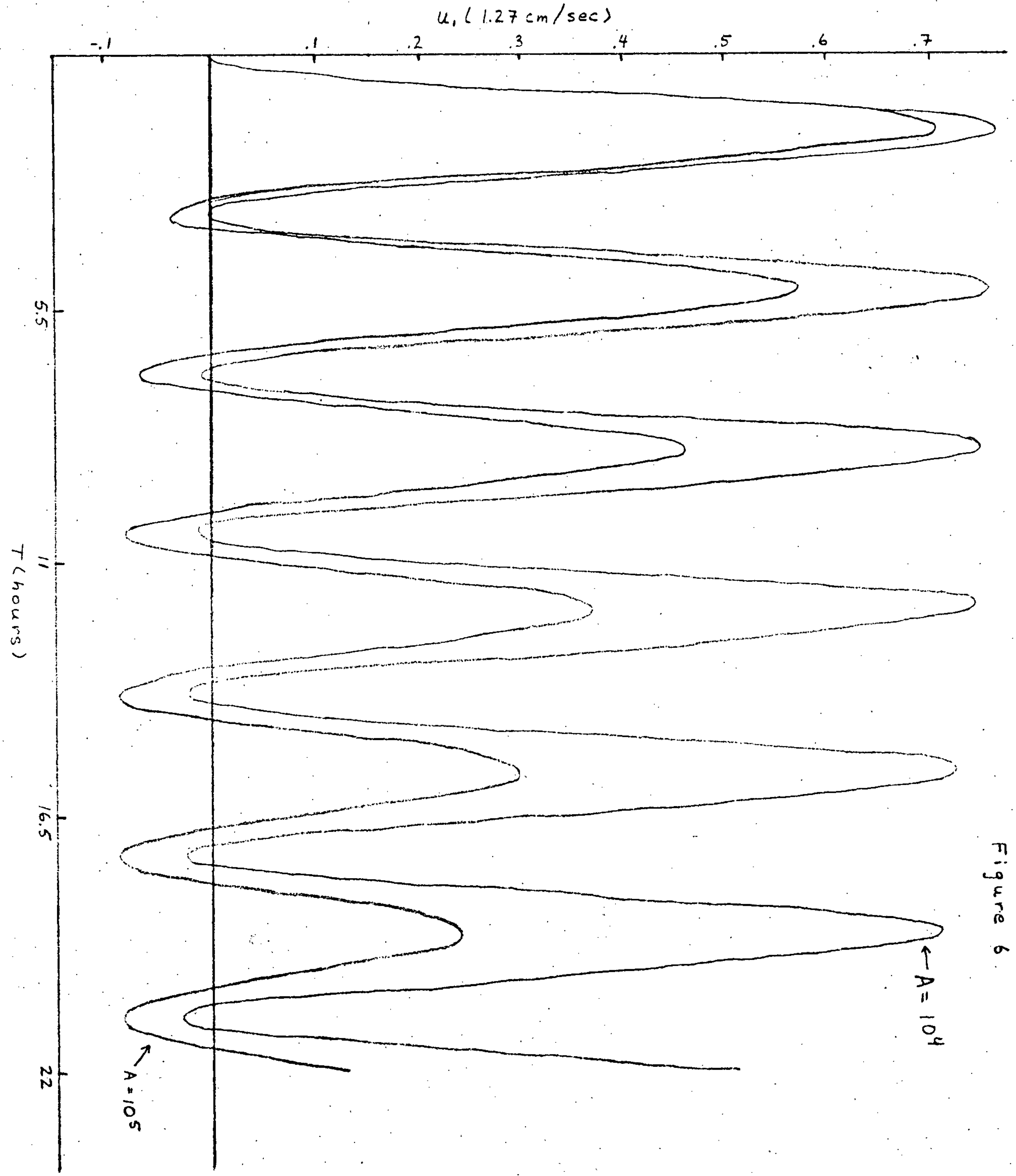

Figure 6

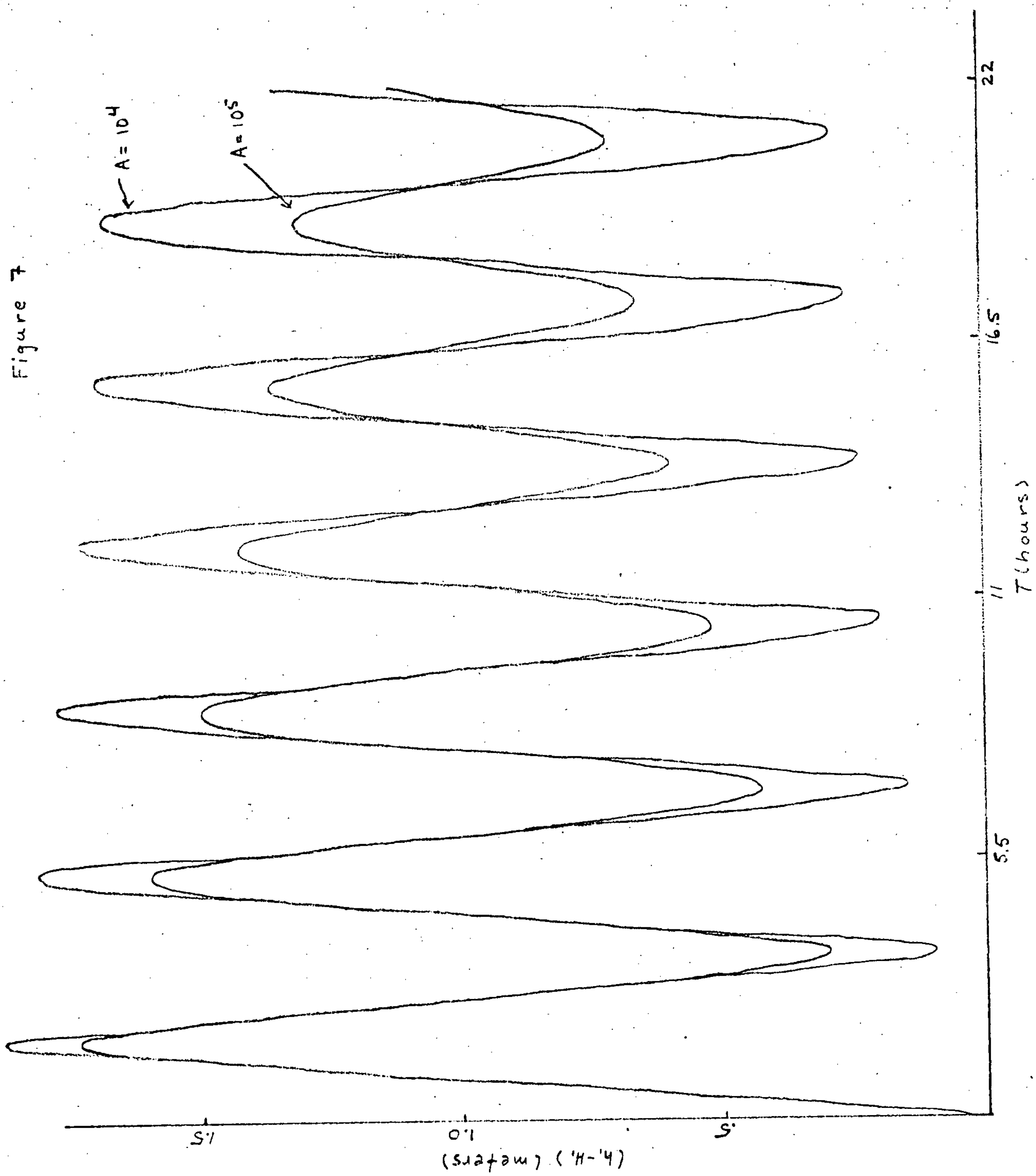

Figure 7

Figure 8

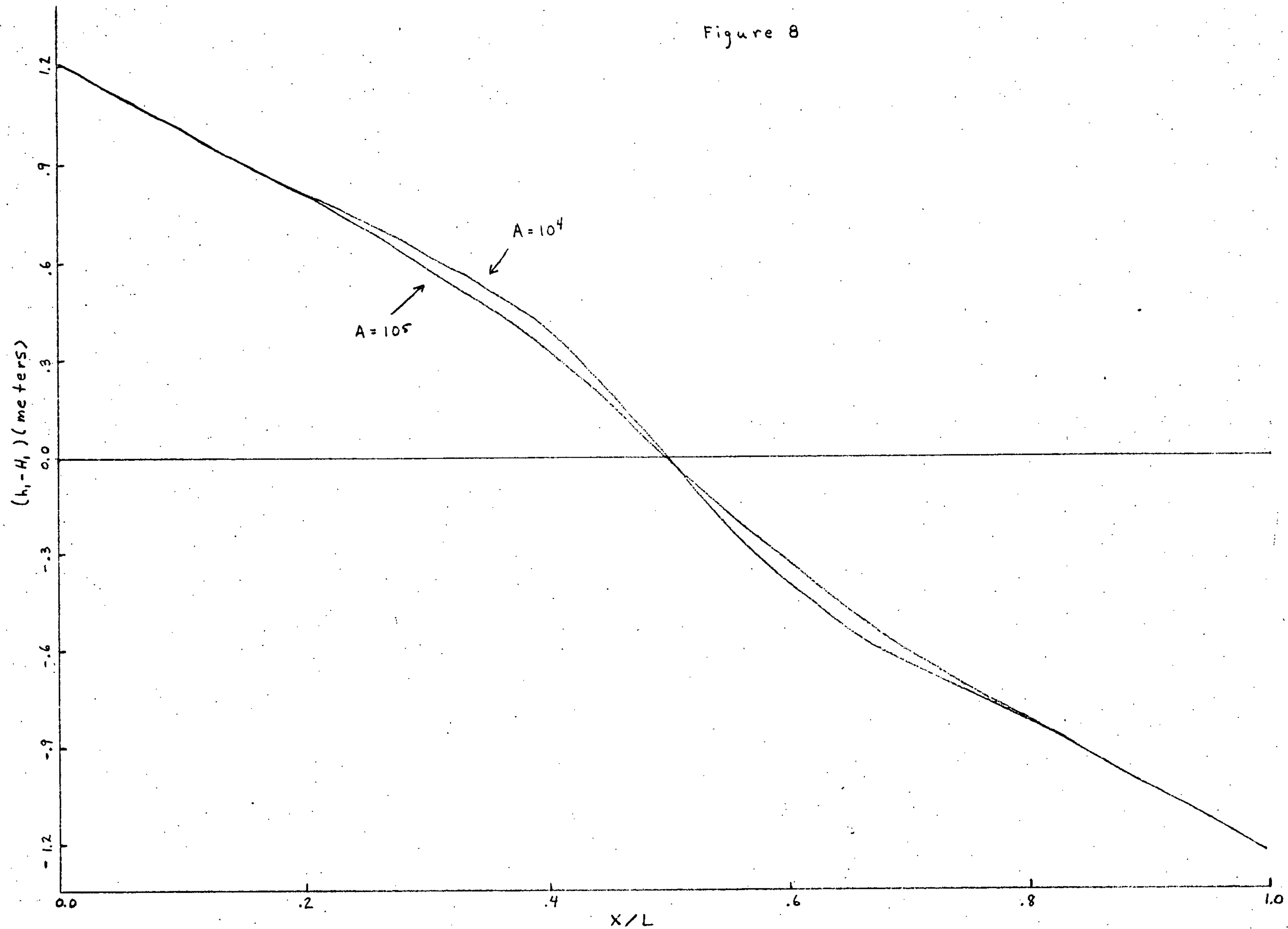

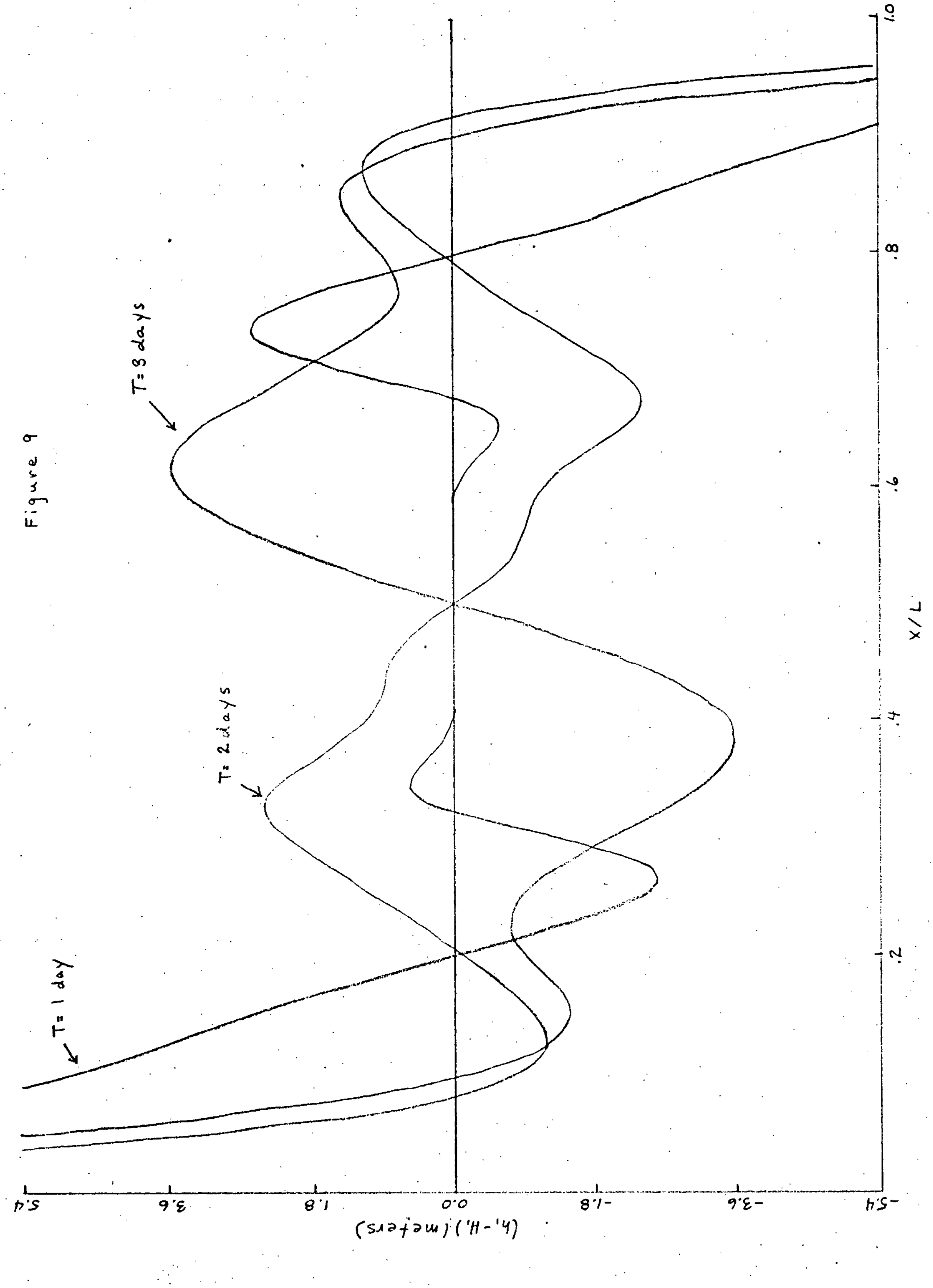

Figure 9

Figure 10

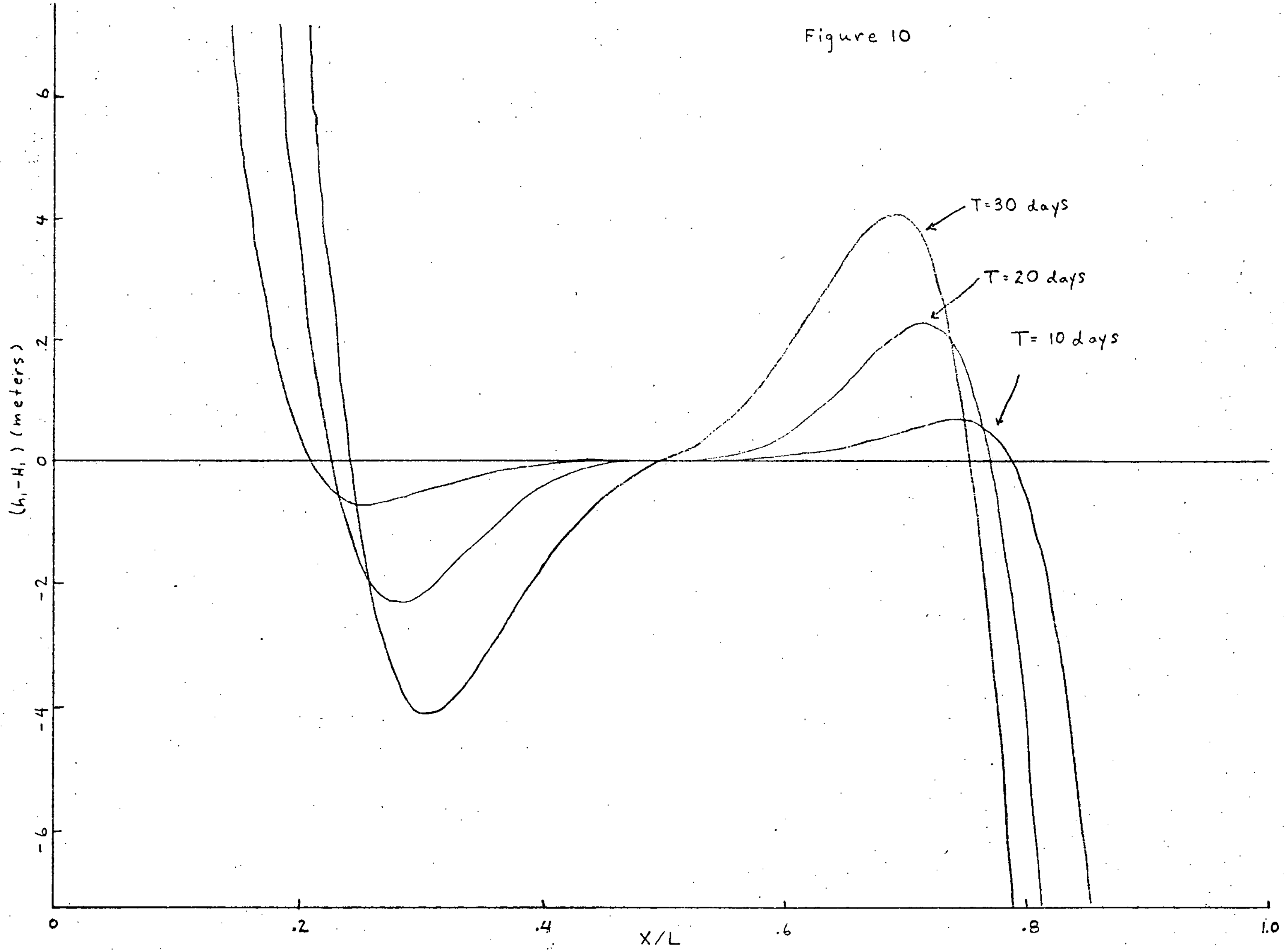

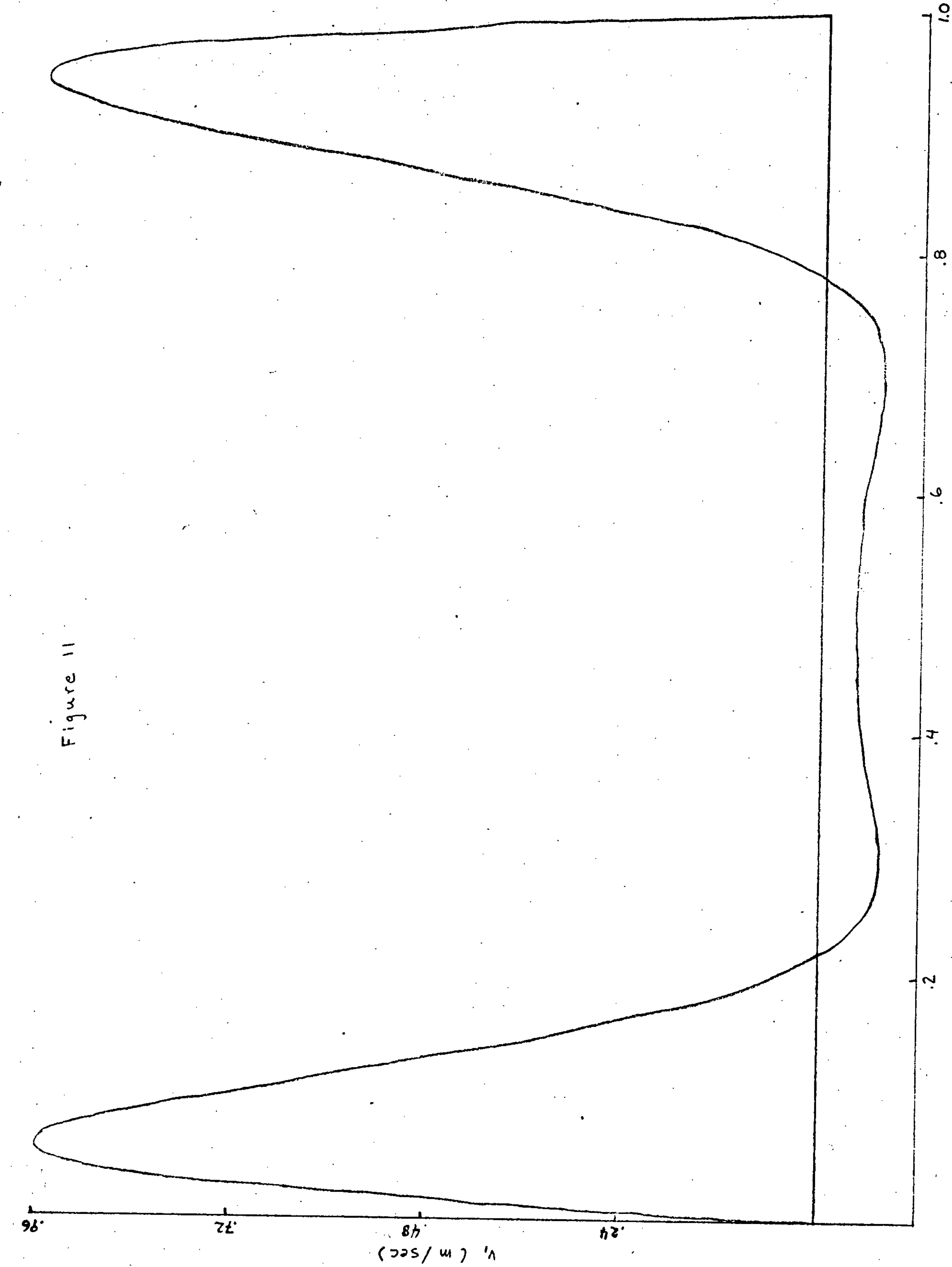

Figure 11

Figure 12

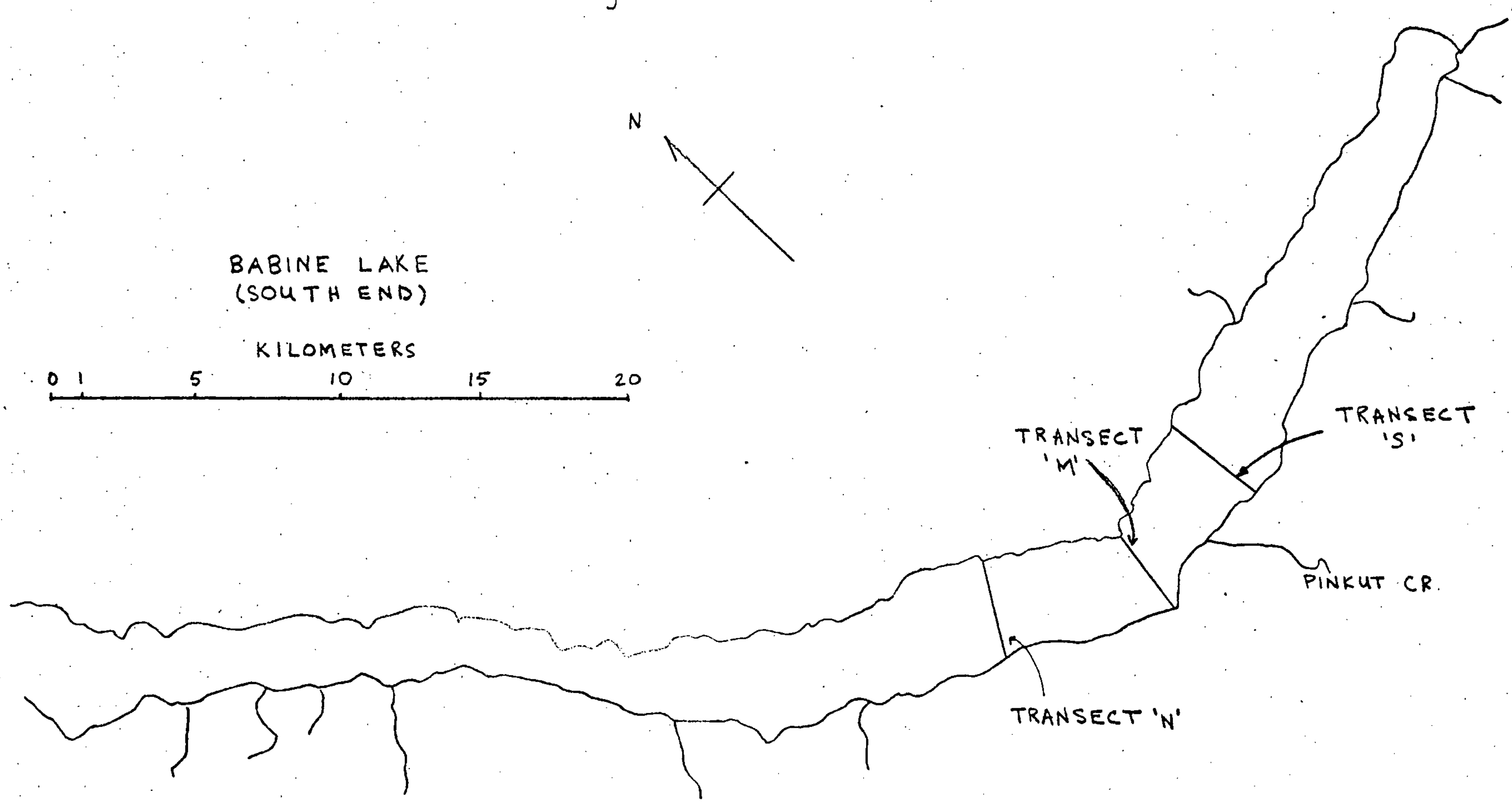
N
BABINE LAKE
(SOUTH END)
KILOMETERS
0 1 5 10 15 20
TRANSECT 'M'
TRANSECT 'S'
PINKUT CR.
TRANSECT 'N'

Figure 13a

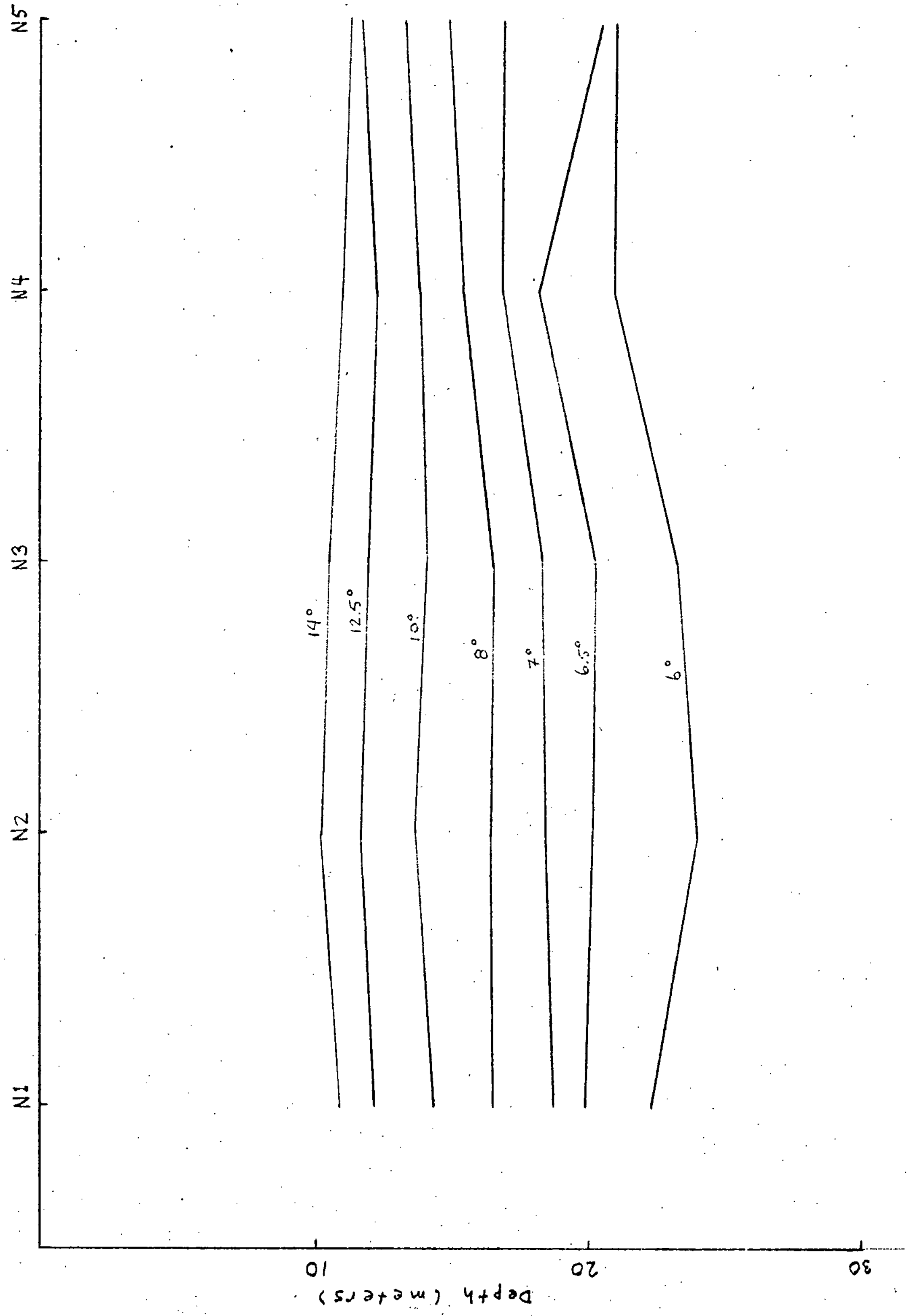

Figure 13b

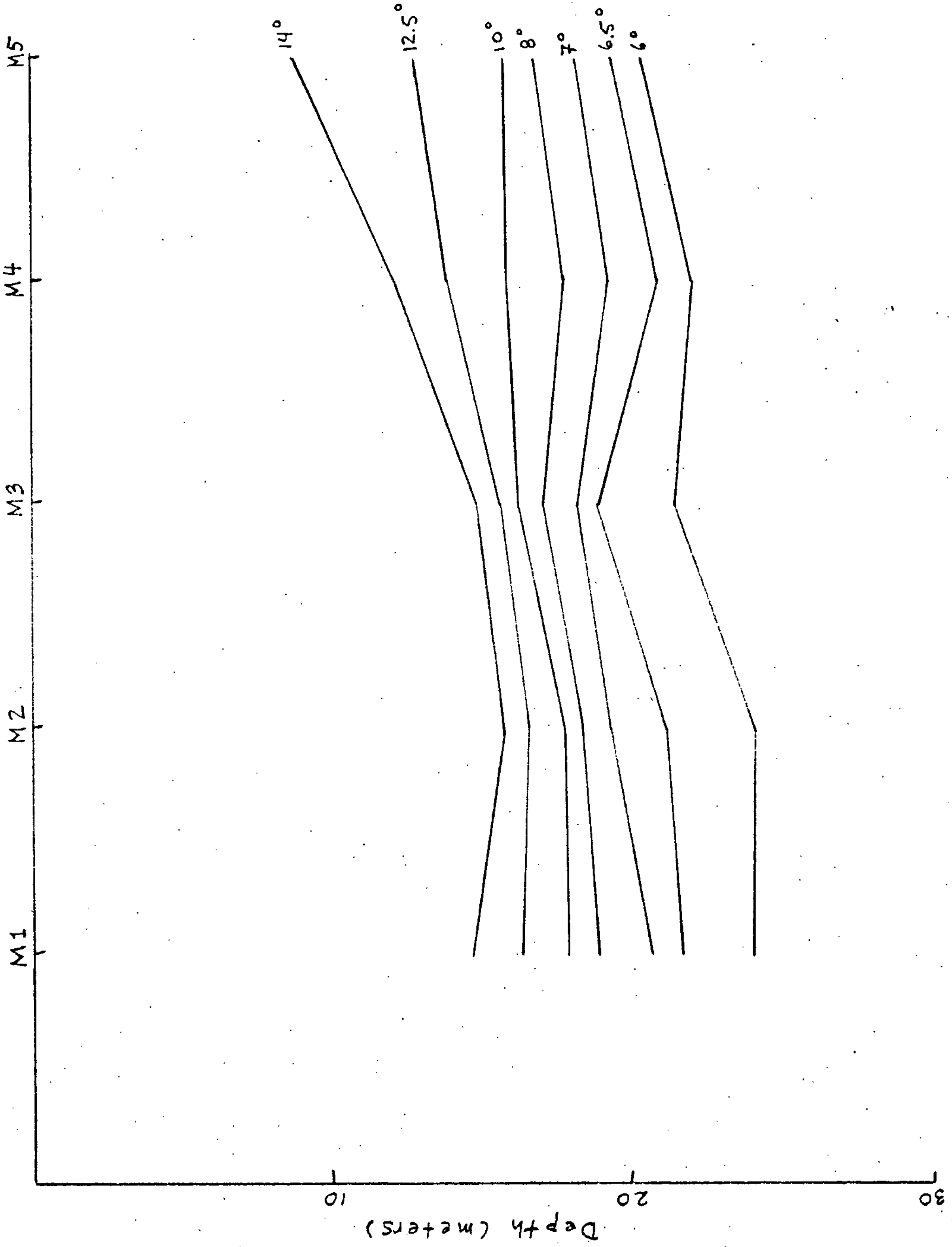

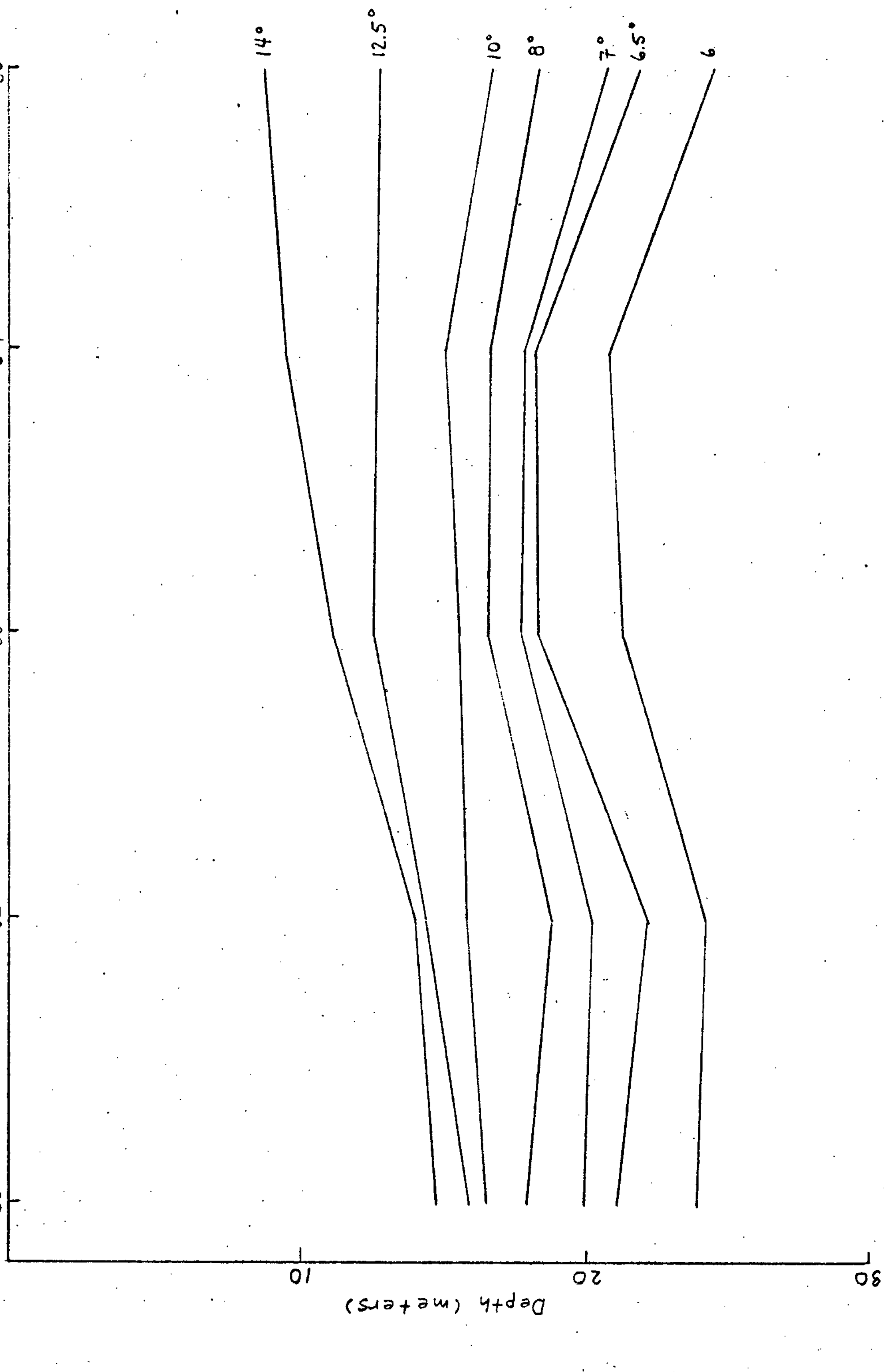

Figure 19a

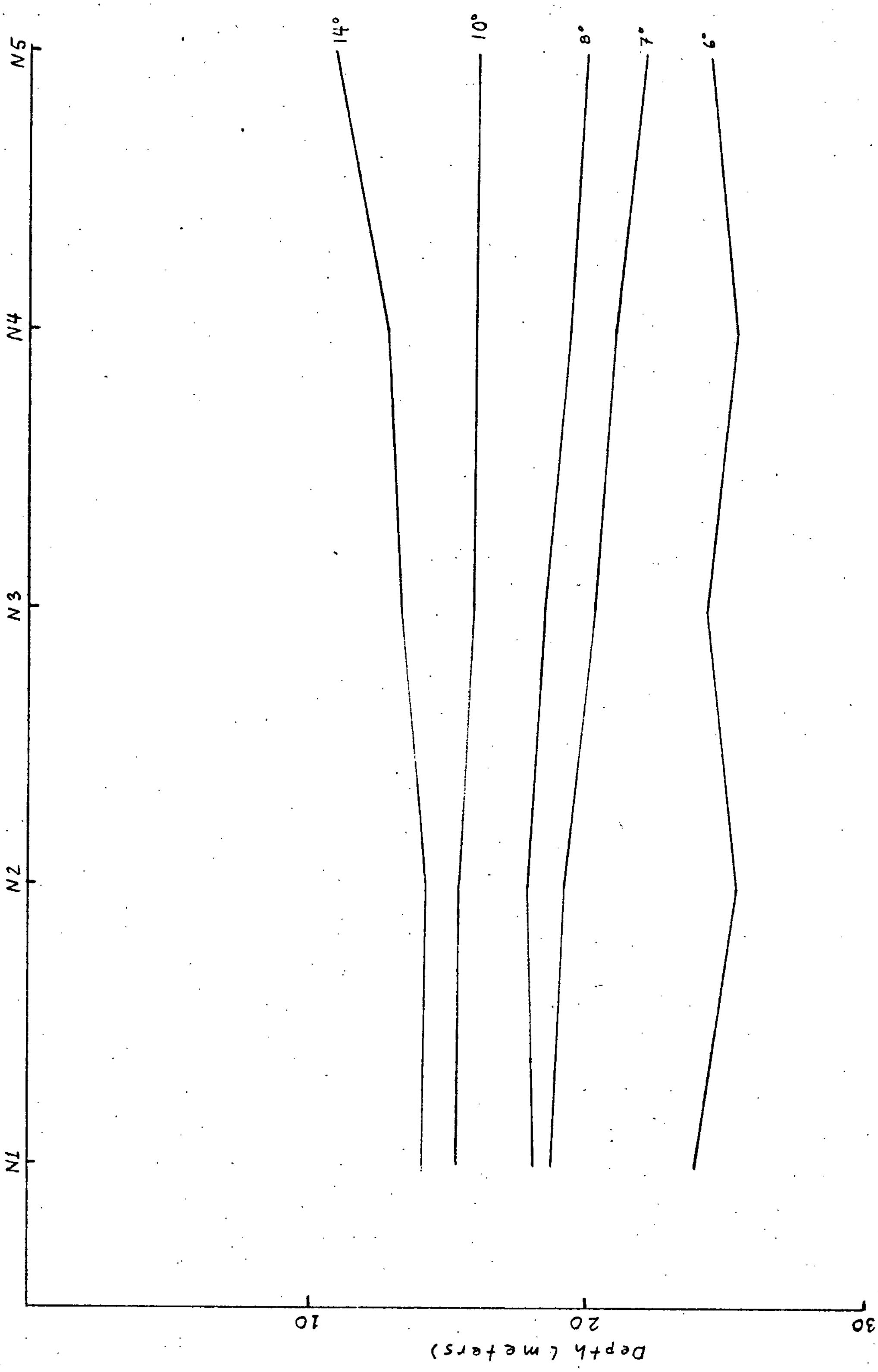

Figure 13 d

Figure 13e

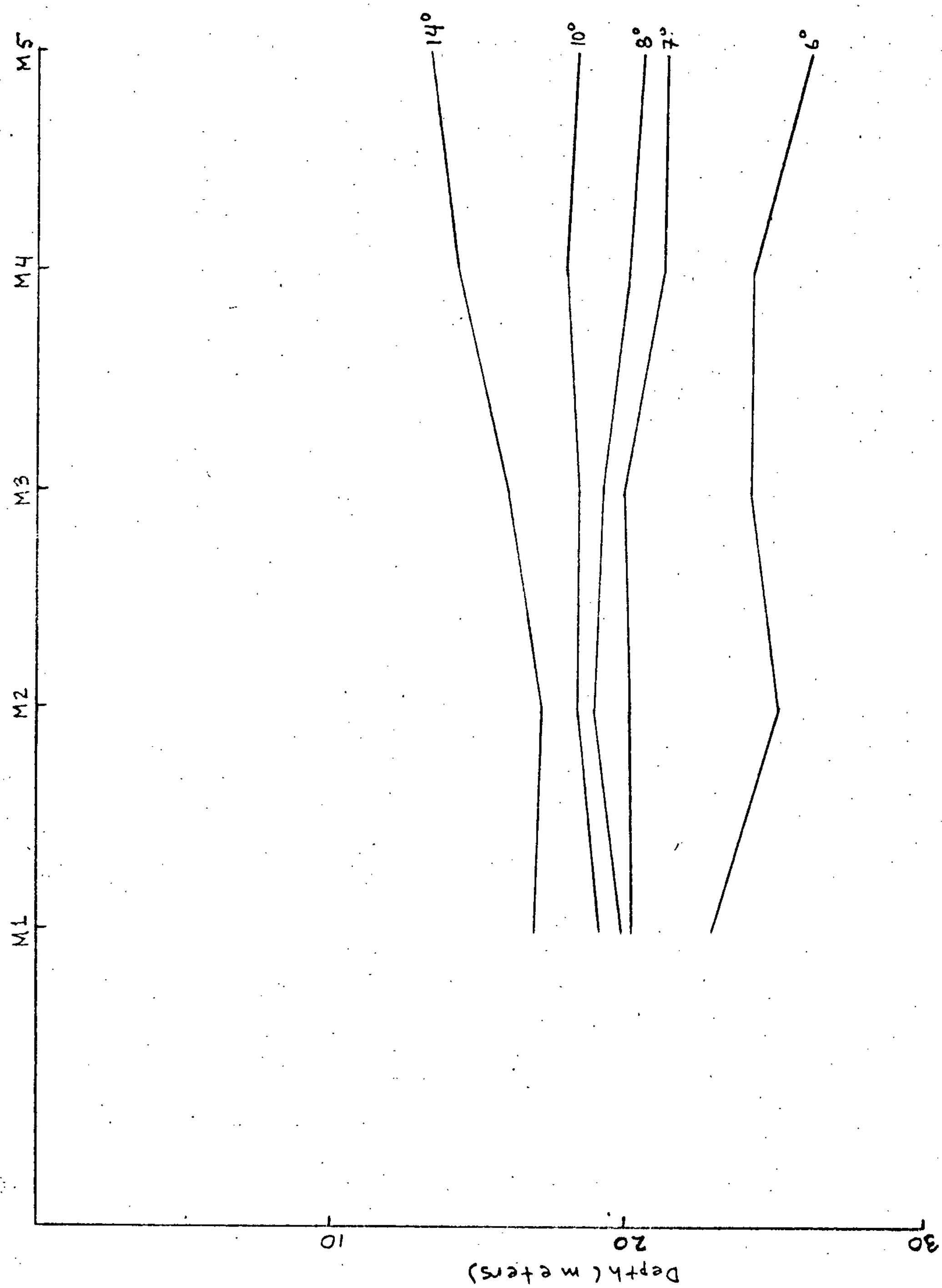

Figure 13f

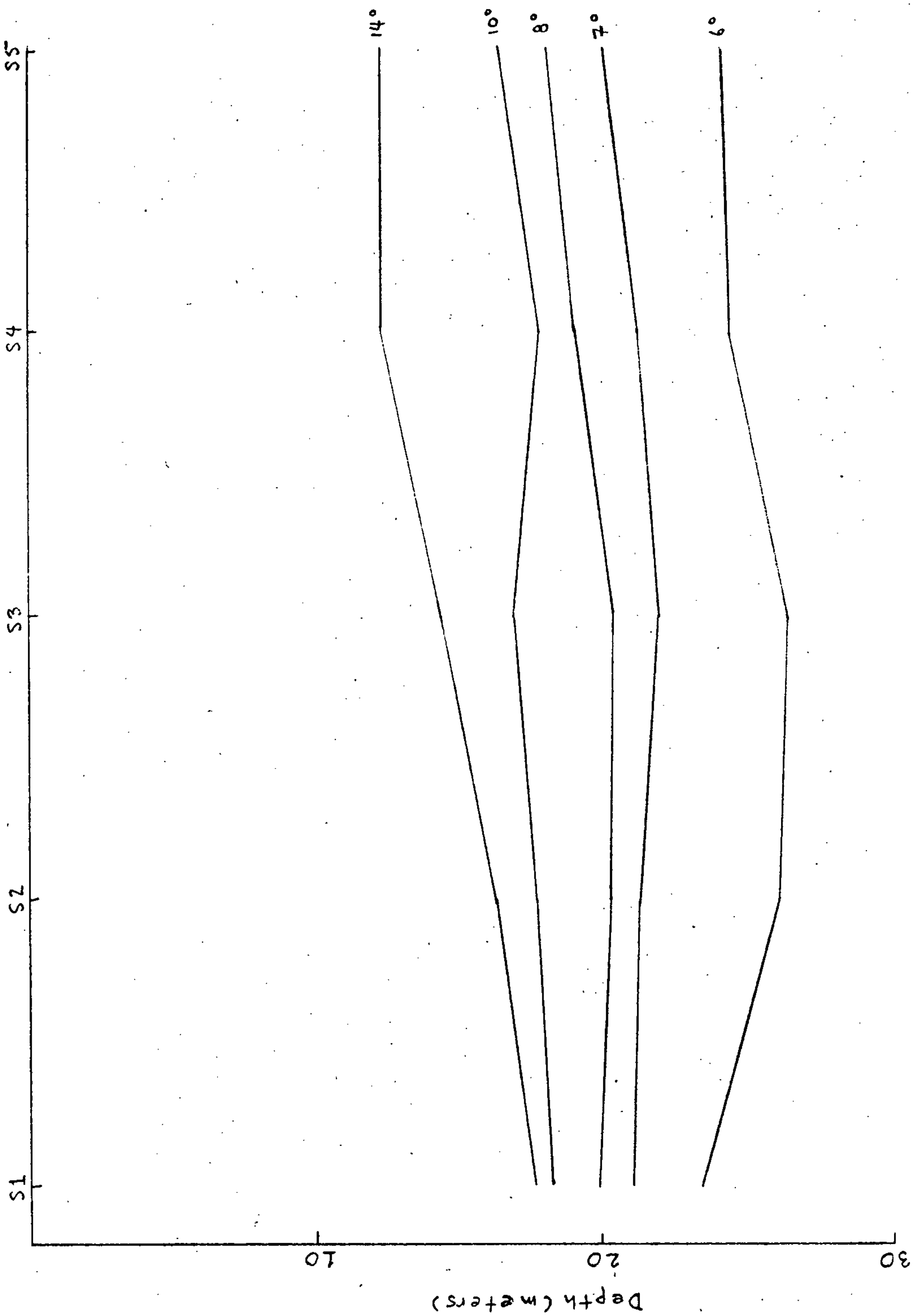

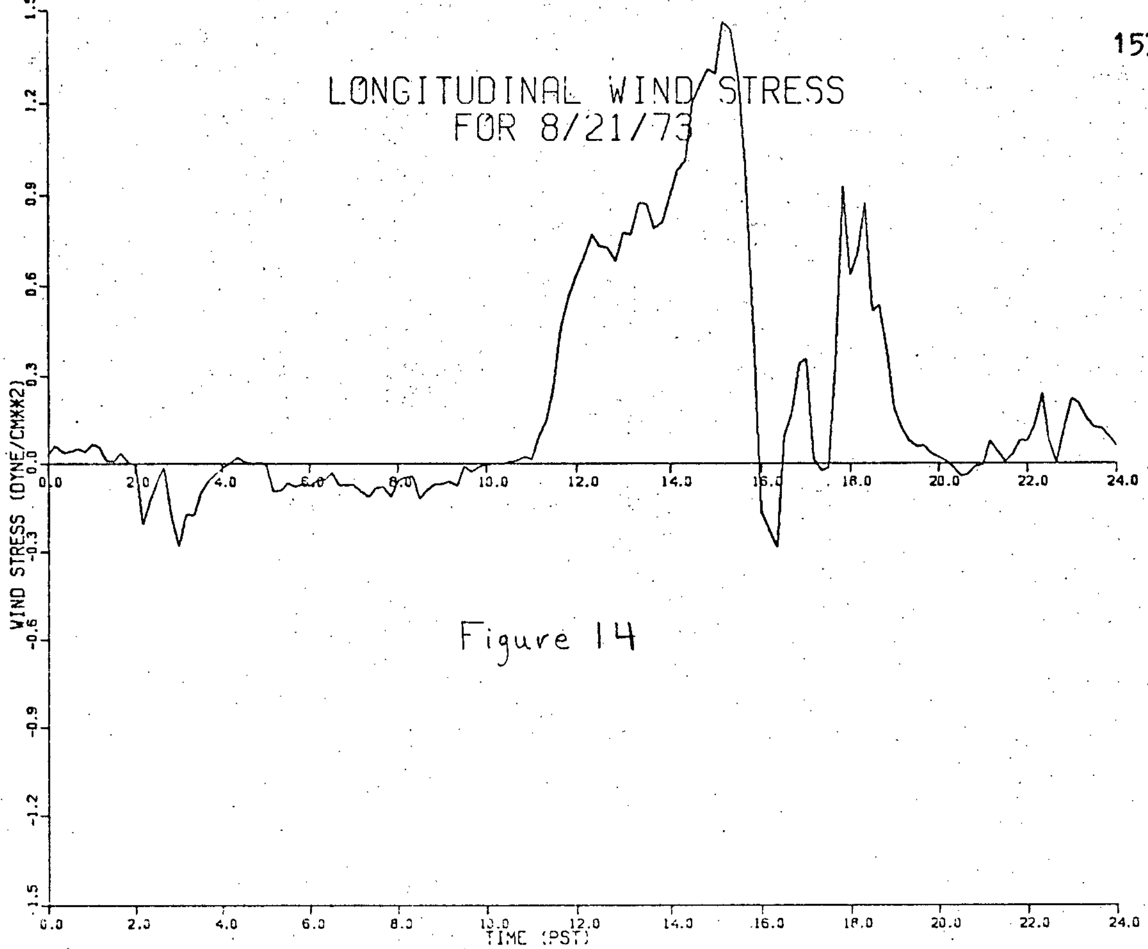
LONGITUDINAL WIND STRESS
FOR 8/21/73
WIND STRESS (DYNE/CM**2)
TIME (PST)

Figure 14

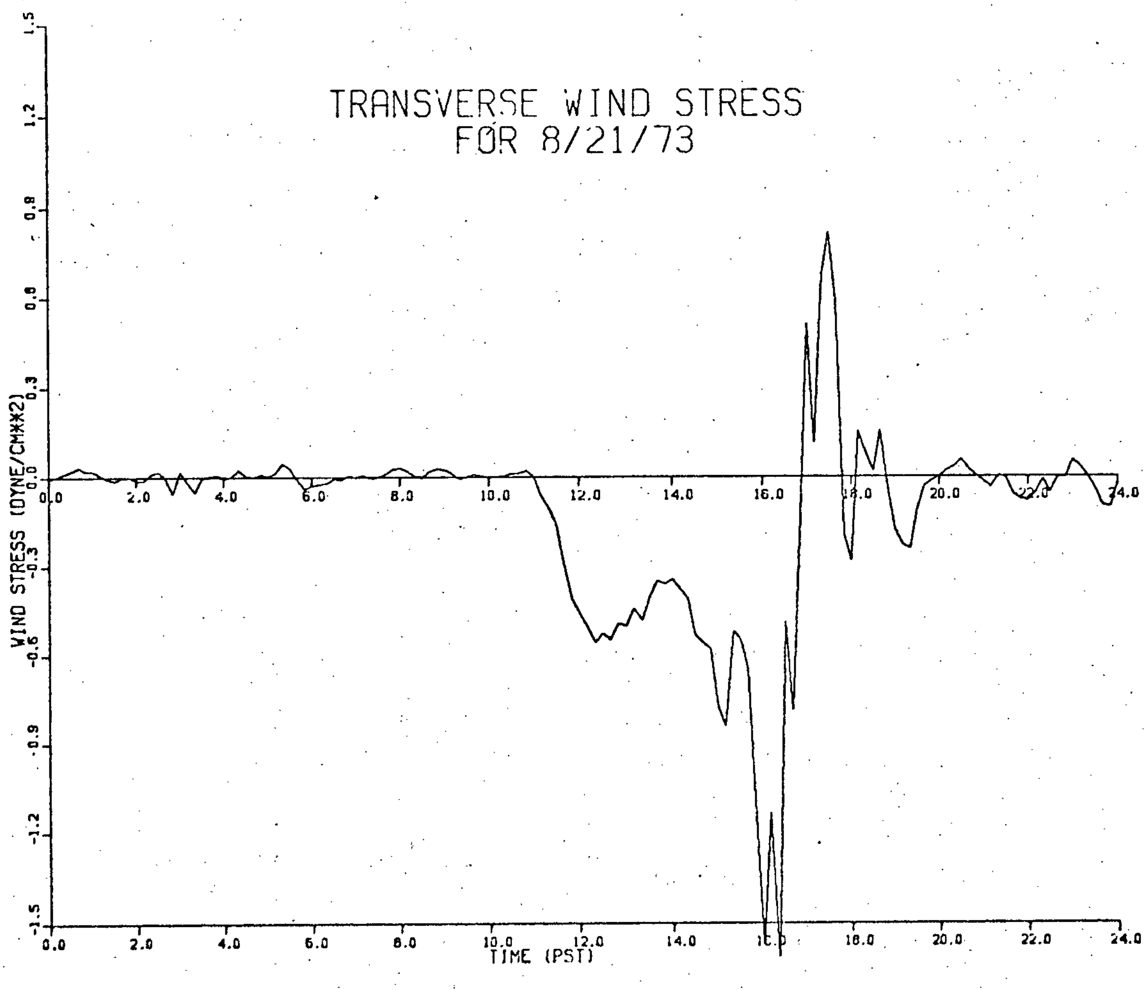
TRANSVERSE WIND STRESS
FOR 8/21/73
WIND STRESS (DYNE/CM**2)
TIME (PST)

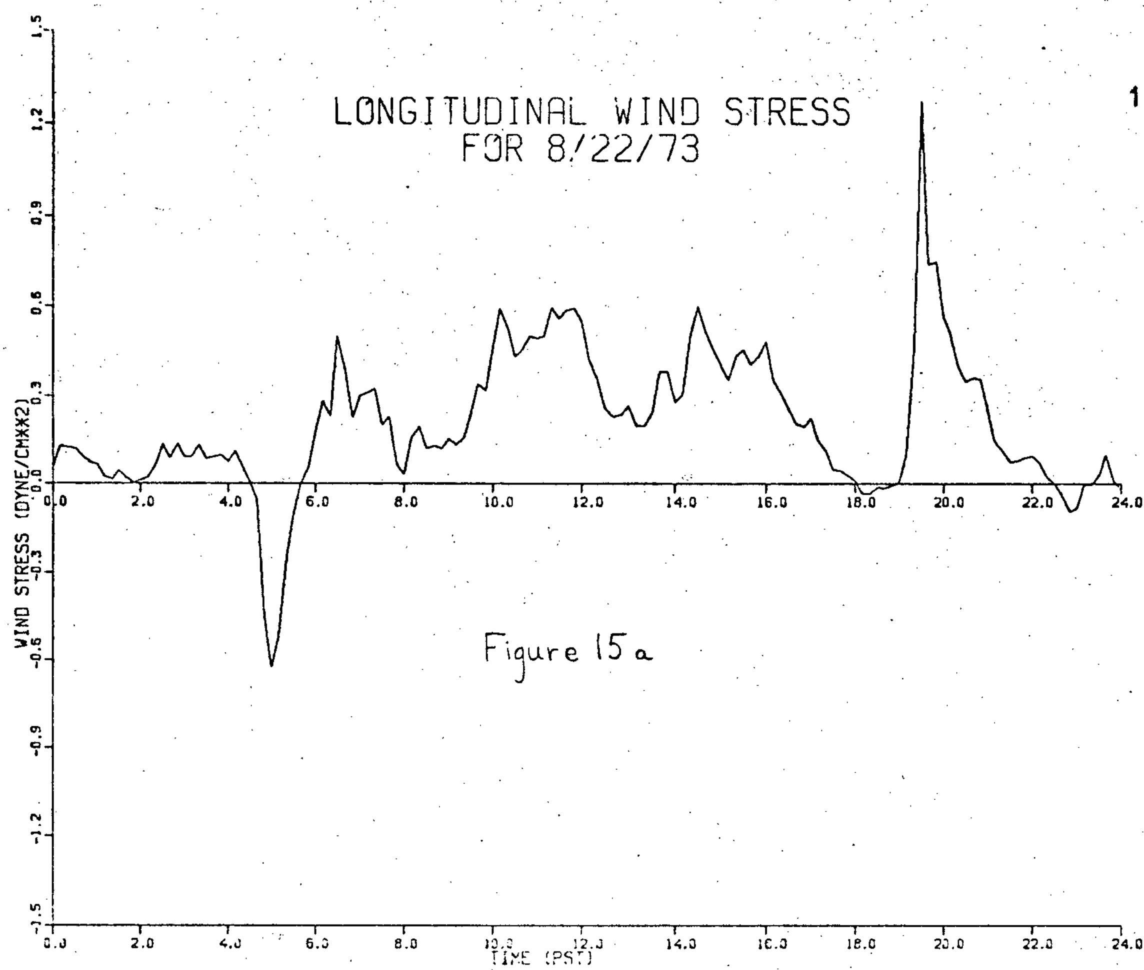
LONGITUDINAL WIND STRESS
FOR 8/22/73
WIND STRESS (DYNE/CM**2)
TIME (PST)

Figure 15a

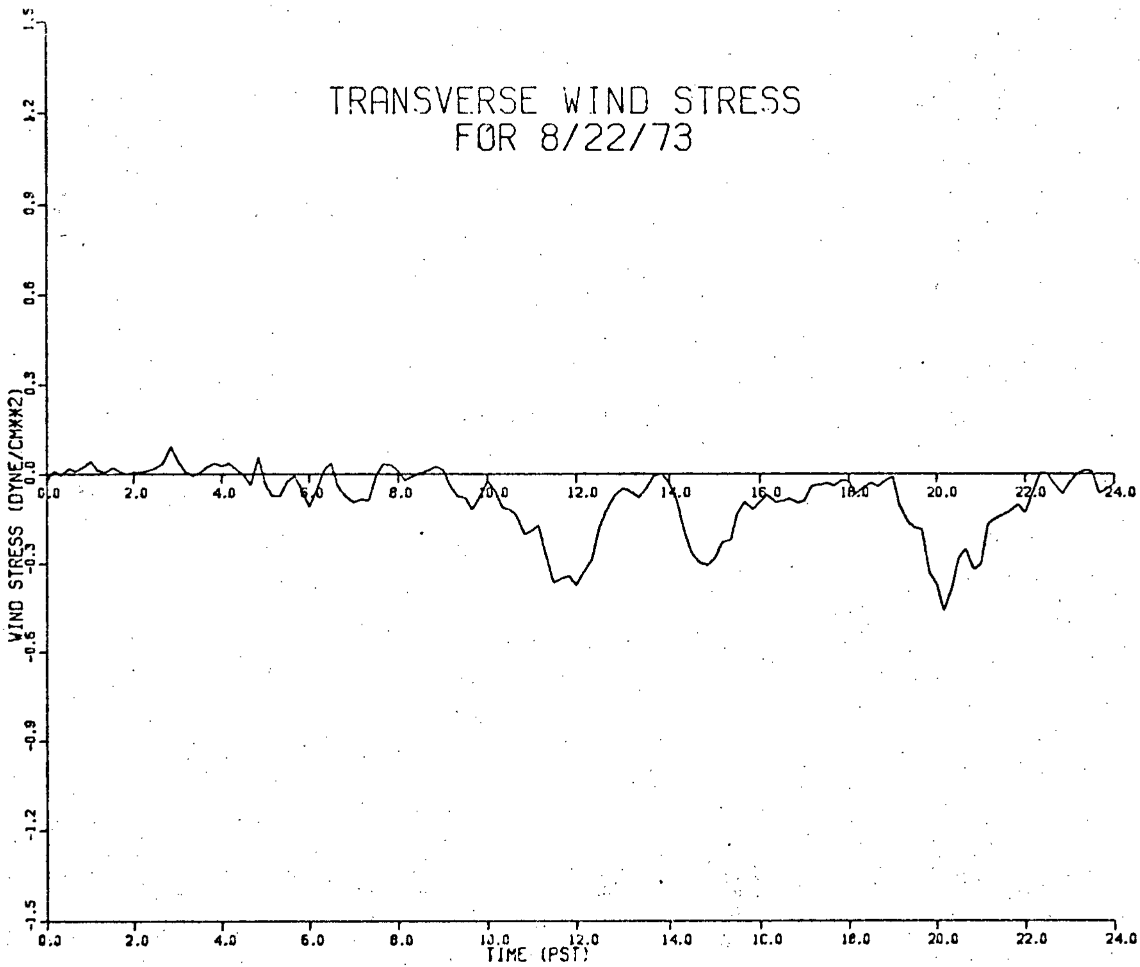
TRANSVERSE WIND STRESS
FOR 8/22/73
WIND STRESS (DYNE/CM**2)
TIME (PST)

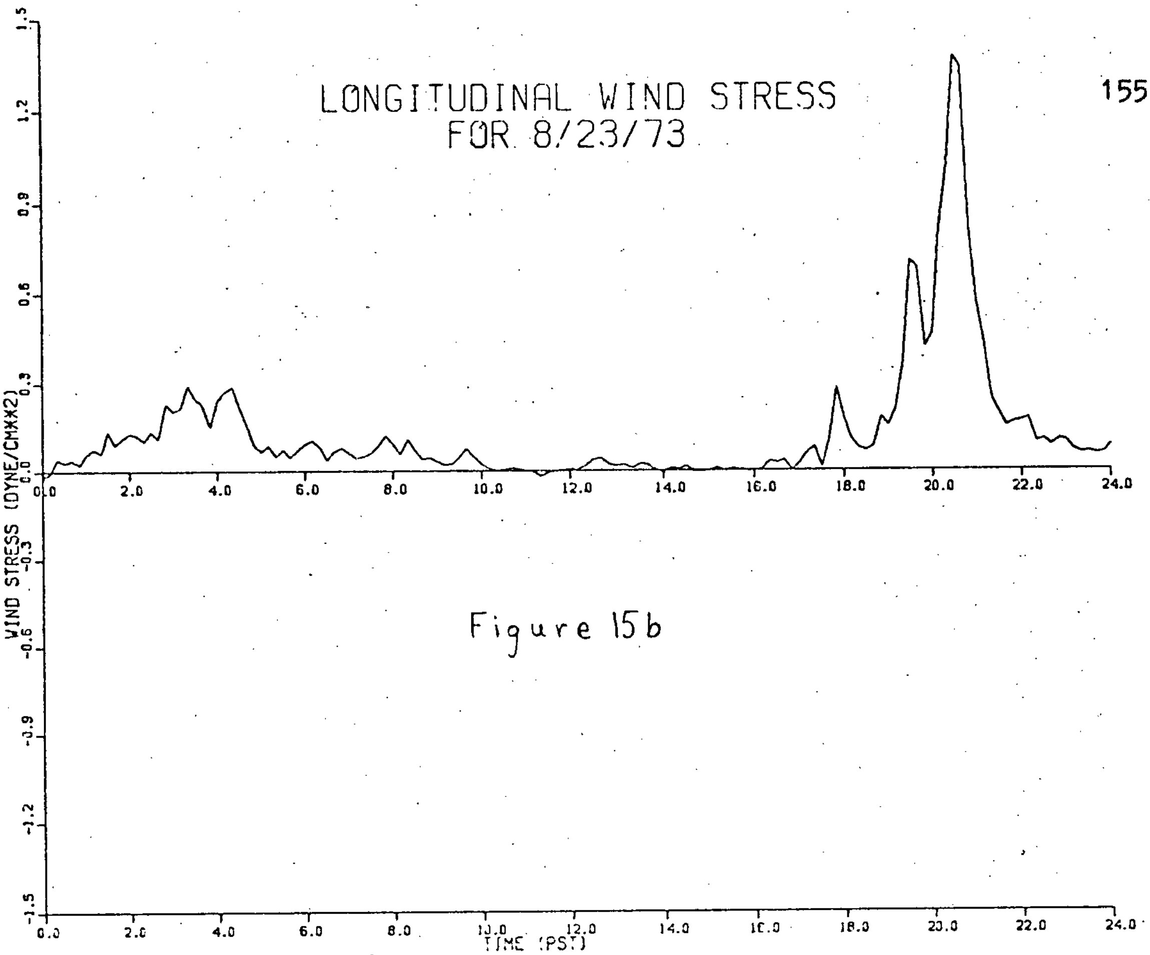
LONGITUDINAL WIND STRESS
FOR 8/23/73
WIND STRESS (DYNE/CM**2)
TIME (PST)

Figure 15b

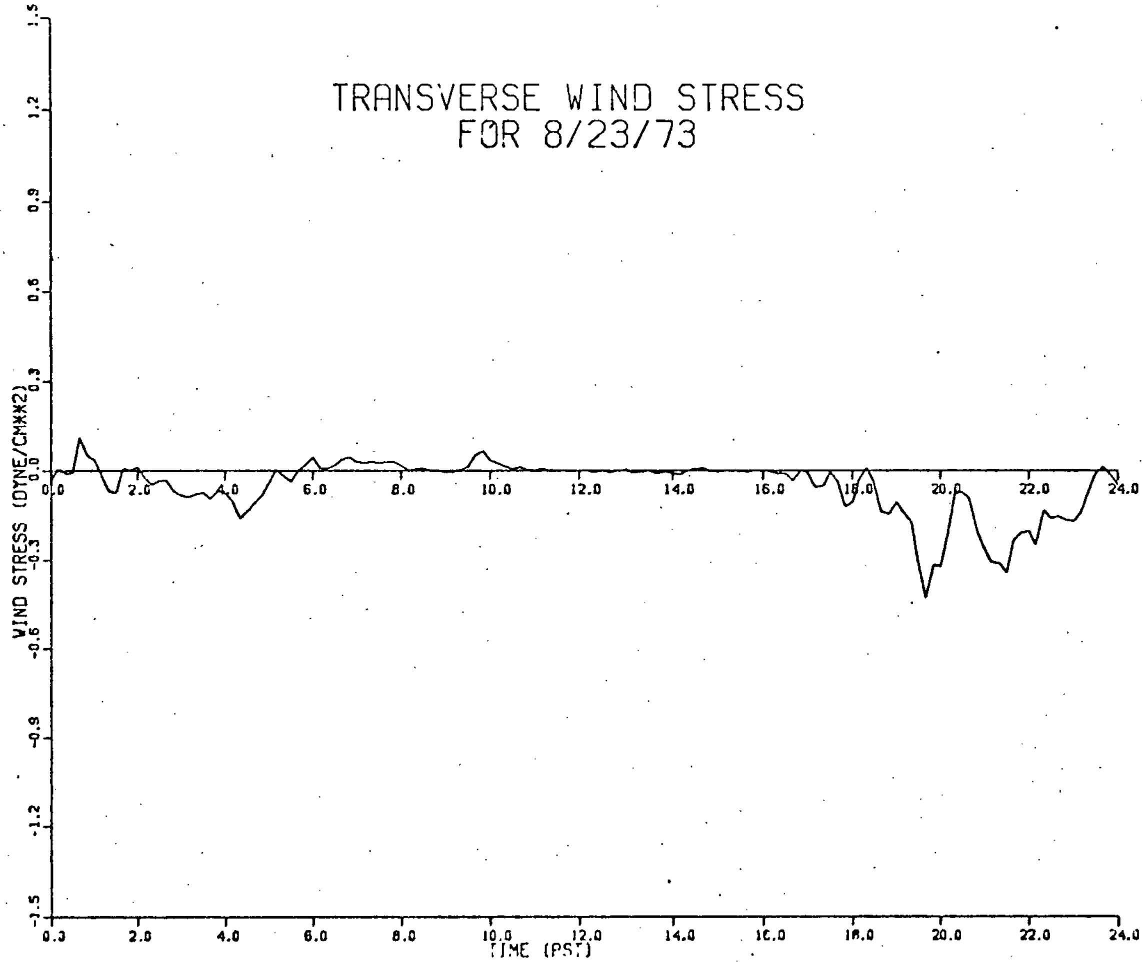
TRANSVERSE WIND STRESS
FOR 8/23/73
WIND STRESS (DYNE/CM**2)
TIME (PST)

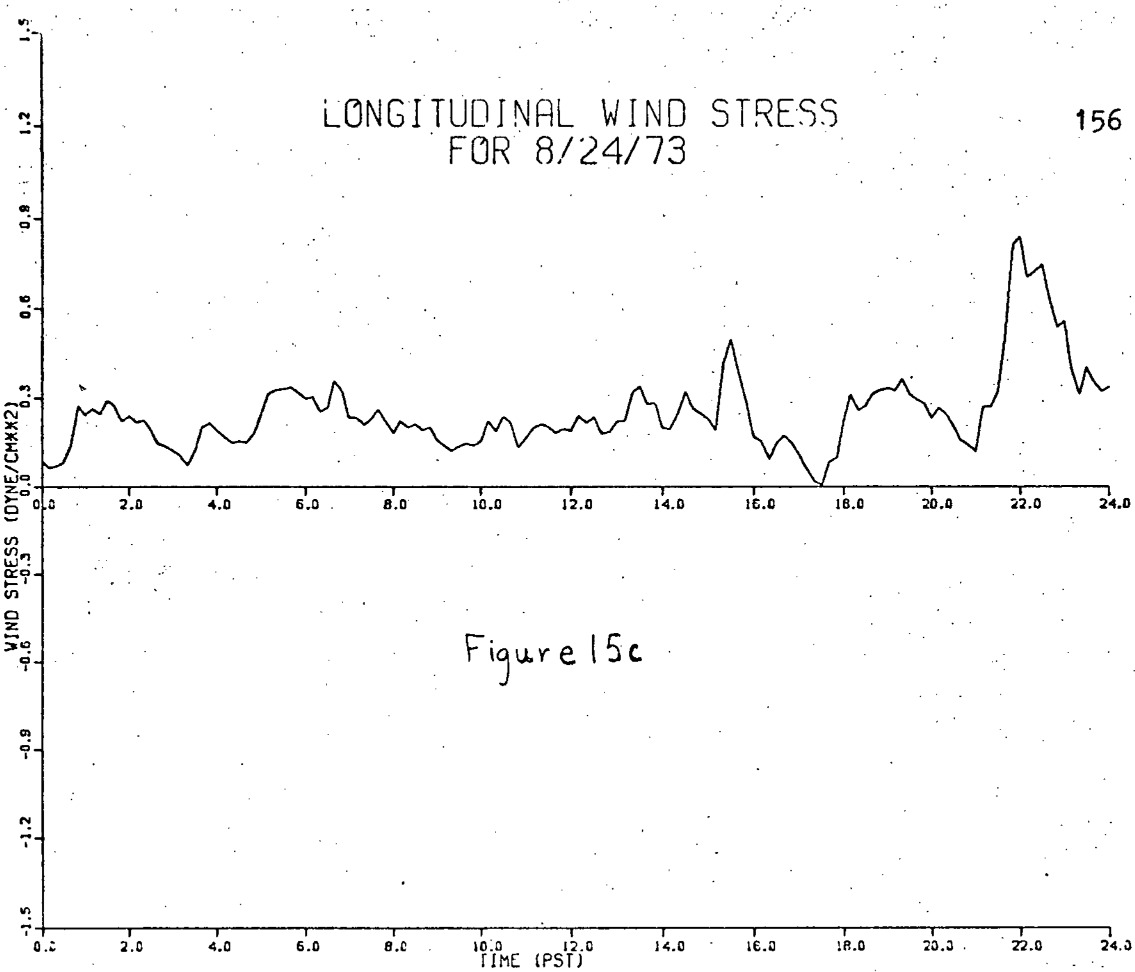
LONGITUDINAL WIND STRESS
FOR 8/24/73
WIND STRESS (DYNE/CM**2)
TIME (PST)
1.5
1.2
0.9
0.6
0.3
0.0
-0.3
-0.6
-0.9
-1.2
-1.5
0.0
2.0
4.0
6.0
8.0
10.0
12.0
14.0
16.0
18.0
20.0
22.0
24.0

Figure 15c

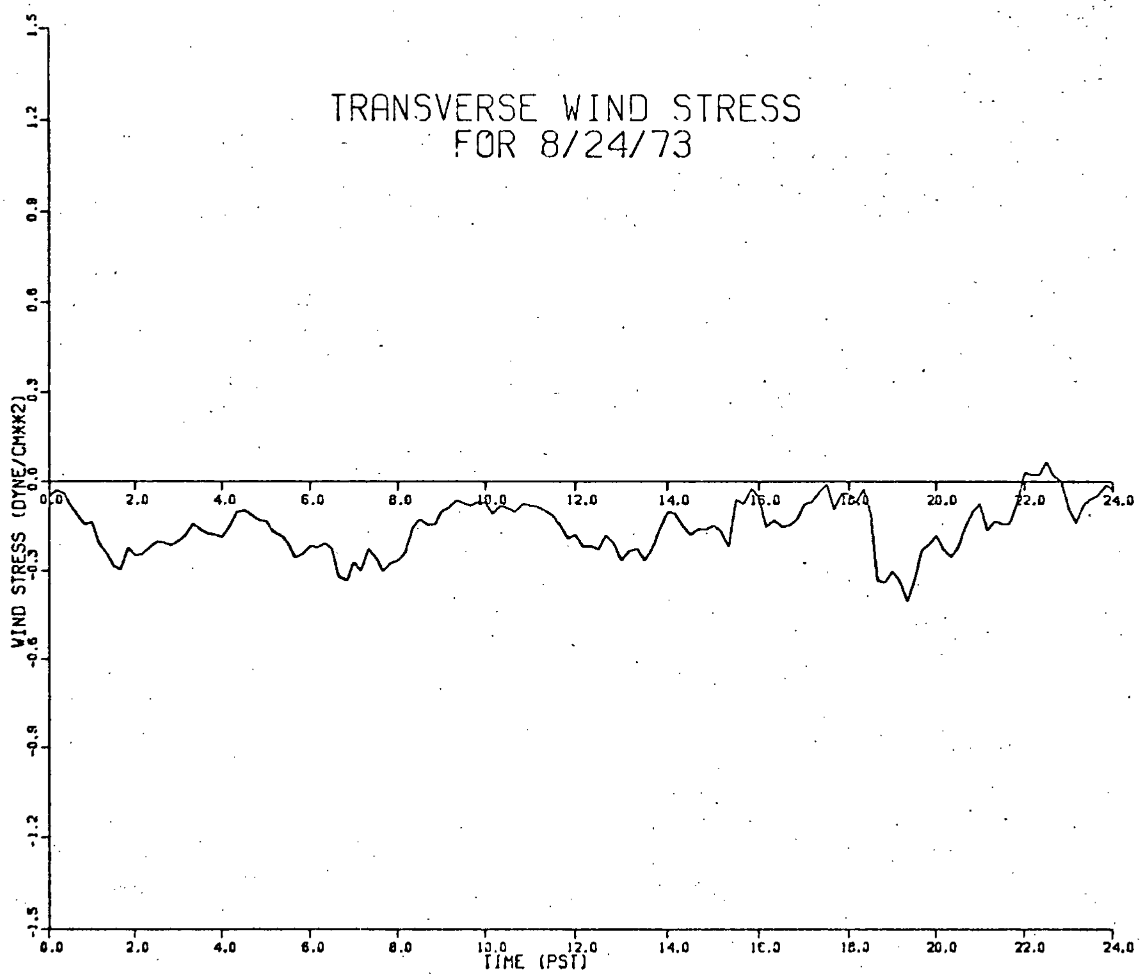
TRANSVERSE WIND STRESS
FOR 8/24/73
WIND STRESS (DYNE/CM**2)
TIME (PST)
1.5
1.2
0.9
0.6
0.3
0.0
-0.3
-0.6
-0.9
-1.2
-1.5
0.0
2.0
4.0
6.0
8.0
10.0
12.0
14.0
16.0
18.0
20.0
22.0
24.0

REFERENCES FOR PART B

Csanady, G. T., 1973: Transverse Internal Seiches in Large Oblong Lakes and Marginal Seas. J. Phys. oceancgr., 3, 439-447.

Farmer, D. M., 1972: The Influence of Wind on the Surface Waters of Alberni Inlet. Thesis, Institute cf Oceanography, University of British Columbia.

Heaps, N. S. And A. E. Ramsbottom, 1966: Wind Effects on the Water in a Narrow Two Layer Lake. Phil. Trans. Roy. Soc. London, 259,391-430.

O'Brien, J. J. and H. E. Hurlburt, 1972: A Numerical Model of Coastal Upwelling. J. Phys. Cceancgr., 2,14-26.

O'Brien, J. J., 1973: Analytical Sclutions fcr Two-Layered Models of the Cnset of a Coastal Upwelling Event. to appear in J. Phys. Oceanogr.